THE PROCEEDINGS OF
THE PHYSICAL SOCIETY

Section B

VOL. 64, PART 11 1 November 1951 No. 383 B

The Diffraction Pattern of Cold Worked Metals: I
The Nature of Extinction

BY W. H. HALL AND G. K. WILLIAMSON
Department of Metallurgy, University of Birmingham

MS. received 19*th October* 1950, *and in revised form* 14*th June* 1951

ABSTRACT. The influence of crystal perfection on extinction is briefly discussed and the possible corrections given. Experimental results for chemically produced copper and annealed aluminium filings have been obtained with a Geiger counter spectrometer using monochromatic radiation. The intensity measurements, and for copper the experimentally determined particle size, were inconsistent with the views that primary extinction occurred, but could be interpreted wholly in terms of secondary extinction, the corrected f values agreeing within $\pm 2\%$ with accepted values. Evidence to show that annealed metals contain residual lattice strain is advanced, in accord with the dislocation theory, and it is suggested that secondary extinction will predominate over primary extinction in all crystals containing such dislocations.

---

§ 1. INTRODUCTION

THE advent of Geiger counter spectrometers (Hall, Arndt and Smith 1949) capable of giving accurate and reproducible measurements of integrated intensities from polycrystalline or powdered specimens has made possible the study of many problems for which film methods have either been inconclusive or have failed. In order that full use can be made of this accuracy it is essential to know the exact nature of and the appropriate correction for extinction.

The work to be described is part of an investigation into the effects of cold work on the reflected intensities in the Debye–Scherrer spectrum of metals and it seems probable from the results that the effect of extinction will entirely mask any effect of cold work. Similarly a knowledge of the nature of extinction will be essential in many of the future applications of accurate intensity measurements, and there are good reasons for assuming the results of this investigation will apply for all powders as used in the Debye–Scherrer type of camera.

§ 2. EXTINCTION

For the Debye–Scherrer spectrum if interaction between the incident and reflected beam is neglected, and if it is assumed that the intensity of the incident beam is reduced only by absorption as it traverses the specimen it can be shown that the integrated intensity (for example Bragg, Darwin and James 1926)

$$\rho = \frac{1}{2\mu} N^2 |F|^2 \left(\frac{e^2}{mc^2}\right)^2 \lambda^3 p A(\theta), \qquad \ldots\ldots(1)$$

in which μ is the coefficient of absorption, N is the number of unit cells per unit volume, F is structure factor corrected for thermal vibration, $\boldsymbol{e}$ is the electronic charge, $\boldsymbol{m}$ is the electronic mass, $\boldsymbol{c}$ is the velocity of light, λ is the wavelength of the incident radiation, p is the multiplicity, θ is the Bragg angle, $A(\theta)$ is a function of θ depending on the geometry of the camera and including the polarization factor.

If interaction between the incident and reflected beams occurs then equation (1) gives a value of ρ which is higher than the experimental value as can be shown by the following argument. Let an x-ray beam be incident on the lattice at the Bragg angle θ. Then each successive plane is able to reflect a fraction q of the incident amplitude with a phase change of approximately $\frac{1}{2}\pi$. Twice reflected radiation will thus be parallel to and approximately π out of phase with the incident beam and destructive interference will occur. If only a few hundred planes are able to reflect this effect will be negligibly small since q has an order of magnitude 10^{-5}. However, if the crystal perfection is such that the phase relationships hold exactly over many thousands of atomic planes the co-operation of all reflected and twice reflected beams may become sufficient to extinguish the incident beam completely and this results in almost total reflection over a narrow angular range of a few seconds of arc, which consequently limits the integrated intensity to a relatively small value. Very few substances appear to behave in this way and it is generally assumed that crystals consist of small crystallites slightly disorientated from one another and containing only a few hundred reflecting planes of linear dimension approximately 10^{-4} cm. or less. Even in such small blocks the perfection of the lattice may be such that interaction has an appreciable effect and reduces the reflected intensity to a value smaller than that predicted by equation (1). Darwin (1922) considered this effect, which he called primary extinction, in detail and has shown that equation (1) may still be used if a correction of the form

$$\rho_{\mathrm{obs}}/\rho=(\tanh pq)/Pq \qquad \ldots\ldots(2)$$

is applied in which ρ_{obs} is the observed integrated intensity, p is the number of atomic planes over which the lattice is perfect, and q is given by

$$q=\frac{n\lambda}{\sin\theta}\frac{\boldsymbol{e}^2}{\boldsymbol{mc}^2}|F|,$$

where n is the number of atoms per unit area of the reflecting plane.

It has been pointed out by Bragg that even for crystals exhibiting no primary extinction the intensity incident on blocks within the crystal may suffer diminution by having a fraction of its intensity reflected by upper blocks. Since (1) is calculated on the assumption that the incident beam is reduced only by absorption, the observed intensity ρ_{obs} will be less than ρ given by (1). Darwin (1922) has shown that this effect which he called ‘ secondary extinction ’ may be regarded as a small increase in the absorption coefficient. This effect will depend on the probability of a block within the specimen reflecting the same pencil of rays as a block at a greater depth in the specimen and on the size of each block. Since in general neither the size nor the angular distribution of the blocks are known it is necessary that any correction shall contain an assumed constant which allows for these two factors.

Darwin showed that if (1) is written $\rho=Q/2\mu$ the observed intensity $\rho_{\mathrm{obs}}=Q/2(\mu+gQ)$ where g is a constant of the crystal.

These equations can be solved for g whence

$$g=(1-\rho_{\mathrm{obs}}/\rho)/2\rho_{\mathrm{obs}} \qquad \ldots\ldots(3)$$

and thus

$$\rho_{\mathrm{obs}}/\rho=1-2g\rho_{\mathrm{obs}}=1/(1+2g\rho). \qquad \ldots\ldots(4)$$

These equations hold for single crystals and powder specimens, but (4) may be applied to powder specimens in two ways. Suppose the powder specimens are composed of randomly oriented groups, the small crystals within each group being approximately parallel. The incident intensity as it penetrates the specimen is reflected by the groups into all the reflections in the Debye–Scherrer spectrum since their orientation is random and (4) must be written $\rho_{\text{obs}}/\rho = 1/(1+2g\Sigma\rho)$. This may be regarded as a constant increase in the coefficient of absorption, its effect being identical for all reflections. It will not affect relative measurements and thus this correction may in general be neglected.

Within each group one crystal fragment may still shield another from some of the incident radiation, both contributing to the same reflection, and in this case (4) will apply.

If both primary and secondary extinction occur together then the corrections (2) and (4) may be applied separately, since primary extinction is dependent only on p and q which are unaffected by secondary extinction, and secondary extinction is dependent on the observed intensity ρ_{obs}, which includes any effect of primary extinction. For simple crystals such as most metals where $|F|$ is a constant multiple of f, the atomic scattering factor, the extinction effect will not vary greatly for reflection from different crystal planes as it would for more complex crystals, in which the value of $|F|$ depends on the indices of the reflecting planes. The magnitude of the extinction effect would therefore be expected to vary smoothly with the order of reflection for such simple crystals, and it has been found convenient to estimate extinction by constructing graphs of f_{obs}/f as a function of the order of reflection $N = h^2+k^2+l^2$ for cubic crystals.

§ 3. PREVIOUS WORK

Very few investigations of the nature of extinction appear to have been made, and, so far as the authors are aware, such work has been carried out exclusively on single crystals. Bragg, James and Bosanquet (1921) showed that the absorption coefficient of rocksalt increased when the rocksalt was reflecting. The effective absorption coefficient was measured in an elegant series of experiments. The observed and calculated atomic scattering factors agreed very closely if the effective absorption coefficient were used instead of the calculated one, and they conclude that rocksalt exhibits secondary extinction only. Similar experiments by Bragg and West (1928) on topaz indicate that both primary and secondary extinction occur.

Brindley (1940), during a study of the effect of cold work on the x-ray diffraction pattern of metals, assumed that primary extinction was the principal effect, and calculated the distance over which the lattice would have to be perfect to account for the extinction. This value was found to be too great to account for the observed line broadening and Brindley suggested that this confirmed the generally accepted view that the line broadening is produced by strains in the crystal. Averbach and Warren (1949) during a study of the changes in integrated intensity produced by cold work suggested that the increase in intensity of the low-order lines could be attributed to a decrease in primary extinction. They suggest that the extinction for the weak 400 reflection will be negligible and on this assumption they show that cold work produces no change in the integrated intensity.

Workers in other fields however have generally assumed secondary extinction to be the most important effect. Daniels and Lipson (1944) used a secondary extinction correction during a study of the intensities of ghost lines which appeared on the Debye–Scherrer spectrum of a copper–nickel–iron alloy in a non-equilibrium state. There is thus a certain amount of confusion as to the nature of extinction and a determination of an appropriate correction is very necessary to enable accurate intensity measurements to be made.

§4. THE EXPERIMENTAL METHOD

The results were obtained using a Geiger counter spectrometer similar to that described by Hall, Arndt and Smith, the automatic resetting devices being sacrificed in the interests of flexibility. Monochromatic radiation was obtained from a curved quartz crystal monochromator, the height at the focus being limited to 5 mm. and the divergence to 2° of arc in order that instrumental line broadening could be reduced to a small value. The beam diverged from the focus on to the flat specimen which was pressed into a shallow cavity in an annealed copper disc which could be moved vertically into the beam and used as a reference specimen. The specimen disc was rotated in its own plane in order that statistical variations in intensity due to finite particle size (Alexander, Klug and Kummer 1948) should be less than 1%. The focused reflected rays entered the counter through a slit 4 mm. high and 0·2 mm. wide subtending 6 minutes of arc at the centre of the spectrometer, the radius of which was 11·46 cm.

Measurements of the intensity entering the counter at specific angular settings were obtained directly from the number of pulses registered on an electronic scaling unit since continuous recording is not capable of giving sufficient accuracy in the measurement of integrated intensities or line breadths. Counts were taken for periods of approximately one minute, the exact time being controlled by a monitoring counter and scaling unit which recorded an arbitrary fraction of the x-ray output and automatically stopped counting after registering 10,400 pulses. Multivibrator quenching units of the type described by Cooke-Yarborough, Floriden and Davey (1949) were used and were set to give an imposed dead time of 200 μsec. The x-ray set was self-rectifying and it was assumed to give a form factor (Arndt 1949, Westcott 1948) of approximately 3 for the CuKα radiation used in these experiments. Thus an effective dead time of 600 μsec. has been used in the dead time correction which for monitored counts has the form (Hall and Williamson 1951) $N_t = N(1+N\tau/T)(1+10400\tau/T)^{-1}$, where N_t is the true count which would be observed if there were no losses, N is the observed count, τ is the effective dead time and T is the period of counting.

Measurements were carried out on one half of the spectrum, i.e. on one side of the incident beam, and in order that the absorption correction should be independent of θ correct setting of the specimen angle relative to the beam is essential. The setting was checked by taking measurements of the integrated intensity on both sides of the beam, in accordance with recommendations made by Bragg (1914) and the angular setting of the specimen adjusted until these two intensities were equal.

Two specimens have been studied, one of aluminium, 99·997% pure, supplied by the British Aluminium Co. Ltd., filed and sieved through a 350 mesh/in. sieve and annealed *in vacuo* at 300° c. for 45 minutes, and the other of chemically produced copper, precipitated from a boiling acidified solution of copper sulphate with zinc dust.

The integrated intensities from the aluminium were obtained graphically by counting the squares under the curve between the line and background on a plot of corrected count against χ the angular setting of the counter. Since the lines were sharp this introduced no appreciable error. The chemically precipitated copper gave much broader lines and the intensities assessed graphically were checked by numerical integration using Simpson's rule, the background level in the two cases being found independently. Differences of up to 10% occurred between the results obtained by the two methods and this was shown to be due to the methods of deciding the background level. In the graphical summation the level was taken to be that at which the curve appeared to reach a constant value, as for example in Figure 1 which shows the 220 reflection, with an apparent background level of 110 counts. For the numerical integration a graph was drawn on a compressed angular, and expanded intensity scale as shown in Figure 2. The level of the background for the 220 reflection from such a graph is 100, and the small difference of 10, becaue it is spread out over many degrees, accounts for the discrepancy between the two methods.

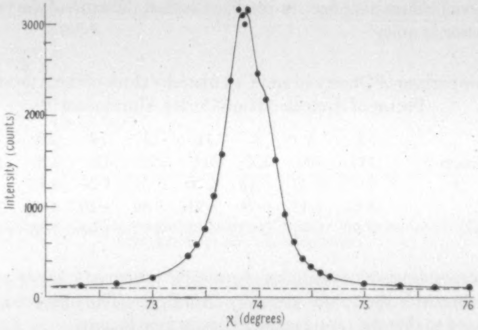

Figure 1. 220 reflection from copper.

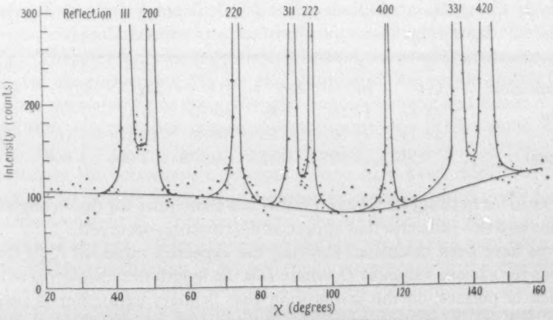

Figure 2. Chemically produced copper background plot.

This background plot shows many interesting features, the most notable being the low level of the background around the weak 400 reflection and the high level between the close 111 and 200, 311 and 222, and 331 and 420 reflections. These two results together suggest that the ' tails ' of the lines extend for a much greater angular range than is generally thought and contribute appreciably to the background level. It is apparent that in any accurate intensity measurement such background plots must be constructed to obtain measurements of the highest accuracy.

§ 5. RESULTS

Relative values of the apparent atomic scattering factor were calculated from the equation

$$I=k|f|^2 p\,\frac{1+\cos^2 2\theta\cos^2 2\alpha}{(1+\cos^2 2\alpha)\sin^2\theta\cos\theta},$$

where α is the Bragg angle of reflection of the monochromatic beam from the quartz crystal and has to be included to allow for the polarization of the beam by the monochromator and k is a constant. The values of the observed atomic scattering factors of aluminium for the various reflections are shown in Table 1 together with the theoretical values given by Brindley (1936).

The observed values have been normalized so that the ratio of the two values for the 422 reflection is unity.

Table 1. Comparison of Observed and Calculated Values of the Atomic Scattering Factor of Annealed High Purity Aluminium

N	3	4	8	11	12	19	20	24
Reflection	111	200	220	311	222	331	420	422
f_{obs}	7·77	7·37	6·18	5·60	5·51	4·24	4·07	3·46
f	8·63	8·13	6·74	5·91	5·69	4·20	4·04	3·46
Ratio	0·90	0·91	0·92	0·95	0·97	1·01	1·01	1·00

The corresponding values for the chemically prepared copper are shown in Table 2 together with the values given by Brindley. The observed values have been normalized so that the ratio for the 331 reflection is unity.

Table 2. Comparison of Observed and Calculated Values of the Atomic Scattering Factor of Chemically produced Copper

N	3	4	8	11	12	19	20
Reflection	111	200	220	311	222	331	420
f_{obs}	18·77	17·28	12·89	10·70	10·11	7·16	6·83
f	17·13	15·70	12·34	10·46	10·17	7·16	6·65
Ratio	0·912	0·909	0·957	0·978	1·006	1·000	·974

The ratio for both spectra is appreciably less than unity for the strong low-order reflections and this indicates that appreciable extinction occurred.

Curves have been calculated showing the expected values of f_{obs}/f for all the reflections for various values of D, where D is the length in centimetres over which the lattice is perfect, on the assumption that primary extinction is responsible for the fall in intensity, using the equation $f_{\mathrm{obs}}/f=[(\tanh pq)/pq]^{1/2}$ where

$$pq=\frac{8D}{a^2(h^2+k^2+l^2)^{1/2}}|f|\frac{\mathbf{e}^2}{\mathbf{mc}^2},$$

and a the lattice parameter. These curves are shown dotted in Figures 3 and 4. The observed values agree best with the curves corresponding to particle sizes between 1 and 2×10^{-4} cm. for aluminium (Figure 3) and 4 and 6×10^{-5} cm. for copper (Figure 4), though in neither case is the agreement satisfactory, mean curves drawn through the experimental points having much smaller curvatures at low values of N than those calculated, the best fit giving a deviation of $\pm 5\%$. An additional check on the possibility that extinction is primary is possible for the copper since the particle size may be estimated from the line broadening. Analysis has been carried out by the method suggested by Hall (1949). Values of $\beta \cos \theta / \lambda$ have been plotted against $\sin \theta / \lambda$ and the intercept at $\sin \theta = 0$ gives the breadth β' due to particle size broadening at $\theta = 0$, which can be used to estimate the particle size in the equation $D = 1/\beta'$. The analysis shown in Figure 5 indicates a value β' of 10^5 cm^{-1} and corresponds to a particle size of approximately 10^{-5} cm., a value one-fifth of that estimated from the attempt to match the intensity results to the primary extinction formulae.

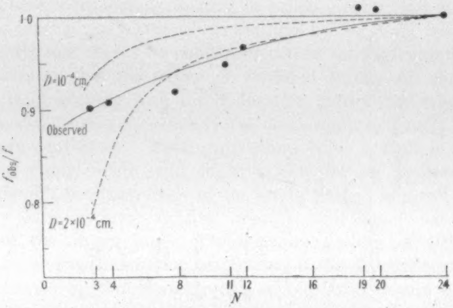

Figure 3. Calculated f_{obs}/f for aluminium assuming primary extinction occurs (dotted lines), and the experimentally observed values.

In view of this divergence from the extinction curves, and the incompatibility of the particle size determinations for copper it is evident that extinction is not primary. The microscopically determined size of the powder grains (i.e. approximately 2μ for the copper and 50μ for the aluminium) are much greater than the particle sizes estimated from extinction and line broadening and hence it must be concluded that the grains have a mosaic structure and will exhibit some secondary extinction.

Accordingly the secondary extinction curves have been calculated from the equation $f_{obs}/f = (1 + kf^2)^{-1/2}$ since ρ in equation (4) is proportional to $|f|^2$ for various values of the constant k. The curves are shown dotted in Figures 6 and 7 for aluminium and copper. The experimentally observed values have been inserted after suitable renormalization. No systematic divergence of the experimentally obtained ratio from the calculated curves $k = 0{\cdot}004$ for aluminium and $k = 0{\cdot}0008$ for copper is apparent, the maximum divergence from the curves corresponding to $\pm 2\%$ in f. The application of a correction for secondary extinction would thus give correct values of the atomic scattering factor within $\pm 2\%$, the experimental error, since this is the maximum deviation from the secondary extinction curve.

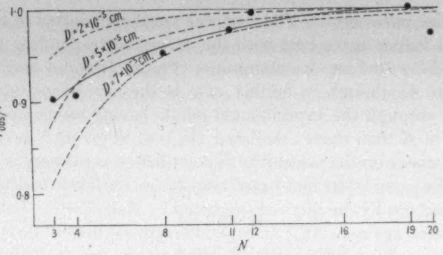

Figure 4. Calculated f_{obs}/f for copper assuming primary extinction occurs (dotted lines), and the experimentally observed values.

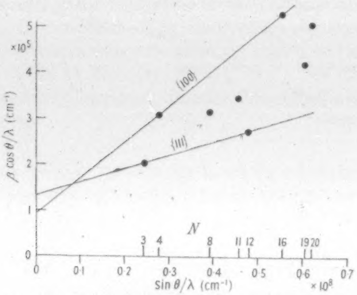

Figure 5. Analysis of the line broadening in copper. β' at $\sin\theta=0$ is approximately 10^5 cm. and the corresponding value of D is 10^{-5} cm.

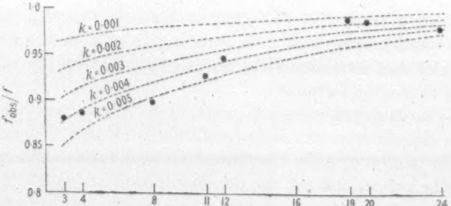

Figure 6. Calculated values of f_{obs}/f for aluminium assuming extinction is secondary. The experimentally determined values fit the curve $k=0·004$ after renormalization.

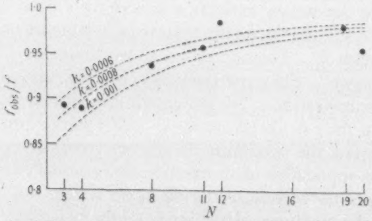

Figure 7. Calculated values of f_{obs}/f for copper assuming extinction is secondary. The experimentally determined values fit the curve $k=0·0008$ after renormalization.

§ 6. CONCLUSIONS

The results quoted above indicate that extinction in filed metals is secondary and that a correction applied to the integrated intensity of the form

$$\rho = \rho_{\text{obs}}(1+2g\rho) = \rho_{\text{obs}}(1-2g\rho_{\text{obs}})^{-1}$$

gives the correct value of the integrated intensity. In addition to the above, the results enable certain conclusions to be drawn as to the state of the annealed aluminium; since the observed line broadening is very small, the distance over which coherent reflection occurs in the aluminium lattice is 10^{-4} cm. or greater. If the lattice were perfect over this distance then appreciable primary extinction would occur as shown in Figure 3. The experimental results have shown that no such extinction is apparent, and hence the lattice must be sufficiently imperfect for the exact phase relationships, leading to primary extinction, to break down, but for the less exact phase relationships required by the Bragg law for reflection to hold. In order that these two conditions can be satisfied simultaneously it is necessary to assume that the lattice of annealed aluminium contains strains. This concept is in keeping with the dislocation theory (for example, Cottrell 1949), which postulates that annealed crystals contain approximately 10^8 dislocation lines per square centimetre. Each dislocation, being a fault in the lattice, is surrounded by strain fields, and these would prevent appreciable primary extinction, although the magnitude of the strain field is so small that it would result in very little increase in line breadth, and hence hardly affect the applicability of the Bragg law. A dislocation density of 10^8 lines/cm^2 is equivalent to an average separation of 10^{-4} cm. if the dislocations are randomly distributed, and the bending introduced into the lattice would be sufficient to prevent coherent reflection over much greater distances than 10^{-4} cm. It has been recently suggested by Frank (1949), and demonstrated by Dawson and Vand (1951), that crystal growth is impossible in the absence of dislocations, and it is probable that they will be present in all crystals, and certainly in metals. It seems that all crystals will thus behave as mosaic crystals, although if the dislocations take up an ordered arrangement the strain-free regions may become sufficiently large for some primary extinction to occur. Primary extinction however will be extremely unlikely in powdered specimens which have been prepared by crushing or filing, since both these processes increase the number of dislocations and will reduce any primary extinction to negligible proportions, and it may be concluded that, for powdered specimens at least, the extinction correction is secondary.

ACKNOWLEDGMENTS

It is a pleasure to acknowledge the encouragement given to us by Professor D. Hanson, Director of the Department of Metallurgy. Generous financial assistance has been received from the Department of Scientific and Industrial Research and this paper is published with the permission of the Director of the National Physical Laboratory.

REFERENCES

Alexander, L., Klug, H. P., and Kummer, E., 1948, *J. Appl. Phys.*, **19**, 742.
Arndt, U. W., 1949, *J. Sci. Instrum.*, **26**, 45.
Averbach, B. L., and Warren, B. E., 1949, *J. Appl. Phys.*, **20**, 1066.
Bragg, W. L., 1914, *Phil. Mag.*, **27**, 881.
Bragg, W. L., Darwin, C. G., and James, R. W., 1926, *Phil. Mag.*, **1**, 897.
Bragg, W. L., James, R. W., and Bosanquet, C. H., 1921, *Phil. Mag.*, **42**, 1.

Bragg, W. L., and West, J., 1928, *Z. Kristallogr.*, **69**, 118.
Brindley, G. W., 1936, *Phil. Mag.*, **21**, 778; 1940, *Proc. Phys. Soc.*, **52**, 117.
Cooke-Yarborough, E. H., Floriden, C. D., and Davey, C. N., 1949, *J. Sci. Instrum.*, **26**, 124.
Cottrell, A. H., 1949, *Progress in Metal Physics*, ed. B. Chalmers (London : Butterworth's Scientific Publications), p. 104.
Daniels, V., and Lipson, H., 1944, *Proc. Roy. Soc.* A, **182**, 376.
Darwin, C. G., 1922, *Phil. Mag.*, **43**, 800.
Dawson, I. M., and Vand, V., 1951, *Nature, Lond.*, **167**, 476.
Frank, F. C., 1949, *Discussions of the Faraday Society*, No. 5, 48.
Hall, W. H., 1949, *Proc. Phys. Soc.* A, **62**, 74.
Hall, W. H., Arndt, U. W., and Smith, R. A., 1949, *Proc. Phys. Soc.* A, **62**, 631.
Hall, W. H., and Williamson, G. K., 1951, *J. Sci. Instrum.*, in the press.
Westcott, C. H., 1948, *Proc. Roy. Soc.* A, **194**, 522.

The Diffraction Pattern of Cold Worked Metals: II Changes in Integrated Intensity

By W. H. HALL and G. K. WILLIAMSON
Department of Metallurgy, University of Birmingham

MS. received 19*th October* 1950, *and in revised form* 14*th June* 1951

ABSTRACT. Measurements have been made, using a Geiger counter spectrometer, of the changes produced by cold work on the integrated intensities in the Debye–Scherrer spectrum of aluminium. It is shown that cold work reduces the integrated intensity of all reflections, this decrease being exactly compensated by a rise in the diffuse background scatter, so that the total reflected intensity is unchanged. These results are at variance with those of previous workers, but the discrepancy can be readily explained by the absence of a correction for extinction in previous work. Brief reference is made to measurements of line width and it is shown that the results support the dislocation theory of plastic deformation.

§1. INTRODUCTION

The effect of cold work on the intensity of diffracted x-rays has attracted considerable attention since a decrease in intensity after cold work was first reported by Hengstenberg and Mark (1930, 1931) who studied molybdenum, tantalum, wolfram, duralumin and potassium chloride. An ionization chamber spectrometer with a wide entrance slit was used and an accuracy of within 1% in the measurement of the integrated intensities was claimed. The intensities of the high angle lines were observed to decrease progressively with increasing Bragg angle, and by analogy with the temperature effect the authors suggested that the decrease was due to an effectively random displacement of the atoms from their mean lattice positions, which they described as a ' frozen heat motion '.

Further work by Brindley and Spiers (1935 a, b) on copper, nickel and a copper–beryllium alloy, by Boas (1937) on gold, by Brill (1937) on iron and by Brindley and Ridley (1938) on rhodium confirmed the results of Hengstenberg and Mark. An exact interpretation was difficult because of the rather large experimental error inherent in the film methods used, and the uncertainty of the correction for extinction; but calculations of the latent energy of lattice distortion made by Boas (1937) and by Haworth (1937) agreed in order of magnitude with the values observed calorimetrically by Taylor and Quinney (1934, 1937).

Recent measurements by Averbach and Warren (1949) on the 400 reflection from α-brass using a Geiger counter spectrometer showed that after cold working the lines developed long diffuse tails, but that at sufficiently great distances from a peak the background level coincided with that of an annealed specimen. They found the integrated intensity above this level to be unchanged by cold work. Large changes in the intensity of the low angle lines were ascribed to variations in primary extinction, the effect of which on the 400 reflection would be inappreciable. Measurements at higher Bragg angles, where any frozen heat motion effect would be greater, do not appear to have been made.

Work by Guinier (1939) had shown that deformation produces a significant rise in the general background level, and since the theory of x-ray diffraction suggests that there should be no change in the total scattered energy, this result appears to be incompatible with that of Averbach and Warren. Their result, however, is dependent on the assumption that any extinction is primary and would thus not vary for the 400 reflection. If extinction is secondary, as suggested by Hall and Williamson (1951), their published data show that a correction of about 7% would need to be applied. Measurements of the changes in line breadth have not, in general, been made simultaneously with measurements of integrated intensity, and thus the present-day theories of these two effects are not closely related. Brindley and Ridley (1939) suggested that a correlation was necessary and found that for copper, nickel and rhodium both effects increased progressively with the hardness of the metal studied.

In the present study measurements of sharp peak intensity, background intensity and line breadths have been made simultaneously with improved accuracy by means of a Geiger counter spectrometer. To simplify the interpretation of line breadth and intensity changes aluminium has been chosen for study, because it is elastically isotropic and exhibits a relatively small extinction effect.

§ 2. EXPERIMENTAL PROCEDURE

Measurements have been made with a Geiger counter spectrometer using monochromatic copper Kα radiation, the experimental details having been described previously (Hall and Williamson 1951). Continuous monitoring of the x-ray output was used to compensate for any random fluctuations, the observation periods being adjusted to approximately one minute. Since several days were required to record each complete spectrum, the long-term reliability of the monitoring equipment was checked at frequent intervals by scanning the peak of the 311 reflection from the annealed copper block containing the specimen. A correction for monitoring drift has been applied to the results where necessary, although this correction never exceeded 2%.

Specimens were prepared by hand filing two samples of aluminium, one more than 99·99% pure, supplied by the British Aluminium Co. Ltd., and the other of normal commercial purity (about 99·7% aluminium). The filings were passed through a 350 mesh/inch sieve and annealed powders were prepared by heating *in vacuo* at 500° c. for 20 minutes. The specimens were finally made by filling a circular cavity 2·5 cm. in diameter and $\frac{1}{2}$ mm. deep in the copper reference specimen with filings which were then moistened with a standard volume (approximately $\frac{1}{4}$ cm^3) of a 5% solution of Canada balsam in xylol) and pressed into position with a glass plate. This method of preparation was very carefully controlled in order that comparative measurements of background level could be made, and the specimen chamber was evacuated to eliminate air scattering.

§ 3. THE DIFFRACTION PATTERN OF COLD WORKED ALUMINIUM

Preliminary experiments showed that the intensities, line breadths and background of the annealed specimens of both the commercial and the high purity aluminium were identical. For this reason only the high purity material was examined in detail in the annealed condition, but measurements were made on specimens of both purities in the filed condition. In all cases the background was examined over the whole range of angles from $\chi = 24°$ ($\theta = 12°$), the lower limit at which the specimen completely filled the beam aperture, to $\chi = 155°$, above which the effects of the tails of the combined 333 and 511 reflections became appreciable. This line was not recorded since it was impossible to include the whole of the tail on the high-angle side. The angular interval between measurements of the background level was normally 10′ in χ, except for a few regions remote from the lines where it was increased to 15′ or very near to the lines where measurements were made at smaller intervals. Frequent observations of the counter background were made with a lead stop in the monochromatic beam, all other experimental conditions remaining unaltered. The counter background remained constant at 55 counts during the experiment and has been subtracted from the observed intensity ordinates.

The resultant x-ray background curves are shown in Figure 1, plotted on an extended intensity scale and a compressed angular scale to accentuate any small changes in level. The effect of cold work is to broaden the bases of the lines and to increase the extent of the tails, especially at high angles. The asymmetry of the bases of the high angle lines from the annealed powder was caused by the α_3 component in the incident beam: after cold working this component tended to be masked by the increase in the tails. The general background levels from both the cold worked specimens were the same, but that from the annealed material was about 15 counts lower, as shown by the dotted line (Figure 1). This very small difference (the peak of the 111 reflection is approximately 20,000 counts) corresponds to 7% of the total integrated intensity of reflection since it extended over a very large angular range. The significance of this result in relation to the measurements of integrated intensity and line width is discussed later.

When estimating integrated intensities difficulty was experienced in defining the range of integration to be used. In previous experiments the measured integrated intensity corresponded to f_T, the atomic scattering factor corrected for thermal vibrations of the atoms in the lattice. The effect of these vibrations is to divert a fraction of the x-ray energy into the background as thermal diffuse scatter, which was detected in the present experiments and is visible, at least in part, as long tails to the lines in Figure 1. If the background in Figure 1 could be resolved completely into the thermal diffuse scatter components for each reflection, then the integrated intensities including this component would lead to values of f, the atomic scattering factor uncorrected for thermal vibrations. Features such as the high background between the 222 and 311 reflections and the low level in the neighbourhood of the weak 400 reflection make it obvious that the diffuse tails extend considerably further than is suggested by a cursory examination. Thus any attempt to draw a smooth curve through the minima of Figure 1 would lead to the exclusion of part of the tails and the integrated intensities above such a curve would correspond to an apparent atomic scattering factor between f_T and f.

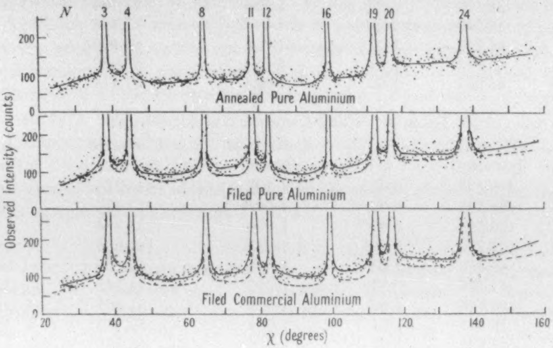

Figure 1. The variation in the background level of aluminium with cold work (filing). The dotted line in the lower graphs is the annealed aluminium background level.

To resolve this difficulty the integrated sharp peak intensity of each line was measured separately, but the diffuse background was integrated for the whole spectrum. The values of the background level used in the integration of the sharp peak intensity were determined in two stages. First the lines were plotted on the more usual intensity scale in which the tails of the lines were not apparent, as in Figure 2, the angular extent of the line being determined by inspection. The corresponding background level could then be found by reference to Figure 1. The ranges of integration were listed and compared, small alterations in level being made in order to achieve a smooth variation of the range of integration with Bragg angle and to ensure that a constant fraction of each line was included. The resultant sharp peak intensities (counts × minutes of arc) were found using Simpson's rule for numerical summation and are listed in Tables 1, 2 and 3. The ratios of the observed and calculated scattering factors f_{obs}/f_T are normalized on the value for the 331 reflection.

Table 1. Annealed Pure Aluminium

Line	Observed Intensity	$\frac{f_{obs}}{f_T}$	Correction Factor	Corrected Intensity	Laue Breadth
3	363,370	0·90	1·330	483,282	14·0
4	182,340	0·92	1·294	235,948	13·2
8	117,030	0·95	1·203	940,789	13·15
11	127,770	0·96	1·156	147,702	13·68
12	38,740	0·99	1·144	44,319	13·73
16	18,900	1·01	1·107	20,809	13·79
19	61,740	1.00	1·079	66,617	14·71
20	61,280	1·01	1·072	65,692	15·21
24	67,910	1·01	1·054	71,577	18·21

Table 2. Filed Pure Aluminium

Line	Observed Intensity	$\frac{f_{obs}}{f_T}$	Correction Factor	Corrected Intensity	Laue Breadth
3	392,641	0·94	1·149	451,145	14·55
4	190,473	0·94	1·133	215,806	13·57
8	126,645	1·00	1·091	138,169	14·64
11	124,623	0·95	1·070	133,347	14·47
12	38,670	0·99	1·064	41,184	14·76
16	16,740	0·96	1·045	17,493	14·84
19	61,262	1·00	1·035	63,406	16·81
20	60,912	1·01	1·033	62,922	17·70
24	66,015	1·00	1·024	67,534	21·63

Table 3. Filed Commercial Aluminium

Line	Observed Intensity	$\frac{f_{obs}}{f_T}$	Correction Factor	Corrected Intensity	Laue Breadth
3	410,122	0·97	1·105	453,185	16·55
4	198,378	0·97	1·094	217,026	16·32
8	123,315	0·99	1·066	131,454	17·01
11	133,730	0·99	1·052	140,684	18·42
12	40,256	1·02	1·046	42,108	18·69
16	17,566	0·99	1·033	18,145	22·67
19	60,044	1·00	1·026	61,605	23·71
20	58,471	1·01	1·025	59,932	26·48
24	67,578	1·02	1·018	68,795	35·69

The ratios of observed to calculated values of the atomic scattering factor f_{obs}/f_T suggest that extinction occurred in all the specimens, and this was shown to be entirely secondary, in agreement with previous results (Hall and Williamson 1951). The magnitude of the extinction effect was estimated by the

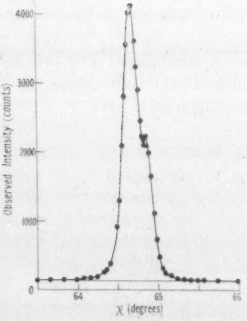

Figure 2. Annealed aluminium line 8 plotted on the normal intensity scale.

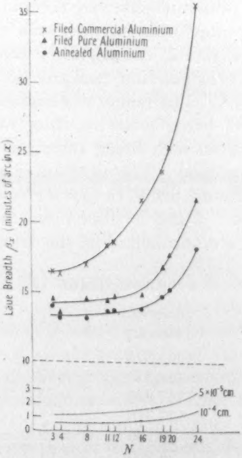

Figure 3. Line breadths in the three specimens. The lower curves are the calculated breadths for two assumed particle sizes.

procedure previously described and the appropriate correction factors are listed in the Tables together with the corrected intensities. The Tables show that the extinction effect entirely masks the effect of cold work, which is to reduce the intensity of all lines. No systematic variation of this reduction with Bragg angle was apparent, the reduction having a mean value of 7%. This result is of great interest and is at variance with the results of previous workers, but the anomaly can be explained in terms of extinction. It has already been shown that the result of Averbach and Warren agrees with this interpretation after appropriate correction for secondary extinction. Similarly a close approximation to the frozen heat motion effect may be obtained if extinction is neglected, and the lowest angle lines of all the spectra are assumed to have equal intensity, as assumed by earlier workers. All the results in the present work, however, are relative to a standard intensity and show that their assumptions are not justifiable.

The total corrected integrated intensities of the lines from the two cold worked specimens are equal within 0·2% and are about 7% lower than that from the annealed specimen, as shown in Table 4.

Table 4

Spectrum	Sharp Peak Intensity Observed	Sharp Peak Intensity Corrected	Integrated Background	Total Reflected Intensity
Pure annealed	1,039,080	1,276,733	877,500	2,154,200
Pure filed	1,077,973	1,191,006	994,500	2,185,500
Commercial filed	1,109,460	1,192,933	994,500	2,187,500

The thermal diffuse scatter corresponding to these intensities is about 250,000 counts × minutes of arc, which is equivalent to an average intensity ordinate of about 30 counts over the whole range of angles. Thus the errors introduced into estimations of f by drawing a smooth background curve through the minima of Figure 1 would have been large. The thermal scatter accounts for only one-third of the observed x-ray background and it is not possible to account quantitatively for the remainder, much of which is Compton scatter. Since this should be constant for all three spectra, a comparison between the total diffracted intensities may legitimately be made by adding the observed integrated background intensity to the total corrected line intensity. From the last column of Table 4 it is seen that there was no appreciable difference in the total intensity diffracted by the annealed and cold worked specimens.

The Laue breadths of the reflections, calculated from the observed line intensities and the α_1 and α_2 peaks found by graphical resolution, are plotted in Figure 3. The breadths from the high purity specimens are much smaller than those from the commercially pure specimen, and this difference is due to the partial recovery (or relief of part of the lattice strain) of the high purity sample. Subsidiary experiments showed that no measurable change in breadth took place during the period of the investigation, the recovery having occurred at the relatively high temperature obtained during filing.

§ 4. DISCUSSION

The results obtained in this investigation have confirmed the increase in background level observed by Guinier. The rise in the background integrated intensity is exactly compensated by a decrease in the total intensity of the sharp peaks, the total diffracted intensity being constant to within 1%. No systematic variation of the integrated intensity of the lines with Bragg angle was apparent, and it is suggested that the ' frozen heat motion ' effects previously reported are a consequence of differential effects of secondary extinction on the diffraction pattern of annealed and cold worked metals.

Comparison of the line broadening and diffuse scattering measurements reveals an important result. Although the line breadths of the cold worked pure aluminium were very little greater than the annealed breadths, the increase in background level was fully as great as that for the specimen of commercial purity, which exhibited much greater broadening. The similarity of the backgrounds of the two cold worked specimens indicates that the amounts of very high strain were similar in both specimens although the less severe long range strains responsible for the line broadening were profoundly different. The continued existence of the most severely distorted regions is difficult to understand unless lattice defects such as dislocations are assumed to be responsible for the diffraction effects. The diffuse scattering must then be attributed largely to the heavy localized distortions near the dislocation lines, and the background measurements indicate that the total numbers of dislocations in the two cold worked specimens were approximately equal. Dislocation theory regards recovery as the migration and rearrangement of dislocations produced during deformation to form arrays of lower strain energy. Such migration is assisted by a rise in temperature and resisted by impurities, which form stable 'atmospheres' round the dislocation and impede their movement (Cottrell 1948, Cottrell and Bilby 1948, Cottrell and Jaswon 1949). The experimental observations are thus fully explained if the numbers of dislocations initially produced by filing were the same, but redistribution to form a more stable arrangement only occurred in the high purity aluminium, recovery in the commercial aluminium being retarded by the impurities present. A further point of interest is the rapid increase in the breadths of the high angle lines of the annealed specimens which could not be attributed to experimental broadening. The broadening caused by particles of sizes 10^{-4} cm. and 5×10^{-5} cm. is shown in Figure 3. The more rapid rise of the experimental curve indicates the presence of internal stresses in the annealed material, as has already been deduced from extinction results. This result which would be expected if dislocations were present is confirmed by Fourier analysis of the line shapes, but exact details will be described in a later paper. Further measurements of line broadening and diffuse scattering from wolfram confirm these results quantitatively. Other evidence leading to the conclusion that dislocations produce the observed effects has been reported by Greenough and Smith (1950) and by Wilson (1949, 1950) who has shown that dislocation strain fields may cause line broadening.

The evidence at present available strongly supports the suggestion that dislocations are responsible for the diffraction effects observed, and it seems difficult to postulate any other radically different type of lattice defect which could explain both the short range and long range strains necessitated by the diffraction effects as reasonably as the dislocation model.

ACKNOWLEDGMENTS

It is a pleasure to acknowledge the encouragement given to us by Professor D. Hanson, Director of the Department of Metallurgy. Generous financial assistance has been received from the Department of Scientific and Industrial Research, and this paper is published with the permission of the Director of the National Physical Laboratory.

REFERENCES

Averbach, B. L., and Warren, B. E., 1949, *J. Appl. Phys.*, **20**, 1066.
Boas, W., 1937, *Z. Kristallogr.*, **96**, 214.
Brill, R., 1937, *Z. Phys.*, **105**, 378.
Brindley, G. W., and Ridley, P., 1938, *Proc. Phys. Soc.*, **50**, 501; 1939, *Ibid.*, **51**, 432.
Brindley, G. W., and Spiers, F. W., 1935, *Phil. Mag.* (7), **20**, 882, 893.
Cottrell A. H., 1948, *Physical Society Bristol Conference Report*, p. 30.
Cottrell, A. H., and Bilby, B. A., 1948, *Proc. Phys. Soc.* A, **62**, 49.
Cottrell, A. H., and Jaswon, M. A., 1949, *Proc. Roy. Soc.* A, **199**, 104.
Greenough, G. B., and Smith, E. M., 1950, *J. Inst. Metals*, **77**, 435.
Guinier, A., 1939, *C.R. Acad. Sci., Paris*, **208**, 894.
Hall, W. H., and Williamson, G. K., 1951, *Proc. Phys. Soc.* B, **64**, 937.
Haworth, F. E., 1937, *Phys. Rev.*, **52**, 613.
Hengstenberg, H., and Mark, H., 1930, *Z. Phys.*, **61**, 435; 1931, *Z. Elektrochem.*, **37**, 524.
Taylor, G. I., and Quinney, H., 1934, *Proc. Roy. Soc.* A, **143**, 307; 1937, *Ibid.*, A, **163**, 157.
Wilson, A. J. C., 1949, *Research*, **2**, 541; 1950, *Ibid.*, **3**, 387.

Outer Brillouin Zones for Face-Centred and Body-Centred Cubic Lattices

By J. F. NICHOLAS

Division of Tribophysics, Commonwealth Scientific and Industrial Research Organization, Melbourne, Australia

Communicated by N. F. Mott; MS. received 27th June 1951

ABSTRACT. In order to resolve some inconsistencies in the literature on the second Brillouin zones of cubic lattices, the shapes of these zones have been recalculated. The results, together with descriptions of the third and fourth zones, are given.

§ 1. INTRODUCTION

For most lattice types the shape of the first Brillouin zone is well known (e.g. Mott and Jones 1936), but the outer zones have rarely been considered. Further, for the face-centred cubic and body-centred cubic lattices, the literature on the shapes of the second zones (Seitz 1940, Brillouin 1946, Berry, Waldron and Raynor 1950) is contradictory and hence it was thought desirable to recalculate the shapes of these zones. In structures having many electrons per atom, the electrons may overlap into the third and fourth zones, and these are also described below.

The boundaries of a Brillouin zone are planes of energy discontinuity in k-space, **k** being the wave-number vector of any wave that is propagating in the lattice. The energy is discontinuous at a point in k-space where the wave (whether an electron wave or an x-ray) associated with this value of **k** would suffer a Bragg reflection. Hence, the planes of energy discontinuity correspond to the Bragg reflections which are characteristic of the lattice considered. Then, the plane of discontinuity in k-space corresponding to a $n_1n_2n_3$ Bragg reflection is normal to the $[n_1n_2n_3]$ direction (in k-space) and its distance from the origin is equal to one half of the reciprocal of the spacing between $(n_1n_2n_3)$ planes in real space. Thus, for a cubic crystal with lattice parameter a, we have a set of planes in k-space with the equations

$$n_1k_x+n_2k_y+n_3k_z=(n_1^2+n_2^2+n_3^2)/2a,$$

where the n_1, n_2 and n_3 can be interchanged to correspond to each system of parallel reflecting planes of the $\{n_1n_2n_3\}$ set in real space; k_x, k_y and k_z are the components of $\mathbf{k}$. Further the magnitude of the discontinuity across any plane is directly dependent on the structure factor for the corresponding reflection (this factor is a function of wavelength but not of the type of wave) (Jones 1934), so that the discontinuity vanishes if the structure factor is zero.

Thus, these planes mark out closed polyhedra centred on the origin and the first zone is the volume inside the first of these. The second zone is then the volume between the outer boundary of the first zone and the next polyhedron, and so on. Furthermore, it can be shown (Seitz 1940) that all zones have the same volume in *k*-space.

§ 2. FACE-CENTRED CUBIC LATTICE

The shapes of the first four zones are shown in Figure 1 (*a*)–(*d*), the bounding planes corresponding to the reflections 111, 200 and 220 only. These planes in *k*-space are

$$k_x + k_y + k_z = 3/2a, \qquad \ldots\ldots(1)$$

$$k_x = 2/2a, \qquad \ldots\ldots(2)$$

$$k_x + k_y = 4/2a, \qquad \ldots\ldots(3)$$

with due allowance for interchanges of axes and of signs. Then the first zone is the well-known truncated octahedron bounded by planes of types (1) and (2), while the outer boundary of the second zone is as given by Seitz (1940), being bounded by simple extensions of the planes defining the first zone. The

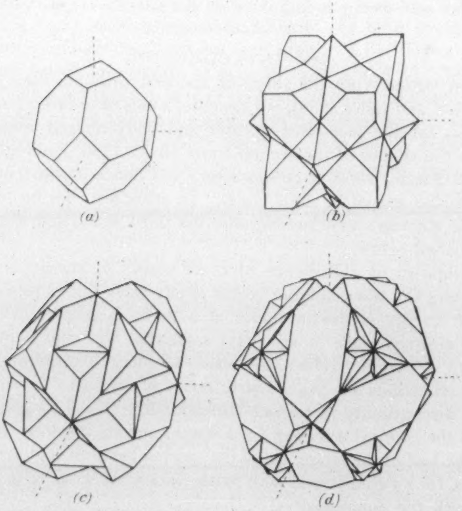

Figure 1. Outer boundaries of the Brillouin zones for a face-centred cubic lattice: (*a*) first zone, (*b*) second zone, (*c*) third zone, (*d*) fourth zone.

modification of the second zone suggested by Berry *et al.* (1950) to allow for {311} planes is incorrect as it can easily be shown that planes of the type

$$3k_x+k_y+k_z=11/2a \qquad \ldots\ldots(4)$$

are completely external to the second zone. Further, this modified second zone does not satisfy the condition that all zones have the same volume.

For the definition of the third zone we have to introduce planes of type (3), and, for that of the fourth zone, extensions of these three sets of planes are sufficient, as planes of type (4) are still external to the zone although they have some lines in common with the outer boundary.

Each zone has a volume of $4/a^3$ and can thus accommodate two electrons per atom, while the volumes of the inscribed spheres are $2{\cdot}72/a^3$, $5{\cdot}00/a^3$, $5{\cdot}85/a^3$ and $11{\cdot}85/a^3$ respectively corresponding to 1·36, 2·50, 2·93 and 5·92 electrons per atom. However, when there are more than 1·36 electrons per atom, the Fermi surface will be far from spherical, its actual shape depending on the magnitudes of the energy discontinuities at the zone boundaries; these discontinuities are a property of the particular substance considered. The calculations of Matyas (1948) and Leigh (1951) show that the energy discontinuities in aluminium are large enough to keep the Fermi surface within the second zone, though it can be seen from the above figures that for very small energy barriers the third electron could overlap into the third zone.

§ 3. BODY-CENTRED CUBIC LATTICE

The shapes of the first four zones are shown in Figure 2 (*a*)–(*d*), the bounding planes corresponding to the reflections 110, 200 and 211. These planes are of the form

$$k_x+k_y=2/2a, \qquad \ldots\ldots(5)$$

$$k_x=2/2a, \qquad \ldots\ldots(6)$$

$$2k_x+k_y+k_z=6/2a. \qquad \ldots\ldots(7)$$

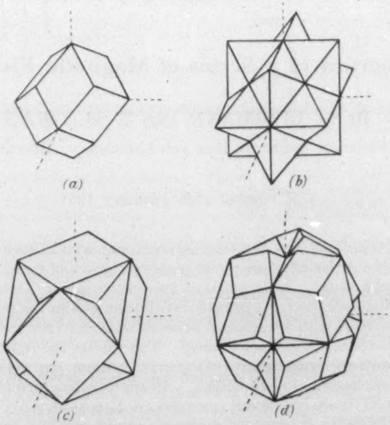

Figure 2. Outer boundaries of the Brillouin zones for a body-centred cubic lattice: (*a*) first zone, (*b*) second zone, (*c*) third zone, (*d*) fourth zone.

Thus, the first zone is the dodecahedron bounded by planes of type (5) and the second zone is formed by extensions of these planes. This should be compared with the second zone described by Seitz and Brillouin who use planes of type (1) as boundaries despite the fact that the structure factor for a 111 reflection is zero in a body-centred lattice and hence the energy is not discontinuous across such planes. Again, the second zone described by Berry *et al.* (1950) has a volume two and a half times that of the first zone and hence does not satisfy the equality of volume condition. The third zone is then bounded by further extensions of these planes together with contributions from type (6) planes, while the outer boundary of the fourth zone consists of planes of types (5) and (7) only.

In this case, each zone has a volume of $2/a^3$, which again corresponds to two electrons per atom, while the volumes of inscribed spheres correspond to 1·48, 2·72, 2·72 and 4·19 electrons per atom respectively. Here, we see that for very small energy discontinuities we would expect a third electron to overlap into the fourth zone, but, in practice, the energy barriers will almost certainly be large enough to prevent this and will usually prevent overlap into even the third zone.

REFERENCES

BERRY, R. L., WALDRON, M. B., and RAYNOR, G. V., 1950, *Research*, **3,** 195.

BRILLOUIN, L., 1946, *Wave Propagation in Periodic Structures* (London and New York: McGraw-Hill), pp. 152–154.

JONES, H., 1934, *Proc. Roy. Soc.* A, **144,** 225.

LEIGH, R. S., 1951, *Phil. Mag.*, **42,** 139.

MATYAS, Z., 1948, *Phil. Mag.*, **39,** 429.

MOTT, N. F., and JONES, H., 1936, *The Theory of the Properties of Metals and Alloys* (Oxford: University Press), pp. 156 ff.

SEITZ, F., 1940, *The Modern Theory of Solids* (London and New York: McGraw-Hill), pp. 298–300.

Imaging Properties of a Series of Magnetic Electron Lenses*

BY G. LIEBMANN AND E. M. GRAD

Associated Electrical Industries Research Laboratory, Aldermaston, Berks.

MS. received 15*th February* 1951

ABSTRACT. The paraxial lens data and the more important first order lens aberrations were determined for a series of symmetrical magnetic lenses of equal lens diameter D but variable air gap width S for a wide range of lens excitations. The range of gap widths covered was $S/D=0{\cdot}2$ to $S/D=2$. The field distribution within the lenses was measured to a high degree of accuracy with a resistance network analogue, and the lens data were then obtained through numerical trajectory tracing. The results are represented as a series of graphs. These results are representative of the most common magnetic electron lenses, and should have useful applications in lens design. An approximate formula for the focal length is $f \simeq 50(DS)^{1/2}V_r/(NI)^2$. A few design examples are discussed.

---

* A shortened paper, giving some of the results of this article, was read before the Congrès International de Microscopie Electronique, held in Paris, 14th–22nd September 1950.

§ 1. INTRODUCTION

THE numerous papers on the imaging properties of magnetic electron lenses* fall broadly into two classes. In one class are those papers which are essentially based on measurements, or at least on measured field distributions, and which are therefore more or less closely related to the lenses used in practice. Some of these papers give a good survey of the paraxial imaging properties, but evaluation of the aberrations which limit the use of electron lenses has only been attempted in a few cases. In the other class are the papers by Glaser (1941), Dosse (1941 a) and Ramberg (1942). These authors assumed certain hypothetical field distributions along the axis of the lens (Glaser: $H(z)=H_0/[1+(z/a)^2]$; Ramberg: $H(z)=H_0 \operatorname{sech}^2 bz$). This allows a calculation of the lens properties, including lens aberrations, with a high degree of numerical accuracy, but results are still only approximate because these hypothetical fields are only approximations to the field distributions found in practical lenses.†

The object of this paper is an investigation of the dependence of the paraxial imaging properties of 'real' lenses and of their more important aberrations, on the geometrical design parameters and on the lens excitation. Preliminary investigations indicated that the main geometrical parameter of a symmetrical lens of internal pole diameter $2R=D$ and pole separation S (see Figure 1) is the ratio S/D. Variations of pole shape, as well as the influence of iron saturation, can be essentially expressed as a modification of the diameter D or the separation S, the extent of such modifications depending on the lens excitation and the shape of the (B, H) curve of the iron used for the pole pieces. This will be discussed more fully elsewhere. In this paper the influence of the relative gap length S/D will be studied through the investigation of the four cases, $S/D=0{\cdot}2$, $0{\cdot}6$, 1 and 2, of a symmetrical magnetic lens of the geometry shown in Figure 1; in view of the remarks made above, this series of lenses should be representative of most cases of ordinary magnetic lenses using iron pole pieces.

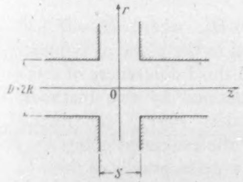

Figure 1. Geometry of investigated lenses.

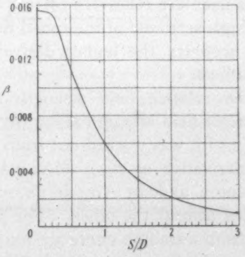

Figure 2. Graph of excitation parameter β as function of relative pole piece gap width S/D. $\beta=k^2V_{\mathrm{r}}/(NI)^2$

The field distribution was measured in each case to a high degree of accuracy on a resistance network analogue described recently by one of the authors

---

* Ruska (1934, 1942, 1944), Becker and Wallraff (1938, 1939, 1940 a, b), von Ardenne (1939, 1941), Glaser (1941), Dosse (1941 a, b, c), Ramberg (1942), Siegbahn (1942), Svartholm (1942), Glaser and Lammel (1943), van Ments and le Poole (1947), and others.

† Glaser's assumed field distribution resembles that found in a magnetic lens under conditions of extreme iron saturation, whereas Ramberg's field corresponds to that of a lens with an indefinitely small pole piece gap.

(Liebmann 1950). The paraxial imaging properties and the main lens aberrations were then computed by an improved ray-tracing method (Liebmann 1949) for these four lenses, as function of the dimensionless excitation parameter* k^2:

$$k^2 = 0{\cdot}022\, H_0^2 R^2 / V_r \qquad \ldots\ldots(1)$$

where $V_r = V(1+10^{-6}V)$ is the relativistically corrected accelerating voltage, and H_0 the maximum axial field strength in gauss, R being measured in centimetres. An alternative form of the excitation parameter k^2 is (in the absence of marked iron saturation):

$$k^2 = 0{\cdot}0087 (H_0/H_p)^2 (S/D)^2 (NI)^2 / V_r = \beta (NI)^2 / V_r. \qquad \ldots\ldots(2)$$

H_p is defined in §2, NI is the number of ampere turns exciting the lens, and the constant β is a function of the relative gap length $\boldsymbol{S}/D$. From the results of the field measurements, given in the next section, one can construct the graph, Figure 2, giving the constant β as a function of S/D.

§ 2. MEASUREMENT OF FIELD DISTRIBUTION

In measuring the field distributions with the resistance network analogue, first a small scale model was set up in each case to ascertain, and correct for, the influence of the network boundary. The final model was set up on such a scale that the lens radius $R=10$ mesh units. The pole piece surfaces were assumed to be equipotentials of M.M.F., and a unit potential difference was applied between them; the potential values $\phi(r,z)$ were recorded to five decimal places. The measured values were then checked by calculating their residuals, and local errors were eliminated by 'relaxation' of the larger residuals. The final potential values used are relatively correct to within better than 2 parts in 10,000. This very high accuracy of the initial field plot is necessary to obtain with sufficiently good accuracy the higher derivatives needed in the computation of the lens aberrations.

The relative field strength $h(z) = H(0,z)/H_0$, where $H_0 = H(0,0)$ is the maximum field strength along the axis, reached in the plane of symmetry of the lens ($z=0$), was worked out from the first and third differences of $\phi(0,z)$. The first derivative of $h(z)$, $dh/dz = h'(z)$, was obtained by two methods, i.e. by differences and by Gundert's method (Gundert 1941), each method being checked against the other. The deviations of the evaluated points for $h(z)$ and $h'(z)$ from a smooth curve are too small to show up in graphs of these functions. The second derivative of $h(z)$, $h''(z) = \phi'''(0,z)/\phi'(0,0)$, was found by differencing the tabulated $h'(z)$ values. A typical plot of points found in this way is shown in Figure 3, relating to the case $S/D=1$. These points, marked by circles, lie on a smooth curve except near the positive maximum where they scatter slightly. Here the values from the averaged curve, representing 'smoothed' values, were used in the computations of the lens aberrations.

With a model of such size that $R=10$ mesh units there is still a small systematic error in plotting the axial field distribution; this is due to the influence of the sharp corners of the model at $r=10$, $z=\pm S/2$. This error can be eliminated by taking field plots for models of such sizes that $R=5$ and 10 mesh units and then extrapolating in the manner previously discussed (see Liebmann 1950). This extrapolation gives a field distribution equivalent to a model size where $R \geqslant 20$ mesh units; this was carried out for the case $S/D = 1$. The effect of the mesh size error on the field values is greater for higher order derivatives, and can be demonstrated in plots of $h''(z)$. The extrapolated values of h'' are shown in Figure 3 by crosses. By carrying out complete computations of the focal length and spherical aberration constant in the case $S/D = 1$, it was shown that the influence of the mesh size error for the model sizes used ($R = 10$ mesh units), is negligible in the final result of the lens computations, being smaller than the computational errors in the evaluation of the lens constants.

---

* The excitation parameter k^2 used here differs from that used by Glaser and others through the replacement of the 'half-width' a by the lens radius R, which is a readily available geometrical constant of each lens.

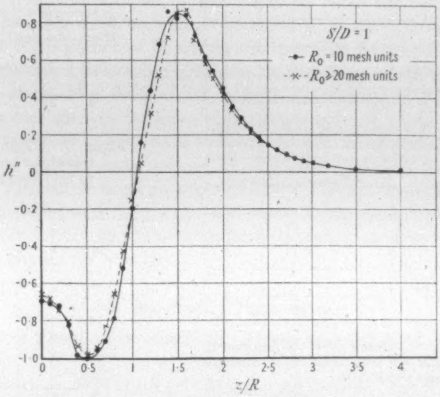

Figure 3. Plot of h'' as function of z/R, showing extent of numerical and mesh size errors ($S/D = 1$).

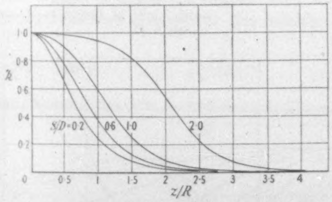

Figure 4. Graph of h as function of z/R for four lenses with different gap width S/D.

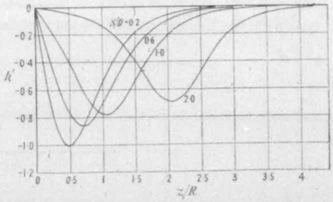

Figure 5. Graph of h' as function of z/R for four lenses with different gap width S/D.

Graphs of $h(z)$, $h'(z)$ and $h''(z)$, all on the same scale, are given for the various lenses in Figures 4, 5 and 6. Only the branches of the curves for $z \geqslant 0$ are shown, as $h(z)$ and $h''(z)$ are symmetrical about the origin, whereas $h'(z)$ is antisymmetrical. All these functions approach the z axis exponentially, and the ratios h'/h and h''/h, used in aberration calculations, approach constant values for sufficiently large values of z.

By writing the field at points at some distance r from the axis in terms of the derivatives of the axial field strength, as known, one can see that the field terms giving rise to geometrical aberrations higher than the third order become of influence only for values of r/R equal to or greater than 0·3 to 0·4; i.e. up to these off-axis distances only third-order aberrations need be considered.

The relationship between H_0, the maximum field along the axis, and H_p, the field strength in the parallel part of the field in the gap between the pole pieces at a great distance from the axis, is given in Figure 7, where the ratio H_0/H_p is plotted as function of S/D. In the absence of marked iron saturation, $H_p = 4\pi NI/10S$.

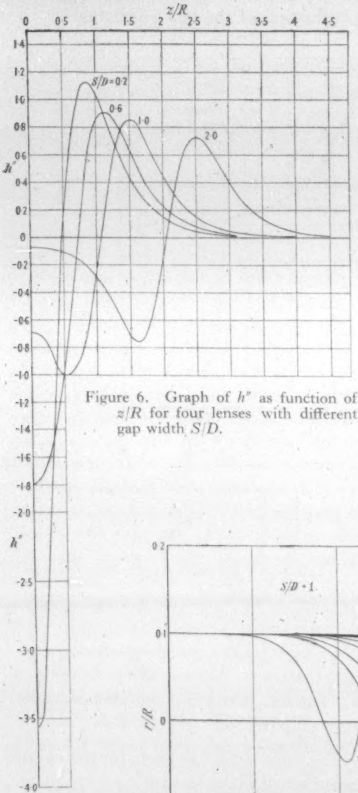

Figure 6. Graph of h'' as function of z/R for four lenses with different gap width S/D.

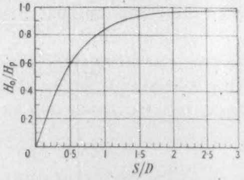

Figure 7. Graph of ratio H_0/H_p of maximum axial field strength H_0 to field strength H_p in air gap.

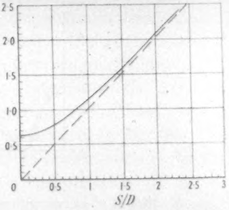

Figure 8. Graph of relative 'half width' a/R as function of gap width S/D.

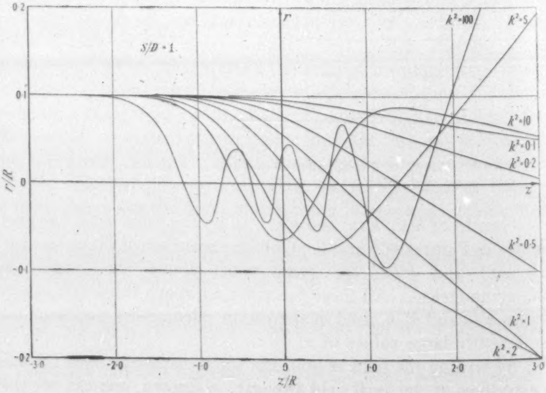

Figure 9. Electron trajectories through lens $S/D=1$, for several values of excitation parameter k^2.

Figure 8 gives a graph of a/R as function of S/D, where a is the 'half width' parameter used by some authors, i.e. the z value for which $h(z)$ has fallen to $h(z)=0{\cdot}5$. For large values of S/D, a/R approaches S/D asymptotically.

§ 3. PARAXIAL IMAGING PROPERTIES OF LENS $S=D$

(i) *Trajectories*

A range of (paraxial) trajectories, approaching the lens parallel to the optical axis, is shown in Figure 9. The ordinate is the off-axis distance in a cylindrical coordinate system rotating about the axis with the electron which is moving through the lens field; the ordinate scale is enlarged ten times compared with the abscissa scale. The intersection of the trajectory with the optical axis (the 'focus') moves towards the lens with an increase in the excitation parameter k^2. For $k^2 \simeq 0{\cdot}2$, the focus comes to lie within the lens field, but the field is still too weak there to exercise a detectable influence on the shape of the trajectory; the focusing action of the lens field which extends to the right of the intersection of the trajectory with the axis becomes noticeable only for $k^2 > 0{\cdot}5$. For stronger excitation, the trajectory is bent back towards the axis after passing through the intersection point with the axis, and for $k^2=2{\cdot}85$ the ray leaves the lens parallel to the axis, but rotated through an angle of 230°. For still stronger excitations, first two intersections, and then more and more intermediate foci are formed. Typical of this oscillatory appearance of the trajectory at very strong excitations is the trajectory shown for $k^2=100$.

(ii) *Rotation of Trajectories*

The rotation of the plane in which the electron moves is given by

$$\Psi(z)=k\int_{-\infty}^{z} h(z)dz=kI(z). \qquad \ldots\ldots(3)$$

The function $I(z)$ from which $h(z)$ was derived is identical with the original function $\phi(0,z)$ except for the multiplication factor $1/\phi'(0,0)$. The resulting total rotation Ψ_1 for the trajectory leaving the lens and the rotation Ψ_0 of the trajectory up to the first focus is given in Figure 10 as a function of k^2. The trajectory will be rotated through the angle $\Psi_1=\pi$ for $k^2=1{\cdot}72$ and $\Psi_1=2\pi$ for $k^2=6{\cdot}85$.

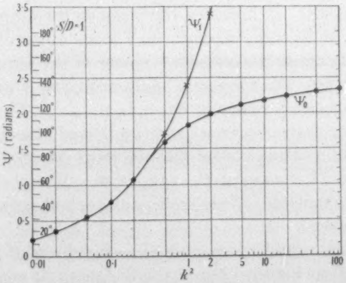

Figure 10. Image rotation for lens $S/D=1$ as function of the excitation parameter k^2. Ψ_0: rotation up to first focus; Ψ_1: rotation when whole length of lens field is used.

(iii) *Cardinal Points*

The paraxial imaging properties of a lens are conveniently described by the positions of the cardinal points, i.e. the foci and the intersections of the principal planes with the axis. In view of the symmetry of the lenses considered here the position of one principal plane and one focus is sufficient, as long as the lens excitation is small enough to keep the focus outside the effective lens field (i.e. $k^2 \leqslant 0{\cdot}5$ for this particular lens). The intersection distance of the focus from the origin (centre of lens) will be denoted by z_f, and the distance of the principal plane by p. The paraxial focal length f is then

$$f = z_f - p. \qquad \ldots\ldots(4)$$

The lens parameters were calculated for several object distances z_a for $k^2 = 0{\cdot}2$, the image distance from the origin being called z_b, to confirm that the lens parameters are truly constant for weak and moderately strong excitations, i.e. that the usual 'lens formula' applies. The result is given in Table 1.

Table 1

z_a/R	$-\infty$	-20	-10
z_b/R	$3{\cdot}172_1$	$3{\cdot}800_8$	$4{\cdot}721_8$
p/R	$0{\cdot}080_7$	$0{\cdot}081_0$	$0{\cdot}080_8$
f/R	$3{\cdot}252_8$	$3{\cdot}253_0$	$3{\cdot}252_9$

It is seen that the focal length and distance of the principal planes from the lens centre are constant within computing accuracy*; we also have here a check of the accuracy of the numerical work.

If the lens excitation is strong ($k^2 \geqslant 0{\cdot}5$ in the present case), we have to distinguish between the case where object and image are both located outside the lens field, and the case where either the object or the image become immersed in the lens field. In the first case, the entire lens field is always used in the image formation, and the lens properties can still be described by the lens formula, using a unique set of cardinal points. The electron microscope projector lens and the focusing lens of the magnetically focused cathode-ray tube belong to this type. The focal length of the lens used in this way will be called f_1, and its virtual focal distance z_1. If, however, the image or the object become immersed in the focusing field, as in many electron microcope objectives, the extent of the lens field used and therefore the refracting power of the lens, will depend on the object position. The lens can then only be described by a unique set of cardinal points if the image position is fixed, for example at $-\infty$. This case is approached in practice when using magnetic lenses with immersed objects. The focal length applicable in this case will be called f_0 and the focal distance (from the centre of the lens) z_0. Figure 11 illustrates the two cases. For very strong excitations f_1 is of an oscillatory character. Only the first branch of f_1 and the focal length f_0 are of practical interest.

The focal distances z_1 and z_0 are plotted as functions of k^2 in Figure 12, the focal lengths f_1 and f_0 in Figure 13, and the distances p_1 and p_0 of the principal planes from the origin in Figure 16.

---

* Electron lenses for which this is true for *all* excitation values, even if the focus comes to lie within the lens field, were called 'Newtonian' by Glaser (Glaser and Lammel 1941). While Glaser's hypothetical lens mentioned before is a 'Newtonian' lens according to this definition, it is found that 'real' magnetic lenses, as investigated in this paper, are not of this type if the excitation exceeds a certain minimum value, different for each lens. Most lenses used in electron microscopes employ excitation values near or slightly above the minimum value.

The first focal distance z_0 decreases monotonically with an increase in k^2, but at an increasingly slower rate the higher k^2. At $k^2=2{\cdot}8_5$, z_0 passes through the origin, and for higher excitations less than half the lens is used in the formation of the first image. The z_1 curve begins to part from the z_0 curve between $k^2=0{\cdot}2$ and $k^2=0{\cdot}5$, and goes to $-\infty$ at $k^2=2{\cdot}8_5$, jumping then to $+\infty$ to decrease monotonically to $-\infty$ at $k^2=9{\cdot}6$, etc.

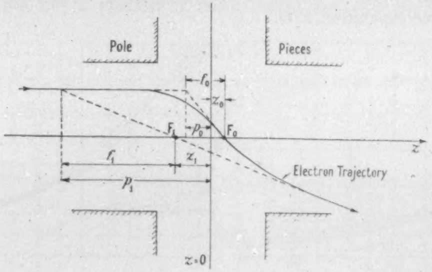

Figure 11. Diagram showing significance of focal lengths f_0 and f_1, of focal distances z_0 and z_1, and of distances p_0 and p_1 of principal planes for centre plane of lens.

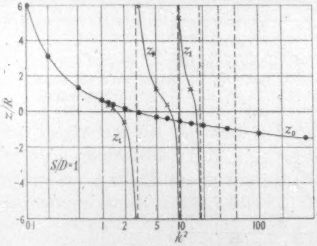

Figure 12. Graph of focal distances z_0/R and z_1/R for lens $S/D=1$ as functions of excitation parameter k^2.

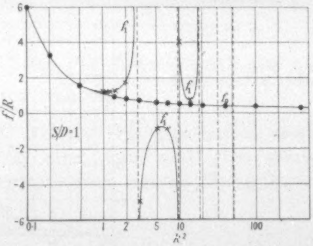

Figure 13. Graph of paraxial focal lengths f_0/R and f_1/R for lens $S/D=1$ as functions of excitation parameter k^2.

The focal length f_0 also decreases monotonically with increasing excitation. The weak lens condition, where $1/f \propto k^2$ is left at about $k^2 \simeq 0{\cdot}2$. At $k^2=1$, we have $f_0/R=1{\cdot}09$, at $k^2=10$, $f_0/R=0{\cdot}51_5$. The focal length f_1 exhibits a first minimum at $k^2=1{\cdot}12$, where $f_1/R=1{\cdot}18$, going to ∞ at $k^2=2{\cdot}85$, and showing a succession of similar loops for higher excitations.

The first minimum of f_1 is of a certain interest because the value of $f_1/R=1{\cdot}18$ represents the shortest focal length which can be obtained by this lens when used as a projector lens. Moreover, the operation of a projector lens near this point makes its image formation almost unaffected by variations in the excitation parameter k^2. The chromatic aberration of the lens at this point is zero, and the amount of the image displacement due to the chromatic change in image rotation, given by

$$\delta = r_i \Delta\Psi_c = (\Delta H/H - \Delta V/2V) r_i \Psi_1, \qquad \ldots\ldots(5)$$

can be made negligibly small in most practical cases ($\Psi_1=2{\cdot}55$ at this point).

§ 4. PARAXIAL PROPERTIES OF THE SERIES OF LENSES $S/D=0{\cdot}2$ TO 2.

The focal distances from the centre planes of the lenses z_0 are plotted for the four lenses $S/D=0{\cdot}2$, $0{\cdot}6$, 1 and 2 as functions of k^2 in Figure 14, the image being assumed at $-\infty$ in each case. The corresponding focal lengths f_0 are plotted in Figure 15, and the distances of the principal planes of the lenses are given in Figure 16. The image rotations Ψ_0 up to the first focus are shown in Figure 17. All these properties of the lenses are seen to depend to a considerable extent on the pole piece separation S/D.

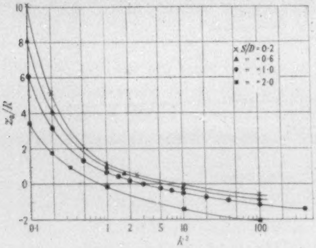

Figure 14. Graph of first focal distances z_0/R for four lenses as functions of excitation parameter k^2.

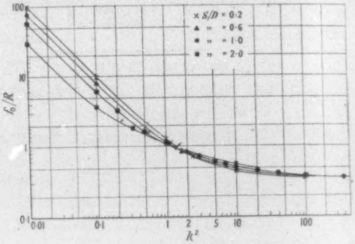

Figure 15. Graph of first focal lengths f_0/R for four lenses as functions of excitation parameter k^2.

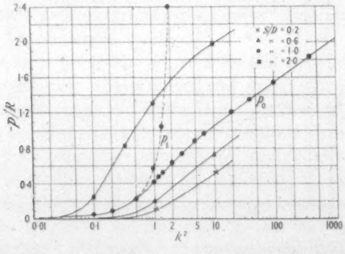

Figure 16. Graph of distances of principal planes from centre planes of lenses for four lenses as function of excitation parameter k^2.

At high values of the excitation parameter k^2 the focal lengths become more nearly equal, and between $k^2=1{\cdot}4$ and $k^2=2$ the curves for the different lenses (Figure 15) cross over; the lenses with the smaller pole piece gaps have the shorter focal length at very high excitations. The differences of focal lengths are then, however, fairly small. (The part played by iron saturation at high excitations will be discussed briefly in a later paper.)

A similar trend is shown by the image rotations (Figure 17), which become more nearly equal with increasing excitation. Eventually, the curves for the different lenses cross over.

In some applications the focal length f_1 is of interest. For weak and moderately strong excitations f_1 and f_0 are of course identical. The points where the curves representing the functions f_1 and f_0 would part are marked in Figure 15 by small arrows. The focal lengths f_1 are plotted in Figure 18 for the four lenses. The application of these results to the design of electron microscope projector lenses is discussed in a following paper (Liebmann, to be published).

If the lens excitation is so low that the lens can be considered a 'weak' lens, i.e. $f \leqslant 4a$, the focal lengths are inversely and the image rotations directly proportional to the lengths of the lens fields, as given by the half-width parameter a (Figure 8). In this region, the focal length can be expressed by this approximate formula, which is correct to within 3%:

$$f/R \simeq 0{\cdot}65(a/R)^{-1}k^{-2}. \qquad \ldots\ldots(6)$$

From equation (6) a practically more useful approximate formula can be derived:

$$f \simeq 50(DS)^{1/2}V_r/(NI)^2, \qquad \ldots\ldots(7)$$

where f, D and S are measured in the same unit, i.e. in centimetres or in inches. Formula (7) is correct to within 10% over the range of S/D values likely to be met in practice for the weak lens condition. For very strong excitations, or for extreme geometries (S/D very small or very large), formula (7) gives always values for f which are too small. The departure from formula (7) begins for excitations which would make $f \lesssim (DS)^{1/2}$.

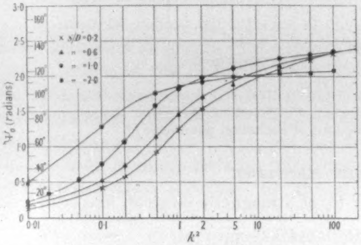

Figure 17. Graph of image rotation up to first focus for four lenses as function of excitation parameter k^2.

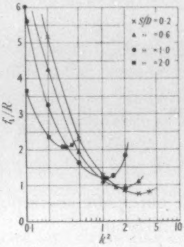

Figure 18. Graph of focal lengths f_1/R for four lenses as functions of excitation parameter k^2.

§ 5. ABERRATIONS OF LENS $S/D=1$

The lens aberrations of greatest importance in well-centred electron-optical systems of perfect rotational symmetry are spherical aberration and chromatic aberration; these are the only aberrations present in images of object points located on the optical axis. Their bearing on the question of resolving power in electron microscopes, or on the maximum electron current densities obtainable in other electron-optical focusing devices is well known. For this reason, the spherical aberration constant C_s and the chromatic aberration constant C_c were determined for the whole range of lens excitations k^2. For the other aberrations only a few values were computed. The image was in all cases assumed to be at $-\infty$, and the aberration values were referred back to the object plane.

(i) *Spherical Aberration*

The spherical aberration constant C_s is defined by

$$\Delta r_i = \delta_s = C_s\alpha^3, \qquad \ldots\ldots(8)$$

where Δr_i is the lateral displacement at the object point of a ray making the angle $\alpha = r_i'$ with the axis.

A graph of C_s/R is given in Figure 19 as function of k^2. One sees that C_s/R falls monotonically from quite high values at low excitations to a value as low as 0·10 at the very high excitation of $k^2=400$. However, present electron microscopes do not use such extreme lens excitations and a more representative value of C_s/R is from 1 to 2.

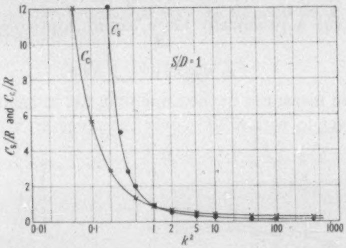

Figure 19. Graph of spherical aberration constant C_s/R and of chromatic aberration constant C_c/R for lens $S/D=1$ as functions of excitation parameter k^2.

(ii) *Chromatic Aberration*

The chromatic aberration constant C_c of a magnetic electron lens is defined by the equation

$$\Delta r_i=\left(\frac{2\Delta H_0}{H_0}-\frac{\Delta V}{V}\right)C_c\alpha, \qquad \ldots\ldots(9)$$

where Δr_i and α have the same meaning as before, and $\Delta H_0/H_0$ and $\Delta V/V$ are the relative fluctuations of magnetic field strength and accelerating voltage. If object and image are both located on the axis, a simple formula, due to Glaser (1940) can be used for the evaluation of C_c:

$$C_c=\int_{-\infty}^{z_i}\left(\frac{r'}{r_i'}\right)^2 dz. \qquad \ldots\ldots(10)$$

A graph of C_c as a function of k^2 is given in Figure 19. The numerical value of C_c is of the same order as the value of C_s, being somewhat lower than C_s at weak excitations and higher at strong excitations. The ratio C_c/f is for all k^2 slightly smaller than unity, which is the limiting value for $k^2\to 0$.

(iii) *The other Geometrical Aberrations*

In order to obtain an estimate of the relative importance of the various first order geometrical aberrations, these were all computed for the case $k^2=1$, using the trajectory tracing method. If the aperture plane is located in the principal plane, the deviations of the 'first order image' point from the paraxial image point can be written as

$$\begin{aligned}\Delta x_i \simeq \Delta r_i &= a_1 r_i^3 + a_2 r_i^2 r_i' f + a_3 r_i r_i'^2 f^2 + a_4 r_i'^3 f^3\\ \Delta y_i \simeq r_i \Delta\Psi_i &= a_5 r_i^3 + a_6 r_i^2 r_i' f + a_7 r_i r_i'^2 f^2.\end{aligned}$$

The seven aberration coefficients $a_1 \ldots . a_7$, referred back to the object plane, are then (in units R^{-2}): distortion $a_1=-0{\cdot}59$, astigmatism and curvature $a_2=1{\cdot}29$, coma $a_3=-1{\cdot}33$, spherical aberration $a_4=0{\cdot}64$, anisotropic distortion $a_5=0{\cdot}86$, anisotropic astigmatism $a_6=-0{\cdot}67$, anisotropic coma $a_7=0{\cdot}58$.

It is seen that all aberration coefficients are of the same order of magnitude. Hence, inserting such aperture angles and object field sizes as are used in practical electron-optical systems (e.g. in electron microscope objectives), one finds that in most cases the effect of all the other aberrations is completely swamped by spherical aberration.*

The next serious geometrical aberration after spherical aberration is usually coma. The two lens constants $(\Delta r_i'/r_i'^2)(R^2/r_a^2)=(\Delta f_0/f_0)(\alpha f_0/R)^2$ and $(\Delta\Psi_0 R^2)/r_a^2=\Delta\Psi_0/(\alpha f_0/R)^2$, which are closely related to the two coma constants, are plotted for a wide range of lens excitations in Figures 23 and 24 (circles). The two plotted functions are of importance in the imaging of more extended object fields with large magnifications.

§6. ABERRATIONS OF THE SERIES OF LENSES $S/D=0{\cdot}2$ TO 2

The most important aberrations of the four lenses are plotted in Figures 20 to 24. In Figure 20 graphs of the spherical aberration constant C_s/R are shown. For low values of the excitation parameter k^2 the lenses differ considerably in their spherical aberration, the lens being the better the greater the relative length of the lens field. For $k^2\simeq 0{\cdot}1$, the ratio of the C_s values for the range of lenses investigated is as high as 100 : 1, but this drops to 8 : 1 for the excitation $k^2\simeq 0{\cdot}5$, which is used in many electron microscopes. As with the focal lengths f_0, the spherical aberration constants for the various lenses become more and more equal the stronger the lenses, and in the region of $k^2=3$ to $k^2=5$ the curves of C_s/R cross over. At the highest excitations, the shorter lens fields give slightly lower C_s/R values, but the differences between the various lenses are small.

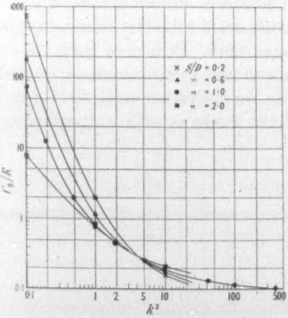

Figure 20. Graph of spherical aberration constant C_s/R for four lenses as function of excitation parameter k^2 when used as objectives.

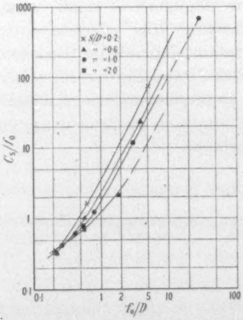

Figure 21. Graph for dimensionless aberration constant C_s/f_0 as function of relative focal length f_0/D for four lenses.

To facilitate a comparison with aberration constants given in the literature, including those for electrostatic lenses, where often insufficient data are given about the relevant dimensions of the lenses, the dimensionless spherical aberration constant C_s/f, sometimes called S or C, is plotted as function of f_0/D in Figure 21.

---

* Coma and astigmatism referred to here are those due to the use of oblique pencils in a perfectly round lens, and are not to be confused with coma and astigmatism due to disorientation or deformation of the pole pieces. These may limit the resolving power in practice more drastically than does spherical aberration.

The chromatic aberration constants C_s are plotted for the four lenses in Figure 22. They change with k^2 very nearly as the focal lengths f_0; for low excitations they approach the f_0 values (at the end of the 'weak' lens range, defined before, the C_c values are about 10% smaller than the corresponding f_0 values). For higher excitations the C_c values for all lenses become nearly equal and have a value of approximately two thirds of the corresponding value of f_0.

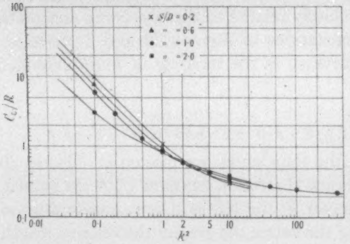

Figure 22. Graph of chromatic aberration constant Cc/R for four lenses as functions of excitation parameter k^2.

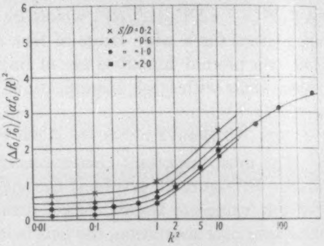

Figure 23. Graph of isotropic coma constants $(\Delta f/f_0)/(\alpha f_0/R)^2$ for four lenses as functions of excitation parameter k^2.

In Figures 23 and 24 the two constants $(\Delta f_0/f_0)/(r_a/R)^2 = (\Delta f_0/f_0)/(\alpha f_0/R)^2$ and $(\Delta\Psi'_0 R^2/r_a{}^2) = \Delta\Psi'_0/(\alpha f_0/R)^2$ related to the isotropic and anisotropic comas are plotted as function of k^2 for the four lenses. The shorter lenses are rather worse than the lenses with the greater length of field. The anisotropic component is almost negligible at small excitations, but becomes preponderant at very high excitations. The effect of coma, when compared with the effect of spherical aberration, depends on the size of the imaged field. It is seen from the curves, Figures 23 and 24, that the relative influence of coma becomes more pronounced with an increase in lens excitation. However, for the rather small field sizes used, for example in electron microscope objectives, coma is still only of secondary importance.

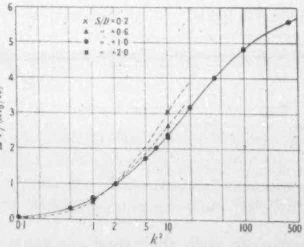

Figure 24. Graph of anisotropic coma constants $\Delta\Psi'_0/(\alpha f_0/R)^2$ for four lenses as functions of excitation parameter k^2.

§ 7. COMPARISON WITH EARLIER WORK

Van Ments and le Poole (1947) published focal data on a series of symmetrical magnetic electron lenses, computed on the basis of measured field distributions within the actual lenses (in the absence of iron saturation). The half widths of the field as function of pole piece separation, and the positions of the foci and the paraxial focal lengths agree closely with the data given here, over the range covered by the previous authors.

Probably on account of the difficulty of measuring aberration constants, few measured values are given in the literature. The most carefully carried out measurement, of a single value of C_s, appears to be Dosse's (1941 b), but the published value requires correction (Dosse 1941 c). As Dosse's lens was asymmetrical, one can only approximately relate his value of $C_s=0{\cdot}34$ cm. to the data given in this paper. However, within this approximation, the agreement with our curves appears very satisfactory. As far as the author's results can be correlated quantitatively with the experimental data of Becker and Wallraff (1938, 1940 b) agreement is good. A remarkable point is that Becker and Wallraff's aberration values for air coils appear to agree with the authors' values obtained for iron containing lenses, if the comparison is made on the basis of equal relative refracting power.

The field distribution assumed by Ramberg (1942) in his calculations of magnetic lens characteristics approaches fairly closely the field distribution measured by the authors for $S/D=0{\cdot}2$; at $k^2=1$ agreement between Ramberg's values for f_0, C_s and C_c and the authors' values for the lens $S/D=0{\cdot}2$ is within 1%.

The extensive calculations by Glaser (1941) are not strictly comparable with the authors' results, as the field distribution assumed by him shows a drop at some distance from the centre of the lens which is too slow when compared with the fields found in actual lenses, even if the iron pole pieces are saturated. This explains the fact that Glaser's C_s/a values show a minimum for a certain value of lens excitation, whereas the C_s/R values of 'real' lenses, used as microscope objectives, show a monotonic decrease with the excitation parameter k^2. However, for moderately strong excitations (between $k^2=0{\cdot}2$ and $k^2=0{\cdot}8$), the data given by Glaser agree within 5% with the authors' data, for a Glaser field with a half width $a=R$, corresponding to a 'real' lens of $S/D=0{\cdot}83$. Thus, the results of many of the discussions based on Glaser's assumed field distribution are very nearly confirmed by the authors' work.

§ 8. APPLICATION TO LENS DESIGN

The various graphs given in the Figures can be used for the design of magnetic electron lenses (of the symmetrical type). The excitation data (in ampere turns) can be related to the excitation parameter k^2 with the help of Figure 2. If such a strong excitation is used that iron saturation will be appreciable, the 'effective' separation ratio S/D will be increased, the amount of increase depending on the degree of saturation. In practice, this increase will amount rarely to more than 20% to 50% beyond the actual geometrical data. The paraxial imaging properties for given k^2 (or conversely, the excitation required for a prescribed position of object and image) can then be read off the curves, Figures 14, 15 and 16. If the excitation is very high, it will be necessary to take into account whether the whole length of the lens field is effective, as in electron microscope projector lenses or in focusing lenses for cathode-ray tubes and similar applications, or whether the object is immersed in the lens field, as in some electron microscope objectives, and some special focusing devices. In the first case, the curves of Figure 18 apply, whereas the lower parts of the curves Figure 15 should be used in the second case.

The information on the principal aberration data is contained in Figures 20, 22 and 23.

Considerations relating to the optimum designs of certain electron microscope lenses are being discussed further (Liebmann 1951, Liebmann, to be published).

As a numerical example of the application of the graphs, consider the design of an electron microscope objective, the following data being given: $V=63$ kv. ($V_r=67$ kv.), $D=0{\cdot}4$ cm., maximum excitation $NI=2{,}500$ ampere turns (nominal). Table 2 gives the evaluation of the lens properties. By interpolation, the most suitable lens can then be selected, taking subsidiary considerations, as desired specimen location, etc. into account. Two sets of numerical values for the shortest lens are given, as it turns out that this lens cannot be worked with the prescribed excitation without running into extreme iron saturation, as indicated by the value for H_p given in brackets. Assuming that this condition will lead to these modifications: effective increase in air gap length 50%, effective increase in lens diameter 10%, loss of ampere turns in iron circuit 20%, we obtain the second set of figures entered for this lens. We see that for a fixed number of ampere turns, lenses with fairly short gaps are mostly preferable.

Table 2

S/D	0·2	0·6	1	2
β	0·0154	0·0101	$0{\cdot}0060_5$	$0{\cdot}0020_2$
k^2	1·44	0·94	0·56	0·19
H_0 (gauss)	10500	8450	6500	3800
H_p (gauss)	(40000*) 21500†	13000	7800	3950
z_0/R	(0·84)	1·00	1·20	1·85
z_0 (cm.)	0·17* 0·22†	0·20	0·24	0·39
f_0/R	(1·00)	1·20	1·50	2·40

S/D	0·2	0·6	1	2
f_0 (cm.)	(0·20*) 0·26†	0·24	0·30	0·48
Ψ_0	(81°)	82°	93°	87°
C_s/R	(1·05)	1·25	1·65	3·8
C_s (cm.)	(0·21*) 0·35†	0·25	0·33	0·76
C_c/R	(0·81*)	0·96	1·2	1·9
C_c (cm.)	(0·16*) 0·22†	0·19	0·24	0·38

$NI=2{\cdot}5\times10^3$ ampere turns, $V_r=6{\cdot}7\times10^4$ volts, $R=0{\cdot}2$ cm.

* Nominal. † Actual.

As a further example, let us work out the nominal number of ampere turns required for a few given focal lengths for fixed anode voltage, say 63 kv., for the four lenses. The result is given in Table 3. It is seen that the shorter lenses are more economical in the use of the excitation power, and that the excitation power needed increases rather more rapidly with a reduction of focal length in the longer lenses. As iron saturation effects are in part equivalent to a lengthening of the pole piece gap, the differences between the lenses of different physical lengths of air gap will be greatly reduced at high excitation values; if the iron has a low saturation flux density the increase of excitation power needed for a relatively small decrease in focal length when f_0/R tends to unity may be quite striking, particularly for lenses of small diameter, which reach the saturation value of H_p for smaller values of f/R.

Table 3. NI at $V_r=6{\cdot}7\times10^4$ volts

f_0/R	$S/D=0{\cdot}2$	$S/D=0{\cdot}6$	$S/D=1$	$S/D=2$
10	670	720	810	1000
5	960	1060	1170	1500
2	1600	1800	2000	3000
1	2500	2850	3700	6700

As a final example, let us consider the effect of scaling the pole piece bore for the gap width $S/D=1$ and a maximum field strength at the pole faces of $H_p=10{,}000$ gauss, or $H_0=8{,}340$ gauss, and the same voltage as before ($V_r=6{\cdot}7\times10^4$ volts). The result of this operation is given in Table 4. Disregarding the increased number of ampere turns required, one sees that the spherical aberration constant C_s has a minimum value for a pole piece diameter of $2R=1{\cdot}0$ cm., although the dependence of C_s on R is not very marked. For different accelerating voltages V or maximum magnetic field strengths H_p the optimum diameter may be greater or smaller. Obviously, other considerations, e.g. easy introduction of a specimen in an electron microscope objective lens, and the avoidance of machining faults, have to play a part in a complete design, but the data derived from the various curves should be of assistance to the designer of electron-optical systems.

Table 4

R (cm.)	0·10	0·25	0·50	1·0
NI (nominal)	1590	3980	7960	15920
k^2	0·23	1·44	5·72	22·9
z_0/R	2·78	0·40	−0·32	−0·80
z_0 (cm.)	0·28	0·10	−0·16	−0·80
f_0/R	2·83	0·92	0·60	0·43

(R cm.)	0·10	0·25	0·50	1·0
NI				
f_0 (cm.)	0·28	0·23	0·30	0·43
C_s/R	8·2	0·61	0·28	0·16
C_s (cm.)	0·82	$0{\cdot}15_2$	0·14	0·16
C_c/R	2·57	0·70	0·43	0·33
C_c (cm.)	0·26	$0{\cdot}17_5$	0·22	0·33
Ψ_0	66°	110°	122°	129°

$H_p=10^4$ gauss, $H_0=8340$ gauss, $V_r=6{\cdot}7\times10^4$ volts, $S/D=1$.

ACKNOWLEDGMENTS

The authors wish to thank Dr. T. E. Allibone for permission to publish this paper, and Miss M. M. MacNaughton for help with part of the numerical work.

Note added on revision. The authors became acquainted with a recently published paper by Lenz (1950) some time after the present paper had been written. Lenz investigated the paraxial lens constants and the more important aberrations of symmetrical magnetic lenses as functions of relative pole separation S/D.

The two papers cover slightly different ground, but the agreement between Lenz's results and the authors' results is very good when referred to the same parameters.

REFERENCES

von Ardenne, M. 1939, *Z. tech. Phys.*, **20,** 289; 1941, *Z. Phys.*, **117,** 602.

Becker, H. and Wallraff, A., 1938, *Arch. Elektrotech.*, **32,** 664; 1939, *Ibid.*, **33,** 491; 1940 a, *Ibid.*, **34,** 43; 1940 b, *Ibid.*, **34,** 230.

Dosse, J., 1941 a, *Z. Phys.*, **117,** 316; 1941 b, *Ibid.*, **117,** 722; 1941 c, *Ibid.*, **118,** 375.

Glaser, W., 1940, *Z. Phys.*, **116,** 56; 1941, *Ibid.*, **117,** 285.

Glaser, W. and Lammel, E., 1941, *Ann. Phys., Lpz.*, **40,** 367; 1943, *Arch. Elektrotech.*, **37,** 347.

Gundert, E., 1941, *Telefunkenröhre*, No. 19/20, 61.

Lenz, F., 1950, *Z. angew. Phys.*, **2,** 448.

Liebmann, G., 1949, *Proc. Phys. Soc.* B, **62,** 753; 1950, *Brit. J. Appl. Phys.*, **1,** 92; 1951, *Proc. Phys. Soc.* B, **64,** 972.

van Ments M., and le Poole, J. B., 1947, *Appl. Sci. Res.* B, **1,** 3.

Ramberg, E. G., 1942, *J. Appl. Phys.*, **13,** 582.

Ruska, E., 1934, *Z. Phys.*, **89,** 90; 1942, *Arch. Elektrotech.*, **36,** 431; 1944, *Ibid.*, **38,** 102.

Siegbahn, K., 1942, *Ark. Mat. Astr. Fys.* A, **28,** No. 17.

Svartholm, N., 1942, *Ark. Mat. Astr. Fys.* B, **28,** No. 16.

The Symmetrical Magnetic Electron Microscope Objective Lens with Lowest Spherical Aberration *

By G. LIEBMANN

Research Laboratory, Associated Electrical Industries Ltd., Aldermaston, Berks.

MS. received 15*th February* 1951

ABSTRACT. Using results recently published it is shown that each of the investigated symmetrical magnetic lenses has an optimum value of the lens excitation parameter, for which the spherical aberration constant is smallest. Taking account of the dependence of the maximum obtainable axial field strength H_0 on the maximum field strength H_p in the pole piece gap, one finds that there is an optimum design of electron microscope objective lens of conventional type which gives a lowest value of spherical aberration and highest resolving power. A modification of this optimum lens as adapted for practical use is described.

§ 1. INTRODUCTION

THE choice of optimum operating conditions or the effect of scaling the dimensions of electron lenses has been discussed briefly by Dosse (1941), Ramberg (1942) and Gabor (1948) and more extensively by Cosslett (1947) and Glaser (1949). The investigations of these authors were based on certain assumed field distributions not directly related to the lens geometry.

In a preceding paper (Liebmann and Grad 1951, to be referred to as I), a series of symmetrical electron lenses was studied, the field distribution being measured on a resistance network analogue. Here the question will be investigated whether there exists among this series of lenses a lens with a lowest absolute value of the spherical aberration constant C_s, i.e. a lens which will be capable of giving the highest resolving power.

§ 2. THE EFFECT OF SCALING OPERATIONS

In Figure 20 of I graphs were shown of the relative spherical aberration constant C_s/R as function of the lens excitation parameter k^2.† It was seen that C_s/R falls monotonically with k^2. For small values of the excitation ($k^2 \simeq 0{\cdot}01$), this drop of C_s/R with increase in k^2 is very rapid, being of the order of k^{-6}, moderating itself gradually to the order of $k^{-1/2}$ at very high excitations ($k^2 \simeq 100$). As k^2 is proportional to R^2, the square of the lens radius, one may therefore expect that C_s, expressed in suitable absolute units, e.g. in centimetres, will behave like R^{-5} for very weak lenses and like $R^{1/2}$ for very strong lenses. If we now take a weak lens and increase its radius R steadily, whilst keeping H_0 and V (or V_r) constant, i.e. if we perform a 'scaling operation'‡, C_s will at first drop steeply, then reach a minimum and then increase again slowly; this minimum will be reached at a certain optimum value R_0 of the lens radius.

---

* A shortened version of this paper formed part of a paper read before the Congrès International de Microscopie Electronique held in Paris, 14th–22nd September 1950.

† The notation here is identical with that of I.

‡ The important point in this scaling operation is that H_0 is not changed, and that therefore the number of ampere turns NI would have to be scaled up in step with the increase in R. If NI were kept fixed, H_0 would change as $1/R$, and k^2 would remain constant. In this case all lens constants, including C_s, would be simply scaled up in the same ratio as R, as long as iron saturation is not predominant, and the magnetic lens would behave as an electrostatic lens would do upon scaling.

Figure 1 shows the effect of such 'scaling operation' on C_s for the lens $S/D=1$. The values marked with circles on the graphs represent the starting values $k^2=k_1^2$ for each scaling operation. The curves, representing C_s in the arbitrary

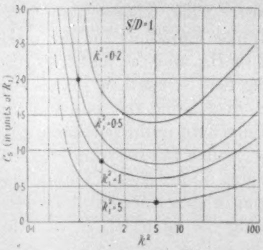

Figure 1. Effect on the spherical aberration constant C_s of scaling the lens radius $R(H_p, V_r$ constant).

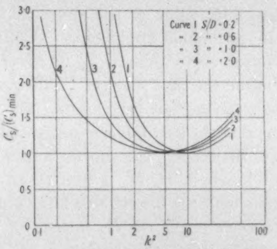

Figure 2. Effect of scaling of the lens radius R on the relative spherical aberration constant $C_s/(C_s)_{min}$ for four lenses of different gap widths.

unit R_1, the starting value of R (which is different for each curve since the same constant H_0 and V_r values were used for the whole group of curves), show the expected trend. All curves are geometrically similar and the minimum value for each curve occurs at $k_0^2 \simeq 5$. R_0, the optimum value of R, is then uniquely determined from $k_0^2 = 0{\cdot}022 R_0^2 H_0^2 / V_r$ by the relation

$$R_0 \simeq 15 V_r^{1/2} H_0^{-1} \text{ (cm.)} \qquad \ldots\ldots(1)$$

and the lowest absolute value of C_s which can be reached with the lens $S/D=1$ is given by

$$(C_s)_{\min} = 0{\cdot}267 R_0 \text{ (cm.)} \qquad \ldots\ldots(2)$$

where the numerical value of $(C_s/R)_0$ is taken from Figure 20 of I. The relations (1) and (2) can be combined to give

$$(C_s)_{\min} = 4{\cdot}05 H_0^{-1} V_r^{1/2} \text{ (cm.)}. \qquad \ldots\ldots(3)$$

Similar relations apply to the other lenses of the series. The 'scaling' curves of all four lenses, showing the relative values of C_s, i.e. $C_s/(C_s)_{\min}$, are plotted in Figure 2, V_r and H_0 being kept constant for each curve. It can be seen that the longer the lens field, the flatter the minimum of the C_s curve, and the lower the corresponding value of k_0^2. The values of k_0^2 and the corresponding values of $R_0 H_0 V_r^{-1/2}$ and of $(C_s)_{\min}(H_0 V_r^{-1/2})$ are given in Table 1.

Table 1

1	2	3	4	5	6	7	8	9
S/D	k_0^2 * (approx.)	$R_0 H_0 V_r^{-1/2}$	$(C_s/R)_0$ †	$(C_s)_{\min} \times (H_0 V_r^{-1/2})$	H_0/H_p ‡	$(C_s)_{\min} \times (H_p V_r^{-1/2})$	z_0/R_0	NI (rel.)
0·2	9	20·2	0·170	3·42	0·263	13·0	0	0·85
0·6	6·5	17·2	0·220	3·78	0·648	5·8	0·05	0·88
1	5	15·1	0·267	4·05	0·834	4·9	0·25	1·00
2	4·5	14·3	0·300	4·30	0·964	4·5	1·10	1·60

* From Figure 2. † From Figure 20 of I. ‡ From Figure 7 of I.

§ 3. THE OPTIMUM OBJECTIVE LENS

Having seen that for each lens of the investigated series there is an optimum excitation parameter k_0^2 and an optimum lens radius R_0, for given values of V_r and H_0, we can now look for the best lens among this series of lenses. Column 5 of Table 1, which gives the values of $(C_s)_{\min} H_0 V_r^{-1/2}$ would appear to indicate that the shorter lenses are slightly superior to the longer ones concerning the absolute value of the spherical aberration constant. This, however, would be an erroneous conclusion. Equation (3), and similar equations for the other lenses, show that $(C_s)_{\min}$ is inversely proportional to H_0, and the higher H_0 the better the lens can be. The practical limit to the field strength is set by iron saturation, but this limits, not H_0 the maximum field along the axis, but the field at the *iron-surfaces* represented by H_p, the parallel field in the pole piece gap. In this respect the shorter lenses are much inferior, as one can see from Figure 7 of I, where H_0/H_p is plotted as a function of the gap width S/D. To find the lens with the lowest absolute value of C_s in our series of lenses, we have therefore to refer $(C_s)_{\min}$ to H_p instead of to H_0. Introducing the factor H_0/H_p into the values listed in column 5 of Table 1 yields the values in column 7, which relate $(C_s)_{\min}$ numerically with H_p and V_r, and which are therefore more correctly representative of the limiting conditions of these lenses. It is seen that the lowest obtainable spherical aberration constant drops markedly with an increase in pole piece separation S/D for small pole piece separation, but at a fairly slow rate for the wider separations. Figure 3 gives a series of graphs showing $(C_s)_{\min}$ as a function of maximum parallel field H_p for a number of typical accelerating voltages for $S/D \rightarrow 2$.

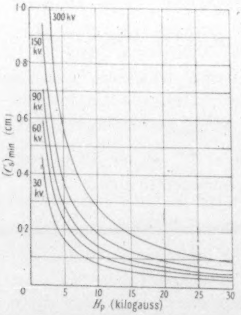

Figure 3. Minimum spherical aberration constant for best symmetrical lens ($S/D \simeq 2$).

Our picture is now nearly complete except for the practical considerations of the position of the object (specimen) and of the number of ampere turns required for the different lenses. This information can be obtained from the data of the preceding paper; it is listed in columns 8 and 9 of Table 1, the relative number of ampere turns NI for H_p constant being taken as 1·00 for the lens $S/D = 1$. The number of ampere turns required increases slowly at first with S/D, and then rather steeply. Still more objectionable is the very deep immersion of the object in the lens field that would be required in the very long lenses. Hence, a good practical compromise is to choose a lens with $S/D \simeq 1$; this lens approaches already quite closely the optimum lens of this series.

§4. THE LIMIT OF RESOLVING POWER

We can now discuss the limit of the resolving power of the ordinary electron microscope, as set by spherical aberration. The resolution limit can be written as

$$\delta = BC_s^{1/4}\lambda^{3/4} \qquad \ldots\ldots(4)$$

where B is a constant of the order unity, depending somewhat on the definition of resolving power and the shape of the scattering characteristic of the object for electrons. A typical value of B is 0·78, given recently by Glaser (1949). The parameter $C_s^{1/4}\lambda^{3/4}$, which is independent of the particular definition adopted for the resolving power, is plotted in Figure 4 as function of the accelerating voltage V, for a lens with $S/D=1$, the relativistic correction having been taken into consideration. The lower curve represents the resolution parameter for optimum values of R_0 with a fixed value $H_p=25{,}000$ gauss ($H_0=20{,}800$ gauss), whereas the upper curve represents this for a fixed value of $R=0{\cdot}5$ cm., H_p (and H_0) varying. As $k_0^2=5$ for both curves, the numbers of ampere turns for the two curves, at the same accelerating voltage, are identical. A typical nominal value of NI at $V=90$ kv. is 9,000 which may have to be increased to some extent on account of incipient iron saturation, particularly for the lower curve. The values of the resolution parameter $C_s^{1/4}\lambda^{3/4}$ at 90 kv. are 4·3 A. for the lower curve ($R_0=0{\cdot}227$ cm.), and 5·3 A. for the upper curve ($H_p=11{,}300$ gauss at 90 kv.).

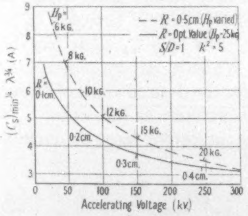

Figure 4. Resolution parameter $\delta=(C_s)_{min}^{1/4}\ \lambda^{3/4}$ as function of accelerating voltage for optimum lens $S/D=1$.

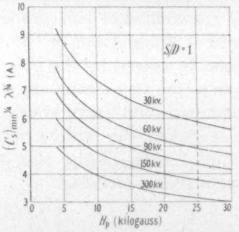

Figure 5. Resolution parameter $\delta=(C_s)_{min}^{1/4}\ \lambda^{3/4}$ for lens $S/D=1$ as function of maximum parallel field strength H_p.

The resolution parameter δ for the best lens $S/D=1$ is plotted for several voltages as function of the parallel field in the pole piece gap in Figure 5. The data given in Figures 4 and 5 show that it should be possible to double the resolving power of the ordinary electron microscope obtained so far before third-order spherical aberration sets a final limit.

§5. COMPARISON WITH EARLIER ESTIMATES

The dependence of the resolving power of the electron microscope on the axial field strength H_0 and on the accelerating voltage was discussed by Cosslett (1947) and by Glaser (1949), using the axial field distribution $h(z)=[1+(a/z)^2]^{-1}$. The relative focal length f/a and the relative spherical aberration constant C_s/a of this field were given explicitly by Glaser (1941), and from this the smallest focal length or the smallest spherical aberration constant can be obtained in units of the 'half-width' parameter a, which in turn can be related to the accelerating voltage V and the axial field strength H_0 by an equation similar to our equation (1). Cosslett (1947) and Glaser (1949) obtained values for the best resolving power which agree very well with those given in this paper (for a comparison, the data of Figures 4 and 5 have to be multiplied by the appropriate value of B). The good agreement of these earlier predictions with that based on the *measured* field distributions used here is ultimately due to the closeness of the C_s/a values for Glaser's assumed field distribution to the spherical aberration values of the 'real' lens with $S/D \simeq 1$, over the most important range of lens excitations, as was pointed out in I (Liebmann and Grad 1951).

§ 6. A PRACTICAL REALIZATION OF THE OPTIMUM LENS

As was mentioned in § 3, the disadvantages of using the very high lens excitations necessary to achieve the optimum lens conditions are not only the great number of ampere turns required, which entails a number of practical difficulties, but the deep immersion of the specimen in the lens field. Even in the lens $S/D=1$, less than half the lens field is utilized for the formation of the image. The serious drawback of the deep immersion is that the half of the lens field not used in the image formation is now a part of the illuminating system, as was discussed by Marton and Hutter (1944). This is illustrated by the schematic diagrams, Figure 6 (*a*), representing the electron lens system, and Figure 6(*b*) representing approximately the light-optical equivalent. In addition to C_0, the condenser lens proper, we have a very strong lens, which we may consider as decomposed in two lenses C_1 and C_2, located between C_0 and the specimen S imaged by the objective lens O. The lens C_1 alone has the same strength as the very strong objective lens O. While it may be possible to adjust the combined illuminating system (C_0, C_1, C_2) for the desired angle of illumination at the specimen, this will be rather difficult in practice as the lenses C_1 and C_2 are coupled with all the adjustments of the objective lens O, including its alignment and its focusing.

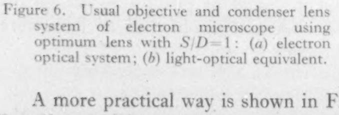

Figure 6. Usual objective and condenser lens system of electron microscope using optimum lens with $S/D=1$: (*a*) electron optical system; (*b*) light-optical equivalent.

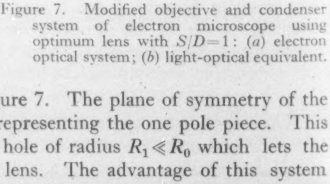

Figure 7. Modified objective and condenser system of electron microscope using optimum lens with $S/D=1$: (*a*) electron optical system; (*b*) light-optical equivalent.

A more practical way is shown in Figure 7. The plane of symmetry of the lens is replaced by a plane iron surface, representing the one pole piece. This plane is perforated by a small cylindrical hole of radius $R_1 \ll R_0$ which lets the illuminating electron beam pass into the lens. The advantage of this system is not only that it reduces the required number of ampere turns to half the previous value, but that it removes the strong condenser component C_1 altogether, and replaces the condenser component C_2 by another one C_3 which is only half as strong as C_2. As will be shown elsewhere, the refractive power of the lens field to the left of S in Figure 7 (*a*), including the focusing action of the pinhole lens of radius R_1, is approximately equal to the refractive power of the field section between the centre plane and the position z_0 of S, being given approximately by

$$(R_0/f)_{C_3} \simeq k_0^2(z_0/R_0). \qquad \ldots\ldots(5)$$

The degree of approximation depends on the relative radius R_1/R_0 of the pinhole. For $R_1/R_0=0{\cdot}1$, a good practical value, the refractive power of C_3 is 25% less than given by equation (5). Hence, for the lens field of type $S/D=1$, and with the k_0^2 and z_0 values given in Table 1, we have $f_{C_3} \simeq R_0$, or $f_{C_3} \simeq 1{\cdot}6 f_0$ where f_0 is the focal length of the objective lens. The reduction of the refractive power of the interacting part of the lens field and its more favourable location with respect to the specimen remove this practical limitation for the use of such strong objective lenses. Similarly it can be shown that the aberrations of the pinhole lens do not reduce the current density or increase the angular spread of the illuminating beam to an appreciable extent.

ACKNOWLEDGMENT

The author wishes to thank Dr. T. E. Allibone for permission to publish this paper.

REFERENCES

Cosslett, V. E., 1947, *J. Sci. Instrum.*, **24**, 40.
Dosse, J., 1941, *Z. Phys.*, **117**, 722.
Gabor, D., 1948, *The Electron Microscope*, 2nd ed., p. 76 (London: Electronic Engineering).
Glaser, W., 1941, *Z. Phys.*, **117**, 285; 1949, *Acta Phys. Austriaca*, **3**, 38.
Liebmann, G. and Grad, E. M., 1951, *Proc. Phys. Soc.* B, 64, 956.
Marton, L., and Hutter, R. G. E., 1944, *Phys. Rev.*, **65**, 161.
Ramberg, E. G., 1942, *J. Appl. Phys.*, **13**, 582.

The Photographic Action of X-Rays

By J. R. GREENING
St. George's Hospital, London S.W.1

Communicated by J. E. Roberts; *MS. received* 25*th April* 1951, *and in amended form* 8*th July* 1951

ABSTRACT. The variation of photographic blackening with intensity, exposure, the thickness of material round the film, the angle of incidence and the wavelength of x-rays, are examined theoretically and, with one exception, experimentally. A detailed theoretical investigation is made of the energy absorption in the silver bromide grains, consideration being given to the energy lost by scatter and fluorescence and to the electron interchange between the silver bromide grains and the surrounding gelatine and other material. It is concluded that for the majority of emulsions there will be no variation of blackening with x-ray intensity and that the photographic density will be proportional to the exposure at low densities. At very short wavelengths the blackening is critically dependent upon the thickness of material round the emulsion. Photographic density decreases with increase of angle of incidence of x-rays, the maximum decrease observed being about 17%. Within the wavelength range examined experimentally (0·020 to 0·354 A.) the photographic density was approximately proportional to the energy absorbed by the silver bromide. The density per röntgen varied by a factor of 42 in this range. The variation of density per röntgen with wavelength and angle of incidence limits the applications of photographic methods of x-ray measurement. Methods by which emulsion manufacturers can reduce these variations are suggested.

§ 1. INTRODUCTION

PHOTOGRAPHIC methods of measuring x-rays would often be very attractive if the accuracy attainable could be made to approach that of ionometric methods. The following investigations of some of the factors affecting the photographic action of x-rays were carried out in the belief that an understanding of the fundamentals of this action would suggest means by which the present limitations of photographic methods could be reduced.

§ 2. THE VARIATION OF BLACKENING WITH INTENSITY

The variation of blackening with x-ray intensity has been investigated by Kroncke (1914), Friedrich and Koch (1914), Glocker and Traub (1921), Bouwers (1923), Dershem (1932), Luft (1933), Bell (1936 a), Mülbach (1937), Morgan (1944) and Tasker (1945). None of these observers found a variation greater than his experimental error, Luft, Bell and Morgan covering an intensity range of 10,000 to 1. Similar results have been obtained for radium γ-rays (Rogers 1931, Rosenberger and Goldhaber 1934, Bell 1936 b) and electrons (Bothe 1922, Ellis and Wooster 1927, Nacken 1930, Becker and Kipphan 1931).

Modern theories of latent image formation (Berg 1948) suppose that for a grain to become developable a certain minimum of energy must be absorbed within a certain maximum of time. If this energy is obtained as the result of more than one discrete absorption event the probability of its being absorbed within the maximum time allowable decreases with decrease of intensity, and so-called low intensity reciprocity law failure occurs. For x-rays the absorption of a single quantum usually renders a grain developable and no reciprocity law failure is to be expected. Films exposed to x-rays of very short wavelength, however, are blackened almost entirely by electrons coming from the surrounding material (see § 4). The specific ionization of these electrons may be such that the passage of a single electron through a grain is not sufficient to make it developable. Consequently some reciprocity law failure might be anticipated when exposing to high-energy radiation emulsions having grains of low sensitivity.

If exposure times are such that they are measured in weeks, the blackening may be appreciably reduced because of the fading of latent images produced early in the exposure. The final effect is the same as that which would result from low intensity reciprocity law failure.

§ 3. THE VARIATION OF BLACKENING WITH EXPOSURE

If the absorption of a single x-ray quantum or the passage of a single electron is sufficient to render a grain developable there should not be a threshold exposure below which no photographic action occurs, the theory of Silberstein (1922) or Charlesby (1940) together with that of Nutting (1913) indicating that the photographic density is proportional to the exposure at low densities.

Initial proportionality between density and x-ray exposure has been observed by Friedrich and Koch (1914), Glocker and Traub (1921), Brindley and Spiers (1933), Jauncey and Richardson (1934), Hirsh (1935), Bell (1936 a) and Herz (1949 a). Similar results have been obtained with radium γ-rays by Rogers (1931), Rosenberger and Goldhaber (1934), Bell (1936 b) and Cowing and Spalding (1949), while the last-named workers, together with Bothe (1922), Ellis and Wooster (1927), Becker and Kipphan (1931) and Cranberg and Halpern (1949) have obtained the same results with electrons of various energies.

Despite this evidence it must not be assumed that the density is initially proportional to the exposure for all emulsions at all wavelengths. As long as a single process of energy absorption renders a grain developable such an assumption is probably true, but when a multiple process of energy absorption is necessary to render a grain developable it is to be expected that a density–exposure curve will exhibit a 'toe', as happens with exposures to visible light. At long x-ray wavelengths Broili and Kiessig (1934) found such a toe for a fine grain emulsion and at very high energies Cowing and Spalding (1949) found a slight toe for exposures to radium γ-rays and ^{32}P beta particles. Bromley and Herz (1950) report that one of their films which had rather insensitive grains showed a toe in the density–exposure curve on exposure to hard x-rays. It is just such a film which might also be expected to show reciprocity law failure (see § 2).

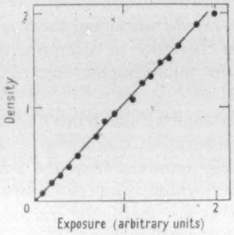

Figure 1. Variation of density with exposure for Ilford Line film exposed to x-rays of wavelength 0·11 A.

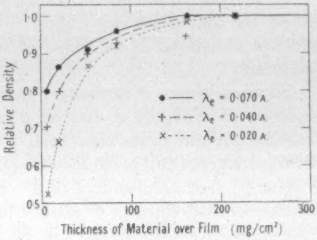

Figure 2. Variation of blackening with thickness of material over film.

We exposed a fine grain emulsion (Ilford Line film) to heterogeneous x-rays having an effective wavelength λ_e of 0·11 A. The results given in Figure 1 show a close proportionality between density and exposure up to densities of at least 1·8. Similar results have been obtained by Ibrahim (unpublished) for a number of longer wavelengths up to $\lambda_e = 0{\cdot}35$ A. Nicholson (private communication) finds similar linearity for exposure to radium γ-rays.

§ 4. THE VARIATION OF BLACKENING WITH THICKNESS OF MATERIAL AROUND FILM

It has been found during measurements of γ-rays with ionization chambers that the ionization varies with the wall thickness of the chamber (e.g. Mayneord and Roberts 1937). It was thought to be essential to determine whether a similar effect occurred in the corresponding photographic experiment. Accordingly films were exposed to x-rays having effective wavelengths of 0·070, 0·040 and 0·020 A. The films were enclosed in thin black paper cassettes (7·27 mg/cm^2) and were backed by 2·2 mm. of Perspex. The tube side of each film was covered with various thicknesses of film base and Perspex. The variation of blackening with thickness of overlying light atom material (expressed as mg/cm^2) is shown in Figure 2.

It will be seen that the blackening builds up rapidly with increasing thickness of overlying material and that the 'blackening deficiency' is greater the shorter the wavelength of the radiation. For radiation of $\lambda_e = 0{\cdot}020$ A. nearly half the maximum blackening is due to electrons coming from outside the black paper cassette. It is evident that films should normally be surrounded by a thickness of material sufficient to establish the maximum electron flux through the emulsion. Such a procedure is also advisable in order to avoid anomalous results due to electrons from the X-ray tube housing or γ-ray source passing through the emulsion. In the present experiments, electrons coming from the air between X-ray tube and film were kept to a minimum by using narrow X-ray beams.

Since the electron emission of the material around the emulsion is of such importance, its atomic number as well as its thickness will affect the blackening observed. Theoretical interpretation of the blackening is facilitated by surrounding the emulsion with material of atomic number close to that of the gelatine and the film base which are inevitably in close contact with the silver bromide grains.

§ 5. VARIATION OF BLACKENING WITH ANGLE OF INCIDENCE OF X-RAYS

In many applications of photographic films to X-ray measurement the X-rays fall on the film at various angles. It is of interest therefore to determine the effect of variations in the angle of incidence on the photographic blackening produced.

Suppose X-rays of intensity I to be falling at an angle of incidence θ on an emulsion of thickness d, and let μ be the linear absorption coefficient of the emulsion for the X-rays concerned. Then the energy removed from the X-ray beam per sec. per cm² of emulsion is $I\cos\theta(1-e^{-\mu d/\cos\theta})$ which, if $\mu d/\cos\theta$ is small, is equal to $I\mu d$, independent of θ. But if $\mu d/\cos\theta$ is not small, the fractional decrease of blackening at $\theta°$ relative to the blackening at 0° incidence

$$= \frac{I(1-e^{-\mu d}) - I\cos\theta(1-e^{-\mu d/\cos\theta})}{I(1-e^{-\mu d})} \qquad \ldots\ldots(1)$$

$$= 1-\cos\theta(1-e^{-\mu d/\cos\theta})/(1-e^{-\mu d}). \qquad \ldots\ldots(2)$$

Thus there is some variation in blackening with changing angle of incidence, but in practice the effect is small. For Ilford Line film the theoretical blackening deficiency at 80° incidence is 0·2% at $\lambda_e = 0{\cdot}110$ A. and 4 to 5% at $\lambda_e = 0{\cdot}327$ A.

An obliquity effect of different origin is to be expected at short wavelengths. Here, as shown above, much of the total blackening is produced by electrons coming from the surrounding light atom material. At short wavelengths most of these electrons are recoil electrons and their general direction of motion is the same as that of the X-rays producing them. Let it be assumed, therefore, that a parallel beam of electrons is falling on the emulsion. (This assumption is somewhat gross as the effects of scatter and the range of original angles of projection of the electrons are ignored, but the qualitative validity of the following argument should not be affected.) If these electrons are completely absorbed in the emulsion, the energy absorption per cm² of emulsion will be proportional to $\cos\theta$. If, however, the electron ranges are much greater than the emulsion thickness the electrons will lose only a small fraction of their energy in the emulsion and the energy absorption will be similar to that in the case of X-rays, i.e. little variation of blackening with angle of incidence should be expected. We may, then, make the following predictions: (i) At long wavelengths there will be a small decrease of blackening with increase of angle of incidence, as given by equation (2). (ii) After allowing for effect (i) a blackening deficiency very roughly proportional to $1-\cos\theta$ will remain. (iii) With decrease in wavelength there will at first be an increase in the blackening deficiency due to (ii) as a greater proportion of the total blackening will be due to electrons originating outside the emulsion. (iv) With further decrease in wavelength the blackening deficiency will pass through a maximum and will thereafter decrease as more of the incident electrons lose only a small fraction of their energy in the emulsion and the absorption process becomes similar to that of X-rays themselves.

The obliquity effect was examined experimentally with radiation of effective wavelengths 0·324, 0·110, 0·070, 0·040 and 0·020 A. For experiments at the two longest wavelengths a strip of film 6 cm. wide was placed in a thin black paper cassette and bent into a cylinder of 5 cm. diameter, emulsion side outwards, round a former consisting of two Perspex discs held about 6 cm. apart by a thin bamboo rod. There was little material therefore which could scatter radiation on to the central portion of the film. The cylinder axis was placed perpendicular to the X-ray beam. Thus the film was irradiated at all possible angles of incidence, the angle of incidence at any point on the film being readily calculated from the geometry of the experiment. For experiments at the shorter wavelengths the film in its black paper cassette was sandwiched between two Perspex cylinders each 2·5 mm. thick. This thickness of material was sufficient to establish the maximum electron flux in the emulsion.

The measured variation of blackening with angle of incidence is shown in Figure 3. Each curve represents the mean of at least twelve sets of density measurements after applying a small correction for the variations of exposure over the films. It will be seen that the predictions made above are all confirmed. The broken line shows the blackening expected if 18% of the total blackening is due to electrons which do not penetrate the emulsion. This is seen to agree fairly well with the experimental results for $\lambda_e = 0{\cdot}040$ A., but the theoretical curve is necessarily very approximate.

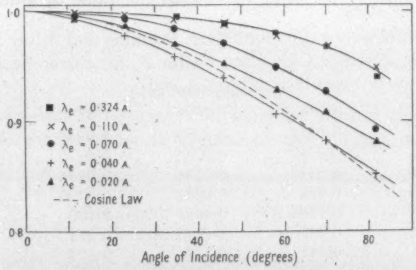

Figure 3. Variation of blackening with angle of incidence.

§ 6. THE VARIATION OF BLACKENING WITH X-RAY WAVELENGTH

The variation of blackening per röntgen with the wavelength of X-rays is of great practical and theoretical interest. Investigations have been carried out by Friedrich and Koch (1914), Glocker and Traub (1921), Berthold (1925), Berthold and Glocker (1925), Bell (1936 a), Pelc (1945) and Bromley and Herz (1950).

The workers named in the last two references showed that the density/röntgen was closely proportional to the energy absorbed by the silver bromide per röntgen, but in calculating this energy absorption they assumed that it was equal to that removed from the primary beam of x-rays by the silver bromide, i.e. that the absorption could be calculated simply from a knowledge of the mass absorption coefficient μ/ρ of silver bromide. In fact the problem is considerably more complex.

(i) *Energy lost by Scatter*

Firstly some radiation is scattered out of the primary beam and is not converted to electron energy. The absorption coefficient used should be $\tau+\sigma_a$ rather than μ, where τ and σ_a are the linear absorption coefficients resulting from photoelectric absorption and the production of recoil electrons respectively.

(ii) *Energy lost by Fluorescence*

Secondly some of the energy absorbed photoelectrically is re-emitted as characteristic radiation. If photons of energy $\boldsymbol{h}\nu$ are absorbed in a K shell of energy $\boldsymbol{h}\nu_K$ a fraction of this energy approximately $\boldsymbol{h}\nu_K w_K/\boldsymbol{h}\nu$ is emitted as characteristic radiation, w_K being the fluorescence yield of the K shell. Calculation shows that for normal photographic emulsions over 90% of the characteristic radiation escapes from the emulsion (see Appendix). Similar effects in the L shells are much smaller and have been ignored. The fraction of the absorbed x-ray energy appearing as kinetic energy of electrons has been calculated for silver bromide assuming $w_K=0{\cdot}77$ for silver and $w_K=0{\cdot}57$ for bromine (Compton and Allison 1935). Values of τ for silver were derived from a survey of published absorption data and τ for bromine was calculated using the general formula suggested by Victoreen (1943). The values of τ for silver bromide were calculated from these values both directly and also after multiplying them by the corresponding values of the factor $1-\boldsymbol{h}\nu_K w_K/\boldsymbol{h}\nu$ to allow for the energy re-emitted as fluorescence radiation. The basic data used are summarized in Table 1, where the final column gives the factor by which $\tau+\sigma_a$ must be multiplied in order to calculate the energy converted to kinetic energy of electrons. It will be seen that the effect of this factor becomes considerable as the silver K absorption edge at 0·484 A. is approached.

Table 1. Values of $(\tau+\sigma_a)/\rho$ for Silver, Bromine and Silver Bromide and the Fluorescence Correction Factor F_1 for Silver Bromide

λ (A.)	$(\tau+\sigma_a)/\rho$ (cm^2/gm.)			
	Silver	Bromine	AgBr	F_1
0·01	0·0248	0·0239	0·0244	1·00
0·02	0·0349	0·0285	0·0322	0·995
0·03	0·0540	0·0344	0·0456	0·977
0·04	0·088	0·0452	0·0700	0·960
0·05	0·128	0·0629	0·100	0·945
0·06	0·200	0·0897	0·153	0·929
0·08	0·441	0·177	0·329	0·897
0·10	0·791	0·321	0·591	0·868
0·12	1·29	0·534	0·969	0·840
0·15	2·34	1·01	1·78	0·798
0·20	5·1	2·32	3·92	0·731
0·25	9·7	4·41	7·45	0·663
0·30	15·7	7·45	12·2	0·598
0·35	24·1	11·2	18·6	0·530
0·40	35·7	16·8	27·7	0·464
0·45	49·3	23·4	38·3	0·397

(iii) *Energy lost by Electron Emission*

The third complicating factor in the calculation of the energy absorption in the silver bromide itself is the electron exchange between the silver bromide and the surrounding gelatine and other light atom material.

Consider first the energy of those electrons originating in the silver bromide which is lost from the emulsion. The problem in effect is to find that proportion of the electron energy liberated in an infinite sheet of material which is lost from the sheet. Following Spiers (1949), who considered a similar problem, it will be assumed that the electrons are emitted isotropically and travel in straight lines a distance R, the 'foil range' of the electrons. In addition it will be assumed that the range R and the energy E of an electron are connected by the formula $R = CE^{1\cdot74}$, an expression in agreement with the ranges calculated by Lea (1946 a) for energies between 2 and 200 kev. and supported by the work of Zajac and Ross (1949). Thus an electron which has travelled a fraction p of its range will retain a fraction $(1-p)^{1/1\cdot74}$ of its original energy, the variation of specific ionization along the electron track thereby being taken into account.

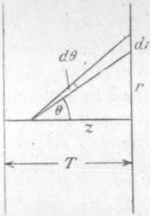

Figure 4. Illustrating calculation of electron energy escaping from a sheet of material.

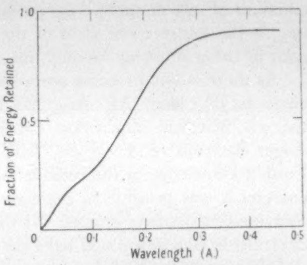

Figure 5. The fraction of the electron energy released in the silver bromide which is retained by the emulsion of Ilford Line film, as a function of wavelength.

If N electrons are emitted per cm^3 of material the number emitted between angles θ and $\theta + d\theta$ (Figure 4) by an element of area dA and thickness dz is $N dz\, dA\, 2\pi r\, dr \cos\theta / 4\pi(r^2+z^2)$. The energy of these electrons which escapes from the right-hand surface of the medium is

$$EN\,dz\,dA\,\frac{2\pi r\,dr\cos\theta}{4\pi(r^2+z^2)} \times \left(1 - \frac{(r^2+z^2)^{1/2}}{R}\right)^{1/1\cdot74}. \qquad \ldots\ldots(3)$$

Therefore the total energy released in the volume element $dz\,dA$ which escapes from the right-hand surface is

$$\tfrac{1}{2}EN\,dz\,dA\,z \int_0^{(R^2-z^2)^{1/2}} \frac{r}{(r^2+z^2)^{3/2}} \left(1 - \frac{(r^2+z^2)^{1/2}}{R}\right)^{1/1\cdot74} dr. \qquad \ldots\ldots(4)$$

Numerical integration of (4) for a series of values of z followed by graphical integration with respect to z made possible the calculation of the fraction of the total energy released in the sheet of material which was retained by the material, as a function of T/R, where T is the thickness of the sheet. These values are as follows:

T/R	0·1	0·2	0·3	0·4	0·5	0·6	0·7	0·8	0·9	1·0
Fraction retained	0·149	0·243	0·323	0·395	0·458	0·514	0·565	0·612	0·649	0·684

Before these data can be used to calculate that fraction of the electron energy liberated in the silver bromide of an emulsion which is retained by the emulsion, it is necessary to know the ranges and energies of the electrons.

(*a*) *Ranges of electrons in photographic emulsions.* The total rectified ranges of electrons in a Kodak NT4 emulsion measured and calculated by Zajac and Ross (1949) were converted to 'foil' ranges by dividing by 1·4 (Williams 1931). These ranges were in good agreement with values quoted by Herz (1949 b). As the same values were obtained by dividing the ranges given by Lea (1946 a) by the density of the emulsion, it was possible to obtain electron ranges over a wider range of energy. It has been assumed that this latter procedure will give correct electron ranges in other emulsions.

(*b*) *Relative numbers and energies of electrons released in silver bromide.* If the absorption of a certain number of quanta each of energy $\boldsymbol{h}\nu$ results in the emission from silver atoms of N photoelectrons each of energy $\boldsymbol{h}\nu - \boldsymbol{h}\nu_{\mathrm{Ag}}$, where $\boldsymbol{h}\nu_{\mathrm{Ag}}$ is the energy corresponding to the silver K absorption edge, there will be $N(1-w_{\mathrm{Ag}})$ silver atoms which return to their ground state by the emission of one or more Auger electrons of total energy approximately $\boldsymbol{h}\nu_{\mathrm{Ag}}$. ($w_{\mathrm{Ag}}$ is the fluorescence yield of the silver K shell.) It will be assumed that each of these atoms emits only one Auger electron and that its energy is $\boldsymbol{h}\nu_{\mathrm{Ag}}$.

As there is one bromine atom for every silver atom, $N[\tau_{\mathrm{a}}(\mathrm{Br})/\tau_{\mathrm{a}}(\mathrm{Ag})]$ photoelectrons of energy $\boldsymbol{h}\nu - \boldsymbol{h}\nu_{\mathrm{Br}}$ will be emitted by bromine atoms, where τ_{a} is the photoelectric absorption coefficient per atom. $N[\tau\,(\mathrm{Br})/\tau_{\mathrm{a}}(\mathrm{Ag})](1-w_{\mathrm{Br}})$ Auger electrons of energy $h\nu_{\mathrm{Br}}$ will, in addition, be emitted by bromine atoms. From a knowledge of the relative numbers of electrons in each group and their energies it was possible to calculate the relative proportions of electron energy contained in the four groups. If the primary X-rays are monochromatic all the electrons in one group will have the same energy.

The proportion of the total energy which appears as the kinetic energy of *recoil* electrons is only significant for wavelengths less than 0·15 A. The total energy of the recoil electrons was calculated by multiplying the total energy of the other four groups of electrons by σ_{a}/τ for silver bromide after correcting τ for energy lost by fluorescence. The mean energies of recoil electrons produced by X-rays of various wavelengths have been given by Lea (1946 b). The percentage of the total energy lying in each group is given in Table 2.

For the emulsion used by us we calculated the fraction of the electron energy liberated in the silver bromide and retained by the emulsion. The results (Figure 5) show that the correction for electron loss from the emulsion is very large at short wavelengths.

(iv) *Energy lost to the Gelatine of the Emulsion*

Not all the electron energy retained by the emulsion is absorbed by the silver bromide; some is absorbed by the gelatine. Provided the ranges of the electrons in the emulsion are large compared with the dimension of a grain and the distances between grains*, the electron flux through a grain and its immediate surroundings will be uniform, and the electron energy will be divided between the silver

---

* For Ilford Line film the average grain diameter is 0·24μ and the distance between grain centres is about 0·4 to 0·5μ. Even at a wavelength of 0·35 A. the range of a silver photoelectron in the emulsion is about 5 grain diameters. However, for coarser grained or more dilute emulsions the theory will begin to break down at shorter wavelengths.

Table 2. The Division of the Total Electron Energy released in Silver Bromide between the Silver and Bromide Photo, Auger and Recoil Electrons

λ (A.)	Percentage of Total Electron Energy in Group				
	$\mathrm{Ag}_{\mathrm{photo}}$	$\mathrm{Br}_{\mathrm{photo}}$	$\mathrm{Ag}_{\mathrm{Auger}}$	$\mathrm{Br}_{\mathrm{Auger}}$	Recoil
0·01	3	1	0	0	96
0·02	16	3	0	0	81
0·03	34	8	0	0	58
0·04	49	12	1	0	38
0·05	58	15	1	0	26
0·06	63	17	2	1	17
0·08	68	21	3	1	7
0·10	69	22	4	1	4
0·12	68	23	5	2	2
0·15	65	26	7	2	0
0·20	60	27	10	3	0
0·25	55	28	13	4	0
0·30	48	28	18	6	0
0·35	39	29	24	8	0
0·40	28	31	31	10	0
0·45	14	32	41	13	0

bromide and the gelatine in the ratio of the products of the number of electrons present and their stopping powers, i.e.

$$\frac{\text{Energy absorbed by AgBr}}{\text{Energy absorbed by gelatine}} = \frac{\text{Mass of AgBr}}{\text{Mass of gelatine}} \times \frac{\text{electrons/gm. AgBr}}{\text{electrons/gm. gelatine}}$$
$$\times \frac{\text{stopping power per electron of AgBr}}{\text{stopping power per electron of gelatine}}.$$

Let this be written $R_1 = R_{\mathrm{m}} \times R_{\mathrm{n}} \times R_{\mathrm{s}}$.

R_{m} is obtained as the ratio of the covering weights of silver bromide and gelatine. As there are $2{\cdot}65 \times 10^{23}$ electrons per gm. of silver bromide and $3{\cdot}21 \times 10^{23}$ per gm. of gelatine*, $R_{\mathrm{n}} = 0{\cdot}825$. The average atomic number associated with silver bromide electrons is 41·9 and that of gelatine electrons is 6·06. The relative stopping powers of electrons of these associated atomic numbers is 0·81, i.e. $R_{\mathrm{s}} = 0{\cdot}81$ (Gray 1949). Thus

$$R_1 = R_{\mathrm{m}} \times \frac{2{\cdot}65 \times 10^{23}}{3{\cdot}21 \times 10^{23}} \times 0{\cdot}81 = 0{\cdot}67 R_{\mathrm{m}}.$$

The fraction of the electron energy retained by the emulsion which is absorbed by the silver bromide is $R_1/(1+R_1)$. For our emulsion this fraction was 0·39.

(v) *Energy gained by Silver Bromide from Surrounding Material*

In order to calculate the energy absorbed by the silver bromide one further factor must be considered. Electrons released in the gelatine of the emulsion and in the material round the emulsion (film base, cassette, etc.) may be absorbed in the silver bromide. Consider a single silver bromide grain in a large volume of gelatine. If the ranges of the electrons liberated in the gelatine are large compared with the dimensions of the grain, the energy absorptions in the silver bromide and the gelatine, due to electrons liberated in the gelatine, are related by

$$\frac{\text{Ergs/gm. AgBr}}{\text{Ergs/gm. gelatine}} = \frac{\text{Electrons/gm. AgBr}}{\text{Electrons/gm. gelatine}} \times \frac{\text{Stopping power per electron of AgBr}}{\text{Stopping power per electron of gelatine}}$$
$$= R_{\mathrm{n}} \times R_{\mathrm{s}}. \qquad \ldots\ldots(5)$$

---

* The average composition by weight of photographic gelatine is carbon 50·8%, hydrogen 6·9% nitrogen 17·5% oxygen 23·9%, and sulphur 0·9% (Yagoda 1949).

For a given X-ray dose the electron energy released per gramme of gelatine is to the electron energy released per gramme of air as $[(\tau+\sigma_a)/\rho]_{\text{gel}}/[(\tau+\sigma_a)/\rho]_{\text{air}}$, fluorescence being negligible for these materials. Thus

$$\frac{\text{Ergs/gm. AgBr}}{\text{Ergs/gm. air}}=R_n R_s \frac{[(\tau+\sigma_a)/\rho]_{\text{gel}}}{[(\tau+\sigma_a)/\rho]_{\text{air}}}. \qquad \ldots\ldots(6)$$

In practice gelatine is not the only material giving rise to electrons that are absorbed in the silver bromide: some electrons originate in the emulsion mounting and the cassette. However, provided these materials are of low atomic number, this complication is of no consequence, for at wavelengths such that the electrons originating in the surrounding light atom material give rise to an appreciable fraction of the total energy absorbed by the silver bromide, τ is negligible for such material. Equation (6) can therefore be written:

$$\frac{\text{Ergs/gm. AgBr}}{\text{Ergs/gm. air}}=R_n R_s \frac{(\sigma_a/\rho)_{\text{gel}}}{(\sigma_a/\rho)_{\text{air}}}. \qquad \ldots\ldots(7)$$

But σ_a/ρ is proportional to electrons/gm., therefore

$$\frac{\text{Ergs/gm. AgBr}}{\text{Ergs/gm. air}}=R_s\times\frac{\text{electrons/gm. AgBr}}{\text{electrons/gm. gelatine}}\times\frac{\text{electrons/gm. gelatine}}{\text{electrons/gm. air}} \qquad \ldots\ldots(8)$$

$$=R_s\times\frac{\text{electrons/gm. AgBr}}{\text{electrons/gm. air}}. \qquad \ldots\ldots(9)$$

R_s has sensibly the same value, 0·81, whether the surrounding material is film base, paper, cardboard or Perspex. Inserting the constants in equation (9) we have

$$\frac{\text{Ergs/gm. AgBr}}{\text{Ergs/gm. air}}=0{\cdot}81\times\frac{2{\cdot}65\times10^{23}}{3{\cdot}01\times10^{23}}=0{\cdot}71. \qquad \ldots\ldots(10)$$

Thus the energy absorbed per gm. of a silver bromide grain from the surrounding light atom material is proportional to the energy absorption per gm. of air at the same point. As an energy absorption of 84 ergs/gm. of air is equivalent to a dose of 1 röntgen, a silver bromide grain receives from its surroundings $84\times0{\cdot}71=59{\cdot}5$ ergs/gm/r. (provided, of course, that electron ranges are greater than the grain dimensions and photoelectric absorption in the surrounding material is negligible).

Consideration has only been given so far to a single grain surrounded by material of low atomic number. In practice there are many grains and the space occupied by grains reduces the volume occupied by the gelatine. Therefore the electron energy originating in gelatine and other light atom material that is absorbed in the silver bromide is rather less than that indicated by equation (10). In our emulsion about 16% of the total volume was occupied by silver bromide. Therefore the calculated contribution to the energy absorption in the silver bromide of electrons liberated in the gelatine must be reduced by 16%. These electrons are recoil electrons for all wavelengths at which they contribute significantly to the energy absorption in the silver bromide, so the fraction of the total energy coming from the light atom material which originates in the gelatine is the same as the fraction of the recoil electron energy originating in the silver bromide which is retained by the emulsion. Calculations on this basis showed that allowance for the 'gelatine space' occupied by silver bromide reduced the overall energy absorption in the silver bromide by 0, 4, 6, 3½ and 1% at 0·01, 0·04, 0·06, 0·10 and 0·15 A. respectively. For most purposes this small correction could be ignored.

(vi) *Overall Energy Absorption in Silver Bromide*

The foregoing results may be combined to give the overall energy absorption in the silver bromide of an emulsion. As X-rays are normally measured in röntgens, 1 r. being equivalent to an energy absorption of approximately 84 ergs/gm. of air, it is convenient to determine the energy ratio ergs/gm. of silver bromide/ergs/gm. of air. The ergs/gm. of silver bromide/r. may then be computed.

For X-ray quanta converted by the silver bromide itself

$$\frac{\text{Ergs/gm. AgBr}}{\text{Ergs/gm. air}} = \frac{[(\tau+\sigma_{\mathrm{a}})/\rho]_{\mathrm{AgBr}}}{[(\tau+\sigma\ )/\rho]_{\mathrm{air}}} \times F_1 \times F_2 \times F_3; \quad \ldots\ldots(11)$$

where F_1 is a correction factor for energy lost by fluorescence and is given in Table 1, F_2 is a correction factor for electron energy lost from the emulsion and F_3 is a correction factor for energy lost to the gelatine.

For X-ray quanta converted in the light atom material round the silver bromide the energy ratio $=0{\cdot}71$ for all wavelengths at which this term is of significance (see equation (10)). For very precise work a small correction should be applied for that fraction of the emulsion volume which is not occupied by gelatine. Therefore, for all X-ray quanta:

$$\frac{\text{Ergs/gm. AgBr}}{\text{Ergs/gm. air}} = \frac{[(\tau+\sigma_{\mathrm{a}})/\rho]_{\mathrm{AgBr}}}{[(\tau+\sigma_{\mathrm{a}})]\rho]_{\mathrm{air}}} F_1 F_2 F_3 + 0{\cdot}71. \quad \ldots\ldots(12)$$

§ 7. COMPARISON OF THEORY AND EXPERIMENT

If the number of grains rendered developable is proportional to the energy absorbed by the grains the density/r. should be proportional to the energy ratio of equation (12) provided all exposures are in the range where density is proportional to exposure. In order to determine the variation of density/r. with wavelength, films were exposed to thirteen beams of heterogeneous X-radiation of effective wavelengths ranging from 0·020 A. to 0·354 A., the exposure in each case being such as to produce a density of about 0·5. The blackenings due to the ten beams of effective wavelength greater than 0·07 A. were all recorded on the same piece of film 16 × 6 cm. Effects due to variations in emulsion characteristics and development conditions were therefore reduced to a minimum. Also the distribution over the film of the exposed areas associated with each wavelength was such that any lack of uniformity in emulsion characteristics and development conditions would only increase the point scatter about the curve relating density/r. and wavelength, and would not affect the general shape of that curve. This procedure was repeated for five other strips of film, and when allowance was made for small (± 5%) variations in development, the average probable error of the measured density/r. was 1·8%.

Owing to the difficulty experienced at short wavelengths of effectively screening those parts of a film it was not desired to expose, all wavelengths could not be recorded on the same film. Separate films were exposed to the radiations of $\lambda_e = 0{\cdot}070$, 0·040, and 0·020 A. The probable error in the values of density/r. at these wavelengths must therefore be rather greater than at the longer wavelengths.

The effective wavelength of a beam was taken to be the wavelength of that monochromatic radiation which had the same linear absorption coefficient in silver when the thickness of absorber was extremely small. It was thought that this would give a wavelength approximately equal to that of the monochromatic radiation having the same absorption in a photographic emulsion.

In Figure 6 the experimental values of relative density/r. are compared with the energy ratio of equation (12). It is thought that the point scatter is due more to errors in λ_e than to errors in density/r. In particular it cannot be expected

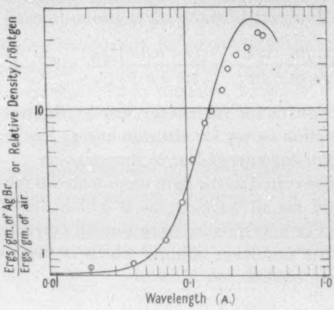

Figure 6. The theoretical wavelength variation of the ratio of the energy absorption/gm. silver bromide to the energy absorption/gm. air (full line) compared with experimental values of relative density/r. (points) for Ilford Line film.

that the experimental results should show such a sharp peak in the region of 0·3 A. as is shown by the theoretical curve, since it is at these longer wavelengths that the X-ray beams used are most heterogeneous.

The agreement between the theory and experiment seems to justify the conclusion that, for the emulsion used, the photographic density is approximately proportional to the energy absorbed by the silver bromide in the wavelength range investigated. It must be borne in mind, however, that a considerable amount of experimental data has been used in deriving the theoretical curve, some of which, e.g. 'foil' ranges of electrons, the form of the energy retention curve (Figure 5) and the values of $\tau+\sigma_a$ for air (see Greening 1948), are in need of additional confirmation.

§ 8. DISCUSSION

It appears that in the application of photographic emulsions to X-ray measurement, intensity variation may be ignored. Further, at low densities the density is usually proportional to the exposure, and providing investigations are confined to this density range, relative exposures of the same film can be obtained from relative densities without rigorous control of development conditions. In those investigations where X-rays are likely to be incident on the film at different angles it must be borne in mind that the blackening varies with angle of incidence. The theoretical explanation of this obliquity effect indicates that it should be less for emulsions of low silver coating weight than for those of high silver coating weight. Furthermore, if anomalous results are to be avoided, the film should normally be surrounded by a thickness of light atom material sufficient to establish electronic equilibrium in the emulsion. The only exception to this would seem to be in studies of the build-up of energy absorption in the neighbourhood of the interface between two different media. We do not propose to discuss these matters in greater detail here.

The variation of density/r. with wavelength does however seem to merit further discussion since it is the factor which imposes the greatest limitation on the application of existing photographic emulsions to X-ray measurement.

Evidence has been presented in this paper showing that at least approximate proportionality holds between photographic density and the energy absorbed by the silver bromide grains for wavelengths up to 0·354 A. Even if this is not so for all emulsions, and it is only true to say that the greater the energy absorption the greater the density, then any method of reducing the wavelength variation of the energy absorbed per röntgen in silver bromide should reduce the wavelength dependence of the film sensitivity. This may be done by reducing the first (wavelength dependent) term of equation (12) relative to the second (wavelength independent) term. Such a reduction may be effected either by reducing F_2 (by decreasing the emulsion thickness) or by reducing F_3 (by decreasing the silver bromide/gelatine ratio). Calculation shows that for a given reduction in silver covering weight it is better to reduce the silver bromide/gelatine ratio than to reduce the emulsion thickness. By using the lowest practical silver covering weight (a useful density must still be obtainable) and the highest practical emulsion thickness, i.e. the lowest practical silver bromide/gelatine ratio, it should be possible to produce a film which has a sensibly constant density/r. for all wavelengths less than about 0·1 A. and a much reduced variation of density/r. with wavelength at longer wavelengths.

Such a film would have many applications in the measurement of very high energy quanta such as are emitted by betatrons, synchrotrons, linear accelerators, Van de Graaff machines and radioactive substances. If used in the 'film badges' carried by personnel exposed to stray radiation from these sources the blackening observed could be expressed in röntgens more accurately than is possible at present, but it may be difficult to retain sufficient sensitivity for this latter application.

In conclusion it may be noted that the theory of §6 may be applied to the calculation of the effects of variations of emulsion thickness and silver/gelatine ratio on the speed of X-ray emulsions. Also the fact that at short wavelegnths a considerable proportion of the photographic blackening is produced by electrons liberated by quanta absorbed in material other than the silver bromide grains, would seem to imply that the currently used terms 'quantum efficiency' and 'quantum yield' (i.e. the number of grains rendered developable per quantum absorbed by the silver bromide) are of rather vague significance when applied to photographic measurements at short X-ray wavelengths.

ACKNOWLEDGMENTS

The experimental work for this investigation was done while the author was working at Westminster Hospital in a department supported in part by the funds of the British Empire Cancer Campaign. The author wishes to thank Dr. C. W. Wilson for discussions during the early part of the work and for his advice during the preparation of this paper. It is a pleasure to acknowledge the kindness of Mr. G. S. Innes in making available the 1 MeV. X-ray machine of St. Bartholomew's Hospital and thus making possible the investigations at wavelengths less than 0·1 A.

APPENDIX

THE SELF-ABSORPTION OF AN INFINITE SHEET EMITTING ELECTROMAGNETIC RADIATION ISOTROPICALLY

Let the thickness of the sheet be T and let its linear absorption coefficient for the radiation it emits be μ.

If N quanta are emitted per cm^3 the number emitted by a volume element of area dA and thickness dz between θ and $\theta + d\theta$ (see Figure 4) is

$$N\,dz\,dA\,2\pi r(r^2+z^2)^{1/2}\,d\theta/4\pi(r^2+z^2) = \tfrac{1}{2}N\,dz\,dA\sin\theta\,d\theta.$$

The number of quanta between θ and $\theta + d\theta$ escaping from the sheet

$$= \tfrac{1}{2}N\,dz\,dA\sin\theta\,e^{-\mu z/\cos\theta}\,d\theta.$$

The total number from the volume element escaping from the right-hand surface of the sheet

$$= \int_{\theta=0}^{\pi/2} \tfrac{1}{2}N\,dz\,dA\sin\theta\,e^{-\mu z/\cos\theta}\,d\theta.$$

Total number from volume of area dA and thickness T escaping from the right-hand surface

$$\doteq \int_{\theta=0}^{\pi/2}\int_{z=0}^{T} \tfrac{1}{2}N\,dA\sin\theta\,e^{-\mu z/\cos\theta}\,d\theta\,dz.$$

But the total number from this volume emitted towards the right-hand surface is $\frac{1}{2}NT\,dA$; therefore the fraction F escaping is

$$\frac{1}{T}\int_{\theta=0}^{\pi/2}\int_{z=0}^{T} \sin\theta\,e^{-\mu z/\cos\theta}\,d\theta\,dz = \frac{1}{\mu T}\int_{\theta=0}^{\pi/2} \sin\theta\cos\theta(1-e^{-\mu T/\cos\theta})\,d\theta$$

$$= \frac{1}{2\mu T} - \frac{1}{\mu T}\int_{0}^{\pi/2} \sin\theta\cos\theta\,e^{-\mu T/\cos\theta}\,d\theta.$$

Putting $\mu T/\cos\theta = y$, which is known to be useful with similar integrals, we have $\sin\theta = -d(\cos\theta) = (\mu T/y^2)\,dy$ and

$$F = \frac{1}{2\mu T} - \mu T\int_{\mu T}^{\infty} \frac{e^{-y}}{y^3}\,dy \qquad \ldots\ldots(13)$$

or, as

$$\int_{\mu T}^{\infty} \frac{e^{-y}}{y^n}\,dy = \frac{1}{(\mu T)^{n-1}}\int_{1}^{\infty} \frac{e^{-\mu T y}}{y^n}\,dy,$$

$$F = \frac{1}{\mu T}\left(\frac{1}{2} - \int_{1}^{\infty} \frac{e^{-\mu T y}}{y^3}\,dy\right).$$

This integral has been tabulated by Placzek (1945). Alternatively, integrating (13) by parts twice, we have

$$F = \frac{1}{2\mu T} - \frac{e^{-\mu T}}{2\mu T} + \frac{e^{-\mu T}}{2} - \frac{\mu T}{2}\int_{\mu T}^{\infty} \frac{e^{-y}}{y}\,dy,$$

and this integral has been more extensively tabulated (e.g. Glaisher 1870, Miller and Rosebrugh 1903, Federal Works Agency 1940). Values of F for a range of values of μT are given in Table 3. For values of μT greater than 5, $F = 1/2\mu T$ to better than 0·1% For higher values of μT the fraction escaping is approximately $1/2\mu T$.

To apply these results to the problem of the absorption of characteristic radiation by a photographic emulsion, an intensity ratio of 4:1 was assumed between silver K_α and K_β radiation giving an effective wavelegnth for silver K

Table 3. The Fraction F of the Radiation Escaping from a Sheet of Thickness T and Linear Absorption Coefficient μ

μT	F	μT	F	μT	F
0·01	0·972	0·25	0·701	0·80	0·445
0·02	0·952	0·30	0·666	0·90	0·416
0·04	0·917	0·35	0·635	1·00	0·390
0·06	0·887	0·40	0·607	1·50	0·296
0·08	0·861	0·45	0·581	2·00	0·235
0·10	0·837	0·50	0·557	2·50	0·194
0·15	0·785	0·60	0·514	3·00	0·164
0·20	0·740	0·70	0·477	4·00	0·124

radiation of 0·546 A., and an approximate mass absorption coefficient μ/ρ in silver bromide of 24. Similarly for bromine characteristic radiation the effective wavelength was taken as 1·017 A. and μ/ρ in silver bromide was taken as 56.

Thus for an emulsion having 0·001 gm. of silver bromide per cm^2, $\mu T = 0·024$ and 0·056 for the silver and bromine characteristic radiations respectively, giving the result that over 90% of the characteristic radiation escapes from the emulsion.

The author is indebted to the referee for drawing his attention to a paper by Tellez-Plasencia and Theron (1950), in which is computed the amount of fluorescence radiation absorbed at any point in an emulsion but originating elsewhere in the emulsion. The treatment is necessarily more complex than that given above and has applications to the calculation of the broadening of line images by fluorescence radiation.

REFERENCES

Becker, A., and Kipphan, E., 1931, *Ann. Phys., Lpz.*, **10**, 15.

Bell, G. E., 1936 a, *Brit. J. Radiol.*, **9**, 578 ; 1936 b, *Ibid.*, **9**, 688.

Berg, W. F., 1948, *Rep. Prog. Phys.*, **11**, 248 (London : Physical Society).

Berthold, R., 1925, *Ann. Phys., Lpz.*, **76**, 409.

Berthold, R., and Glocker, R., 1925, *Z. Phys.*, **31**, 259.

Bothe, W., 1922, *Z. Phys.*, **8**, 243.

Bouwers, A., 1923, *Z. Phys.*, **14**, 374.

Brindley, G. W., and Spiers, F. W., 1933, *Phil. Mag.*, **16**, 686.

Broili, H., and Kiessig, H., 1934, *Z. Phys.*, **87**, 425.

Bromley, D., and Herz, R. H., 1950, *Proc. Phys. Soc.* B, **63**, 90.

Charlesby, A., 1940, *Proc. Phys. Soc.*, **52**, 657.

Compton, A. H., and Allison, S. K., 1935, *X-rays in Theory and Experiment* (New York : Van Nostrand), p. 488.

Cowing, R. F., and Spalding, C. K., 1949, *Radiology*, **52**, 423.

Cranberg, L., and Halpern, J., 1949, *Rev. Sci. Instrum.*, **20**, 641.

Dershem, E., 1932, *Phys. Rev.*, **42**, 908.

Ellis, C. D., and Wooster, W. A., 1927, *Proc. Roy. Soc.* A, **114**, 266.

Federal Works Agency, Works Projects Administration, City of New York, 1940, *Tables of Sine, Cosine and Exponential Integrals.*

Friedrich, W., and Koch, P. P., 1914, *Ann. Phys., Lpz.*, **45**, 399.

Glaisher, J. W. L., 1870, *Phil. Trans. Roy. Soc.*, **160**, 367.

Glocker, R., and Traub, W., 1921, *Phys. Z.*, **22**, 345.

Gray, L. H., 1949, *Brit. J. Radiol.*, **22**, 677.

Greening, J. R., 1948, *Brit. J. Radiol.*, **21**, 75.

Herz, R. H., 1949 a, *Photogr. J.* B, **89**, 89; 1949 b, *Phys. Rev.*, **75**, 478.

Hirsh, F. R., 1935, *J. Opt. Soc. Amer.*, **25**, 229.

Jauncey, G. E. M., and Richardson, H. W., 1934, *J. Opt. Soc. Amer.*, **24**, 125.

Kroncke, H., 1914, *Ann. Phys., Lpz.*, **43**, 687.

Lea, D. E., 1946 a, *Actions of Radiations on Living Cells* (Cambridge : University Press), p. 24; 1946 b, *Ibid.*, p. 12.

Luft, F., 1933, *Veröff. des Wiss. Zentral-Lab. Agfa*, **3,** 245.
Mayneord, W. V., and Roberts, J. E., 1937, *Brit. J. Radiol.*, **10,** 365.
Miller, W. L., and Rosebrugh, T. R., 1903, *Trans. Roy. Soc. Canada*, **9,** 73.
Morgan, R. H., 1944, *Radiology*, **42,** 471.
Mülbach, E., 1937, *Z. wiss. Photogr.*, **36**, 269.
Nacken, M. J., 1930, *Phys. Z.*, **31,** 296.
Nutting, P. G., 1913, *Phil. Mag.*, **26,** 423.
Pelc, S. R., 1945, *Proc. Phys. Soc.*, **57,** 523.
Placzek, G., 1945, *Math. Tables Project*, Report No. M.T.1.
Rogers, J. S., 1931, *Proc. Phys. Soc.*, **43,** 59.
Rosenberger, H., and Goldhaber, G., 1934, *Strahlentherapie*, **51,** 45.
Silberstein, L., 1922, *Phil. Mag.*, **44,** 257 and 956.
Spiers, F. W., 1949, *Brit. J. Radiol.*, **22,** 521.
Tasker, H. S., 1945, *Photogr. J.* B, **85,** 75.
Tellez-Plasencia, H., and Theron, P., 1940, *Sci. Indust. Photogr.*, **21,** 361.
Victoreen, J. A., 1943, *J. Appl. Phys.*, **14,** 95.
Williams, E. J., 1931, *Proc. Roy. Soc.* A., **130,** 310.
Yagoda, H., 1949, *Radioactive Measurements with Nuclear Emulsions* (New York : Wiley), p. 87.
Zajac, B., and Ross, M. A. S., 1949, *Nature, Lond.*, **164,** 311.

A Study of Rectification Effects at Surfaces of Germanium and Lead Sulphide

By C. A. HOGARTH and J. W. GRANVILLE
Physics Department, The University, Reading, Berks.

Communicated by R. W. Ditchburn; *MS. received* 2nd *May* 1951.

ABSTRACT. Previously reported results of polishing and chemically etching the surfaces of germanium crystals are confirmed. The effects of vacuum heat treatment are investigated and it is found that treatment of this kind at temperatures between 500 and 900° c. can improve the rectification characteristics considerably. The treatment does not spoil the optical quality of a polished surface and in this connection may provide an advantage over chemical etching. Similar effects are obtained with deficit-conducting lead sulphide. Modifications to the surface structures of the crystals by various treatments are investigated by electron diffraction.

§ 1. INTRODUCTION

It has been known for a number of years that if a metal is polished, a surface layer of character different from that of the bulk, frequently referred to as a Beilby layer, is produced. Work performed on germanium rectifiers (see Benzer 1949) has shown that diodes with poor rectification characteristics are obtained if the point contact is placed on a polished surface, and special etching techniques were developed. When the surface layer has been removed by etching, the rectification characteristics are greatly improved and the value of the peak back-voltage may be increased considerably.

In a previous communication (Granville and Hogarth 1951), the authors have described how the surface layers produced by polishing germanium and lead sulphide specimens can modify the point-contact thermo-electric effects. Chemical etching and heat treatment *in vacuo* were found to reduce or to suppress entirely the anomalous thermo-electric effects found for polished surfaces. In the present work the results of these treatments on the rectification characteristics of germanium and lead sulphide crystals are examined. Thermal treatment *in vacuo* can improve the rectification characteristics, and the effect of this treatment on the surfaces of germanium crystals is examined by electron diffraction.

§ 2. EXPERIMENTAL METHODS

The probe contact manipulator previously described (Granville and Hogarth 1951) was employed for the investigation of the diode properties of various germanium and lead sulphide surfaces. A simple electrical circuit was employed and the voltage–current characteristics were displayed on a calibrated D.C. oscilloscope. The whisker contact was made from 0·005 in. tungsten wire pointed by electrolytic etching and a contact thrust of 3 gm. wt. was employed. The investigation showed that when the point was clean and not seriously blunted the exact diameter of the contact point was not a critical factor affecting the diode characteristic. Reproducibility could, therefore, be obtained with the above arrangement.

Of the various parameters associated with a high inverse voltage diode, the peak back-voltage was selected for measurement as this is a quantity which gives a useful indication for the performance of rectifiers of this type (Benzer 1949), and which can be rapidly measured. In some experiments peak inverse power was also measured.

A particular spot on the semiconductor surface could not be precisely located after the specimen had been removed from the bed of the manipulator for heat treatment. Thus, to form an estimate of the changes produced by surface treatment, a method of averaging had to be employed. A small area, about 4 mm^2, was located on the surface under investigation, either by coordinates drawn with a diamond or, where this was impracticable, by the natural contours of the surface. In this area fifty separate contacts were made in succession in a regular network, and the arithmetic mean of the fifty values of peak back-voltage was taken as characteristic of the small region of surface. This method gave reproducible values for the average peak back-voltage.

Cleaved surfaces were obtained by shattering a germanium ingot or a lead sulphide crystal, and the freshly broken surface could be tested without further treatment. Where perfectly plane cleaved surfaces were not available on a particular specimen, the flattest area available was tested. Polished surfaces were usually prepared by grinding with Aloxite 50 and polishing with 0000 emery paper. Chemical etching of germanium was carried out with a mixture of HF, HNO_3, and water containing a trace of cupric nitrate.

Heat treatments up to 900° C. were carried out on certain of the germanium specimens and it was not, therefore, practicable to make permanent soldered connections to the germanium to act as large area base electrodes; instead, the specimen was held firmly in a clip. A contact of low resistance was still obtained and there was no observable change in the measured peak back-voltage compared with measurements made using a soldered base electrode. The heat treatment was performed in an all-glass vacuum system at a pressure of 10^{-4} to 10^{-5} mm. Hg.

Two types of heat treatment were employed, to illustrate the effects of varying the temperature and the duration of heating. Firstly, the germanium specimen was polished, tested for rectification and then heated for 1½ hours at 200° C. It was then removed from the furnace and tested again, and the process was repeated at 400° c., 600° c., 800° c. and 900° c. The second type of experiment involved the vacuum treatment of germanium specimens at 500° c. for various periods, allowing the specimen to cool between each heat treatment. The heat treatment of lead sulphide was carried out in a similar manner except that temperatures were much lower.

It is known that thin films of germanium deposited by vacuum evaporation on to unheated substrates show a very low degree of order as determined by electron diffraction tests. This is also in agreement with the results of electrical measurements on such films. Layers deposited in this way on etched germanium substrates produced marked changes in the photo-voltaic and thermo-electric properties. It therefore seemed desirable to see whether there are corresponding changes in the rectification properties. The procedure adopted was to polish and etch chemically a germanium crystal, and measure the average peak back-voltage and current for a given small area. A film of germanium was then deposited and the average peak back-voltage and current of the same area was measured. The crystal was then again etched and tested, a new film deposited, and so on. The film thicknesses were measured by the multiple-beam interferometry technique as described by Tolansky (1948).

The germanium specimens used, which included both polycrystalline and single crystal specimens, were taken from ingots supplied by Messrs. Johnson, Matthey, or from material re-cast in these laboratories. The lead sulphide specimens used were from photo-voltaic cells of German origin, and had shown the transistor effect (Banbury, Gebbie and Hogarth 1951). Their voltage–current characteristics have been described by Henisch and Granville (1951).

§ 3. EXPERIMENTAL OBSERVATIONS

The results of experiments on rectification properties may be summarized as follows:

(i) The results of polishing and chemically etching germanium surfaces are shown in Table 1. The internal consistency of the results shows that the present experimental method is a useful one for testing the diode characteristic, and the results are in agreement with those reported by Benzer (1949).

Table 1. Average Peak Back-Voltages for Germanium after various Surface Treatments

Specimen no.	B11	A8	B4	E14
Cleaved surface	47	34	49	18
Polished surface	23	20	21	13
Polished and etched surface	55	29	55	22

(ii) Figure 1 shows the average peak back-voltage on two polished surfaces and one cleaved surface of a germanium crystal after heating to different temperatures. The cleaved surface was examined for comparison with the polished ones. Up to 600° c. the average peak back-voltage for the cleaved surface is approximately constant while that on each polished surface steadily increases to about double its original value. At higher temperatures the values of peak back-voltages decrease for each surface. The most rapid rise of peak back-voltage occurs for heat treatment at about 500° c.

(iii) Figure 2 shows the average peak back-voltage on a cleaved surface and two polished surfaces of germanium after heating to 500° c. for different periods.

For the first half-hour the value on the cleaved surface remains substantially constant, while those for the polished surfaces increase to more than double their original values. After this time the three surfaces behave in a similar manner indicating that any further changes occurring are not due to the different initial characters of the surfaces.

(iv) Table 2 shows the results of tests made on seven germanium specimens after heating to various temperatures for one hour. The average peak back-voltages on polished surfaces have all greatly increased after baking while those on cleaved surfaces have remained almost unaltered. For specimens B16 and B17 the effect of chemical etching *after* the vacuum heat treatment was examined, and the values of peak back-voltage were found to have increased slightly. This behaviour is similar to that reported by Benzer (1949) for the effect of etching cleaved surfaces.

Table 2. Average Peak Back-Voltages for Germanium after various Heat Treatments

Specimen No.		Before heating.		Baking temp.	After heating	
		Polished	Cleaved	(°c.)	Polished	Cleaved
I	B 16	18	36	900	35	39
II	B 17	16	30	900	30	31
III	B 24	12	32	600	23	34
IV	B 24	15	32	600	32	34
V	B 25	11	23	600	18	24
VI	B 26	15	43	500	40	44
VII	B 26	16	43	500	38	44

(v) Examination with a high-power microscope failed to indicate any change in appearance of the polished germanium surfaces after thermal treatment.

(vi) The surfaces produced by thermal treatment are very stable and tests made over a period of weeks show no change in values of peak back-voltage.

(vii) It was found that the rectification efficiency of a cleaved crystal of PbS was also reduced by polishing. A suitable etching solution is not described in the literature and various possibilities were tried. It was found that a 60% solution of perchloric acid, used in the form of a drop, in contact with the polished surface for a few minutes caused a considerable improvement in rectifying properties. A typical increase in peak back-voltage was from 6·5 to 9·5 volts.

(viii) Figure 3 shows the effect of vacuum treatment on two polished surfaces of deficit-conducting lead sulphide. The effects of vacuum treatment for various periods at 100° c. are shown, and it is seen that the peak back-voltage increases by about 15% for treatments up to 30 minutes and then remains constant.

(ix) It was observed that the deposition of an amorphous germanium layer on the etched surface of a germanium crystal impaired the rectifier performance. Figure 4 (*a*) shows that there is a gradual decrease of the peak back-voltage as the layer thickness increases. The average peak inverse current is greater for thicker layers as shown in Figure 4 (*b*). Values of peak back-voltage and current for the same area, which had been polished *after* the evaporation experiments, are also recorded in Figure 4. The peak inverse power, measured by taking the average of the products of voltage and current at the turnover region, is plotted as a function of thickness of the layer in Figure 4 (*c*), and is seen to be substantially constant and of similar value to that shown for the etched and polished surfaces.

§4. ELECTRON DIFFRACTION EXPERIMENTS

Electron diffraction reflection photographs were taken for various germanium surfaces using a 75 kv. beam and with a distance of 25 cm. from specimen to screen.

Typical results are given in Figure 5 (Plate *). Figure 5 (*a*) shows such a photograph for a polished and chemically etched surface of a germanium specimen cut from a small ingot. Figure 5 (*b*) shows the result for the same specimen after grinding and polishing its surface and Figure 5 (*c*) the result for the ground and polished surface after treatment at 450° c. for $1\frac{1}{2}$ hours. The presence of sharp spots but absence of Kikuchi lines in Figure 5 (*c*) shows that the previous amorphous layer has recrystallized into fairly large, but not perfect, crystals.

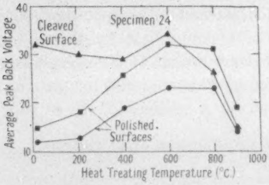

Figure 1. Average peak back-voltage on cleaved and polished surfaces of germanium after vacuum-baking at various temperatures for $1\frac{1}{2}$ hours.

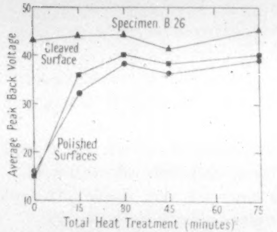

Figure 2. Average value of peak back-voltage on cleaved and polished surfaces of germanium as a function of duration of baking at 500° c.

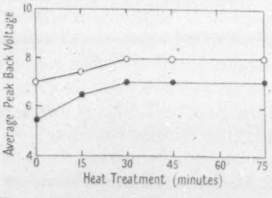

Figure 3. Changes in performance of two lead sulphide rectifiers after vacuum treatments at 100° c.

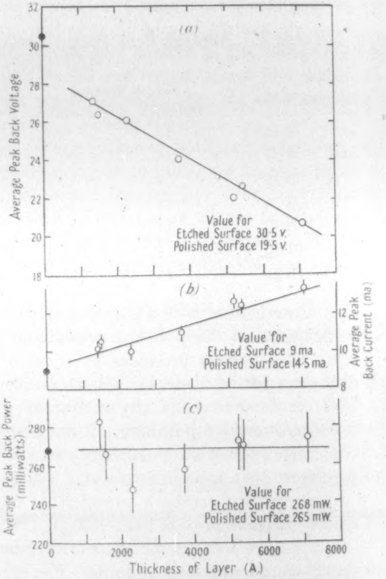

Figure 4. (*a*) peak back-voltage, (*b*) peak inverse current and (*c*) peak inverse power as functions of thickness of deposited amorphous layer on germanium.

---

* For Plates see end of issue.

Examination of several photographs taken after the crystal had been heated to 400–500° C. *in vacuo* has shown that there is no generally preferred direction of orientation of these crystallites. Figure 5 (*d*) shows the same crystal surface after further vacuum treatment at 850° C. The crystalline character of the surface is now comparable with that of a chemically etched specimen. Photographs taken with an evaporated layer of germanium on a substrate of polished and chemically etched germanium show an amorphous structure for the film much as in Figure 5 (*b*). The electron diffraction results thus confirm the nature of the surface processes as inferred from the electrical measurements.

§ 5. DISCUSSION

The experimental results described here show how the various treatments given to the surfaces of germanium and lead sulphide can modify their rectifying properties. They are consistent with the view that polishing the crystals produces an amorphous surface layer and that this layer can be removed by chemical etching or by thermal treatment *in vacuo*. In the case of germanium, a layer with similar properties may also be produced by the deposition of a thin germanium film evaporated on to an unheated etched surface of germanium.

The production of a crystalline surface by heat treatment of a polished or evaporated layer is similar to the results of Finch (1937) who found that polished calcite surfaces appeared amorphous when examined by electron diffraction, but that recrystallization occurred on heating. In the case of germanium, when the finish of the surface is of importance, and where specimens of particular shape, e.g. curved surfaces for infra-red lenses, are required, recrystallization of the amorphous polish layer may be preferable to its removal by chemical etching. The experiments in which the amorphous surface layer is simulated by means of an evaporated film enable us to form an estimate of the thickness of the layer produced by polishing the crystal. If the lines of Figures 4 (*a*) and 4 (*b*) are extrapolated to the values of peak back-voltage and current for the same surface after grinding and polishing, a value may be deduced which for this particular specimen is 8,000 A. This is of the order previously suggested by König (1948) in a general discussion of Beilby layers. Interferometric studies of a polished germanium crystal which had undergone a representative etching process as used in these experiments yielded an upper limiting value of 10^{-4} cm. for the thickness of the layer produced by the polishing process.

The constancy of the peak inverse power for different surface treatments of the germanium shown in Figure 4 (*c*), is in agreement with the view put forward by Hunter (1951), and verified by Bennett and Hunter (1951), that the maximum inverse voltage is determined by thermal effects at the contact. A detailed theoretical analysis of the conditions which obtain at a point contact in the presence of an amorphous surface film would demand a knowledge of the energy relations in an amorphous substance as well as information concerning surface levels. There is also the possibility of current spreading within the amorphous film and of rectification effects at the junction between the amorphous and crystalline material. In this case increasing the film thickness would increase the spreading and hence the area of current flow at this junction. The system is thus too complicated to lead to detailed conclusions concerning mechanisms by which the presence of evaporated or polish layers produce the effects here described.

Previous work on the voltage–current characteristics of lead sulphide crystal diodes (Henisch and Granville 1951) has shown a great similarity between this material and germanium. The similarity may again be noted when the results of chemical etching and vacuum heat treatment of surfaces of the two materials are compared.

ACKNOWLEDGMENTS

The authors would like to make grateful acknowledgment to Professor R. W. Ditchburn for his encouragement in this work and to Dr. T. B. Rymer and Dr. H. K. Henisch for helpful advice and stimulating discussions.

REFERENCES

Banbury, P. C., Gebbie, H. A., and Hogarth, C. A., 1951, *Semi-Conducting Materials*, Ed. H. K. Henisch (London : Butterworth's Scientific Publications), p. 78.
Bennett, A. I., and Hunter, L. P., 1951, *Phys. Rev.*, **81**, 152.
Benzer, S., 1949, *J. Appl. Phys.*, **20**, 804.
Finch, G. I., 1937, *Trans. Faraday Soc.*, **33**, 425.
Granville, J. W., and Hogarth, C. A., 1951, *Proc. Phys. Soc.* B, **64**, 488.
Henisch, H. K., and Granville, J. W., 1951, *Semi-Conducting Materials*, Ed. H. K. Henisch (London : Butterworth's, Scientific Publications), p. 87.
Hunter, L. P., 1951, *Phys. Rev.*, **81**, 151.
König, H., 1948, *Optik*, **3**, 201.
Tolansky, S., 1948, *Multiple-beam Interferometry* (Oxford : Clarendon Press).

A Vibrating Cantilever Method for the Investigation of the Dynamic Elasticity of High Polymers

By K. W. HILLIER
Imperial Chemical Industries Ltd., Butterwick Research Laboratories, Welwyn, Herts.

MS. received 10*th May* 1951

ABSTRACT. A method is described for obtaining dynamic values of Young's modulus at low frequencies (20 c/s. to 100 c/s.) by using the forced resonance of a vibrating cantilever. Provision has been made for keeping the apparatus at a constant temperature and a few measurements of the dynamic modulus are given for polythene at 30° c. and 40° c. The theory of the vibrations of a cantilever including viscous internal damping is discussed. The results continue previous work carried out at higher frequencies by a different method and indicate the continuity of the dynamic modulus–frequency relation between 20 kc/s. and 20 c/s. for polythene. 'Static' measurements have also been carried out and agree with those published earlier. Even at the lowest frequency the dynamic modulus is still three times the 'static' value; and it is concluded that lower frequencies should be investigated.

§1. INTRODUCTION

In recent papers from this laboratory (Hillier and Kolsky 1949, Hillier 1949) on the dynamic elasticity of high polymers it was concluded that the measurements should be extended in frequency so as to cover as wide a range as possible. The method described in those papers has been exploited as far as possible and results have been obtained over a range of frequencies from 0·5 kc/s. to 30 kc/s. For accurate measurements of the velocity of sound (the method employed to determine the dynamic value of Young's modulus) a filament at least as long as two wavelengths of sound in the material at the imposed frequency is needed. For most high polymers having a velocity of sound of the order 10^5 cm/sec. at ordinary temperatures the wavelength at 0·5 kc/s. is 200 cm. This is practically the limit of the constant temperature apparatus that was available and other methods of measurement applicable to lower frequencies were considered. Since it was thought desirable to continue to measure Young's modulus two modes of oscillation of the specimen were considered: longitudinal compression and expansion and transverse oscillations of a beam, in particular, a cantilever. The latter appeared to offer advantages as it was simpler to clamp; also, values of the 'static' modulus at comparable strains could be obtained. An apparatus was therefore designed and built employing this method.

§ 2. METHOD

The method is illustrated in Figure 1. The specimen is rigidly clamped at one end and has a small magnetic pole piece A at the other. A polarizing field from a D.C. electromagnet B was applied and the specimen made to vibrate by the coil C through which was fed an alternating current of variable frequency. The amplitude of the oscillations of the end A of the specimen was measured by the travelling microscope M. This end of the specimen was illuminated by a stroboscope S whose frequency was adjusted until the vibrations appeared sufficiently slow for accurate measurements to be made. The resonant frequency of the specimen could then be determined and, from this the elastic modulus of the material. The method was successfully used by Davies and James (1934) to measure the elastic modulus of metal specimens, and a full account of the theory is given in their paper.

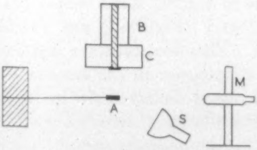

Figure 1.

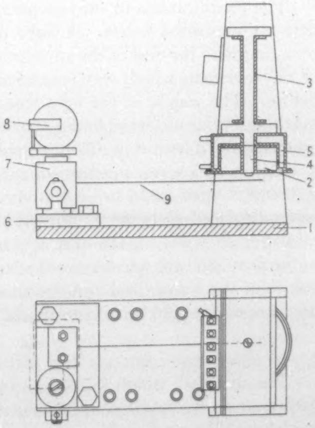

Figure 2.

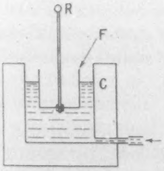

Figure 3.

In previous work (Hillier 1949) it has been shown that the 'static' modulus derived from an ordinary tensile test on monofilaments differed considerably from the dynamic modulus derived from the velocity of propagation of sound along the monofilament. Some doubt as to the validity of the comparison wa raised since the measurements in the dynamic test involved only very small strains of the order 0·01 % whereas the tensile test could not be used with less than 1 % strain. With the vibrating cantilever method identical strains could be used and a truer comparison made.

§ 3. APPARATUS

The apparatus was constructed with a duralumin frame to reduce spurious magnetic effects and this frame carried the specimen clamp and coils with their soft iron core. It is shown, not to scale, in Figure 2. The main frame 1 held the coil formers, 2 and 3, soft iron core 4, and a water cooling jacket 5 surrounding the driving coil. The base of the frame was drilled and tapped at several points so that the platform 6 could be fastened at several distances from the axis of the coils thus giving lengths of specimens between 5 and 20 cm. This platform carried the specimen clamp 7 and a reversible electric motor drive 8 to move the specimen in a plane parallel to the axis of the coils. The whole apparatus was put inside a constant temperature oven so that the temperature could be maintained to within 1° c. The specimen 9 was viewed through the glass door of the oven by a long focus travelling microscope which was fitted with a micrometer eyepiece to give accurate measurements of the amplitude of vibration. The specimen was illuminated by a stroboscope (Scophony Type HPS) also placed outside the oven. The D.C. polarizing coil was fed from a 24 v. accumulator battery with a rheostat and ammeter to control the current. The driving coil was fed from a 70-watt power amplifier excited by a wide-band resistance capacity oscillator (Dawe Instruments Type 400B) whose frequency was checked against a standard frequency crystal oscillator by an oscilloscope.

The modifications to the equipment necessary to obtain 'static' stress–strain data are described below. A light duralumin float F (Figure 3) was attached by a ring R to the end of the cantilever specimen. This float caused a deflection of the specimen which was measured with the microscope in the same way as before. The weight of the float was so adjusted that it deflected the bar to the maximum value observed in the dynamic tests. The 'Perspex' cistern C was then gradually filled with water from outside the constant temperature oven by raising a reservoir on a screw mechanism and readings of the specimen position and the water level were made at fixed intervals. A simple calculation of the volume of water displaced gives the increment of force removed from the specimen. The measurements were made only when the water level was on the vertical sides of the float and care was taken not to trap a bubble of air beneath the float. From values of the water level and specimen deflection the stress and also the strain on the specimen can be calculated and the value of the 'static' modulus obtained.

§ 4. EXPERIMENTAL

The specimen which was 3 mm. square and 10 cm. long was fitted at one end with a small mild steel pin (1·6 mm. diameter, 8·4 mm. long) by heating the pin to about 150° c. and pushing it into the specimen for about half its length. The end of the pin was ground flat and polished and a fine scratch made across it. The specimen was then clamped so that the scratch on the pin was perpendicular to the plane of vibration. The apparatus was placed in the oven, and when at the set temperature, the position of the specimen was adjusted to a convenient distance from the coils by the electric drive on the specimen clamp. The polarizing field was switched on and the current adjusted to the maximum value to be used, generally 1·0 amp. The driving coil was then energized and the variation in the amplitude of oscillation with frequency, the resonance curve, obtained; this amplitude was measured at set frequencies about 1 to 2 c/s. apart. The polarizing current was reduced to a lower value and the position of the specimen altered until the centre of the oscillations was the same as that observed at the higher current. Since the field strength is a function of the distance from the coil as well as a function of the current through it only by thus keeping the distance constant could the variation in the current be used as a measure of the field strength. Resonance curves were plotted for four or five different values of the polarizing coil current: a typical set is shown in Figure 4. The frequency at which the maximum amplitude occurred was ascertained and plotted against polarizing current and the line extrapolated to zero current, i.e. zero field strength, as in Figure 5. This extrapolated value of the frequency was taken as the resonant frequency of the specimen in a similar manner to that described by Davies and James (1934). The measurements were repeated for different lengths of specimen and at different temperatures. From these values of the resonant frequency f_0 at zero field strength the elastic modulus was calculated as described below.

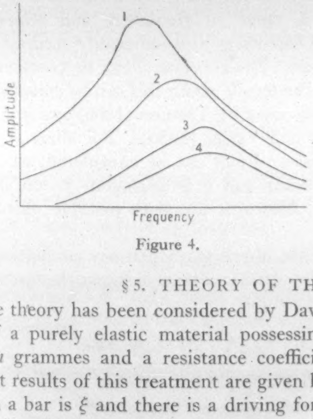

Figure 4.

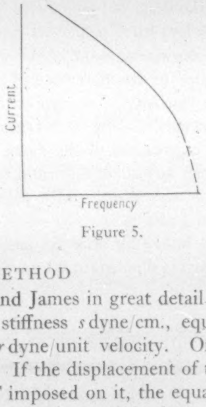

Figure 5.

§ 5. THEORY OF THE METHOD

The theory has been considered by Davies and James in great detail for the case of a purely elastic material possessing a stiffness s dyne/cm., equivalent mass m grammes and a resistance coefficient r dyne/unit velocity. Only the relevant results of this treatment are given here. If the displacement of the end of such a bar is ξ and there is a driving force F imposed on it, the equation of motion is $md^2\xi/dt^2 + rd\xi/dt + s\xi = F$. When $F = 0$ and r is small the free resonant frequency of the system f_0 will give a measure of the stiffness since $f_0 = (s/m)^{1/2}/2\pi$.

In actual experiments the value of the amplitude of the displacement ξ_m is observed as a function of f and the variation of this function studied as a function of the polarizing current. It has been shown that the maximum value of ξ_m occurs at a frequency f_1 differing from and always less than f_0. To obtain a value for f_0 the values of f_1 at differing field strengths must be extrapolated to zero field strength and driving signal.

The transverse vibrations of a thin elastic rod having a mass M attached at the free end have been fully discussed by Prescott (1946). If the rod is of length l, cross sectional area a and density ρ and is composed of material with Young's modulus E, the frequency of the fundamental normal mode f_0 is given in the equation

$$(k/2\pi)(E/\rho)^{1/2} = l^2 f_0/z^2 \qquad \ldots\ldots(1)$$

where k is the radius of gyration of the cross section perpendicular to its plane of motion and z is given in the equation

$$\frac{1+\cosh z\cos z}{\cosh z\sin z-\sinh z\cos z}=cz, \qquad \ldots\ldots(2)$$

c being the ratio of the mass at the end M to the mass of the rod ρla. A graphical method was used to determine z by which it was possible to obtain values accurate to within 0·2% without any difficulty. By using the value of f_0 obtained by extrapolation to zero field strength as explained above and this value z, the modulus E could be determined.

The theory has so far been confined to purely elastic materials and it is now proposed to indicate the deviation from this theory to be expected when using high polymer materials. It is well known (Alfrey 1948) that such materials do not obey a simple Hooke's law and that time derivatives of the strain must be incorporated in any stress–strain relationship. The simplest form of this is given in Voigt's equation $\sigma=E\epsilon+\zeta d\epsilon/dt$ where σ is the stress, E the elastic constant, ϵ the strain and ζ/E is referred to as the relaxation time of the material. In a previous paper (Hillier 1949) it has been shown that this is inadequate to describe the behaviour of polythene over a range of frequency and temperature; nevertheless for a restricted range of frequency it is sufficiently accurate to be a useful characterization of the polymer. The constant ζ can be considered as a 'viscosity' of the material and if ϵ is the tensile strain this can be considered as a 'tensile viscosity'. A similar term was used by Trouton (1906) and is discussed by Bosworth (1949) and Lethersich and Pelzer (1950). For shear strain ϕ a second expression of the form $\sigma_\varphi=n\phi+\eta\, d\phi/dt$ can be considered, where σ_φ is the shear stress, n the rigidity modulus and η is analogous to the ordinary viscosity of a fluid. The paper by Bosworth discusses possible relationships between ζ and η.

The following analysis based on the above two equations connecting stress and strain is due originally to Suyehiro (1928). Figure 6 shows the forces acting on a section of the bar a distance x from the clamped end, δx in length, of cross sectional area A and density ρ. Then the equation of motion for a displacement y is:

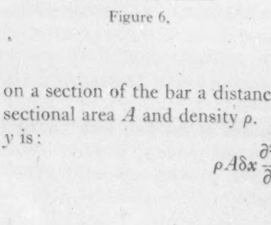

Figure 6.

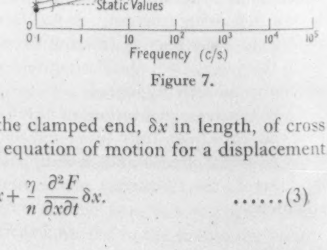

Figure 7.

$$\rho A\delta x\frac{\partial^2 y}{\partial t^2}=\frac{\partial F}{\partial x}\delta x+\frac{\eta}{n}\frac{\partial^2 F}{\partial x\partial t}\delta x. \qquad \ldots\ldots(3)$$

If the moment of inertia about the axis is I, then couples acting on the specimen producing rotation $\partial y/\partial x$ are

$$\frac{\partial M}{\partial x}\,\delta x+F\delta x-\frac{\zeta}{E}\frac{\partial^2 M}{\partial x\partial t}\,\delta x+\frac{\eta}{n}\frac{\partial F}{\partial t}\,\delta x,$$

where M is the bending moment, and the equation of rotary motion is

$$\rho I\delta x\frac{\partial^2}{\partial t^2}\left\{\frac{\partial y}{\partial x}\right\}=-\frac{\partial M}{\partial x}\,\delta x+F\delta x-\frac{\zeta}{E}\frac{\partial^2 M}{\partial x\partial t}\,\delta x+\frac{\eta}{n}\frac{\partial F}{\partial t}\,\delta x. \qquad \ldots\ldots(4)$$

Eliminating F between (3) and (4) we find

$$\rho A\frac{\partial^2 y}{\partial t^2}=\rho I\frac{\partial^2}{\partial t^2}\left\{\frac{\partial^2 y}{\partial x^2}\right\}-EI\frac{\partial^4 y}{\partial x^4}-\zeta I\frac{\partial^5 y}{\partial x^4\partial t}.$$

If the bar is thin compared with its length and only the lower modes of transverse vibration are considered then this equation reduces to

$$\frac{\partial^2 y}{\partial t^2}+\frac{EK^2}{\rho}\left\{\frac{\partial^4}{\partial x^4}+\frac{\zeta}{E}\frac{\partial^5}{\partial x^4\partial t}\right\}y=0. \qquad \ldots\ldots(5)$$

At $x=0$, $y=0$ and $\partial y/\partial x=0$ which are the conditions for a clamped end and at the free end $x=l$,

$$EK^2A\left\{\frac{\partial^2}{\partial x^2}+\frac{\zeta}{E}\frac{\partial^3}{\partial x^2\partial t}\right\}y=0, \text{ implying no shear force}$$

and

$$EK^2A\left\{\frac{\partial^3}{\partial x^3}+\frac{\zeta}{E}\frac{\partial^4}{\partial x^3\partial t}\right\}y=Le^{-i\omega t} \text{ the applied traction.}$$

The applied force is assumed to be sinusoidal and the real part of $e^{-i\omega t}$ is taken as the oscillatory term. It is assumed that the steady state solution is of the form $y=Y_{(x)}e^{-i\omega t}$ and equation (5) becomes

$$(d^4Y/dx^4)(K^2/\rho)(E-i\omega\zeta)=\omega^2 Y. \qquad \ldots\ldots(6)$$

Let $N^4=\omega^2\rho/K^2(E-i\omega\zeta)$, then equation (6) can be written $d^4Y/dx^4=N^4Y$. The general solution of this equation is

$$Y=a\cosh Nx+b\sinh Nx+c\cos Nx+d\sin Nx.$$

Putting in the boundary conditions the solution becomes

$$Y=a(\cosh Nx-\cos Nx)+b(\sinh Nx-\sin Nx),$$

where $$b=-a(\cosh Nl+\cos Nl)/(\sinh Nl+\sin Nl).$$

It can be shown that the displacement y_l of the free end $x=l$ is given by

$$y_l=\frac{e^{-i\omega t}LN}{2\rho A\omega^2}\,\frac{(\cosh Nl+\cos Nl)(\sinh Nl-\sin Nl)-(\sinh Nl+\sin Nl)(\cosh Nl-\cos Nl)}{1+\cosh Nl\cos Nl} \qquad \ldots\ldots(7)$$

This expression cannot be used analytically to obtain values of E and ζ from the observed values of y_l but it has been used to calculate resonance curves for systems with assumed and possible values of the parameters. The following parameters were used: $E=10^9$ dyne/cm², $\rho=0{\cdot}9$ gm/cm³, $K^2=0{\cdot}0025$ cm², $l=10$ cm. The resonant frequencies, i.e. y_l maximum, were obtained in the form of the pulsatance ω, for three values of ζ, (*a*) $\zeta=0$; (*b*) $\zeta=3\times10^6$ dynes/unit vel.; (*c*) $\zeta=10^7$ dynes/unit vel. The required values of ω were then (*a*) $\omega=58{\cdot}6$; (*b*) $\omega=58{\cdot}6$; and (*c*) $\omega=53$. It is clear that for higher values of ζ the use of the resonant frequency of a cantilever to measure the elastic response of the material is not trustworthy.

The frequency dependence of the elasticity of high polymers can be represented by a complex modulus (Nolle 1950) by analogy with dielectric theory (Cole and Cole 1941). It can be shown that if E'' is the imaginary part of Young's modulus then ζ will be equivalent to E''/ω. The real part of the modulus is as before merely the normal Young's modulus represented by $E'\equiv E$. The usefulness of the resonant frequency for the determination of elastic modulus can then be expressed in terms of the ratio $E''/E'=\omega\zeta/E'$. If this ratio exceeds 0·2 then there will arise a serious error in the estimation of E' from ω_0 (Nolle 1948). From previous work however (Hillier 1949) it was known that the order of magnitude of the ratio E''/E' was less than 10^{-1}, and the simple expression equation (1) was therefore used to calculate E. No attempt was made to measure ζ or E'' as the nature of the coupling between the electrical and mechanical circuits rendered this too inaccurate.

Table 1 gives values for the modulus of elasticity for polythene calculated from the resonant frequencies f_0 obtained at several temperatures. Figure 7 shows a graph of the values plotted against frequency together with values already published and derived from the velocity of sound in monofilaments. It is seen that the values agree very well and form an extrapolation of the previous results.

Table 1

Temperature	30° c.			40° c.	
f_0(c/s.)	46	53·3	76·5	35·8	67·5
E (dyne/cm^2)	$1{\cdot}96\times10^9$	$2{\cdot}15\times10^9$	$2{\cdot}75\times10^9$	$1{\cdot}54\times10^9$	$2{\cdot}04\times10^9$

Table 2 gives values of the 'static' modulus, the mean of several experiments at each temperature. The values agree well with values obtained by extension of thin filaments of the same grade of polythene reported previously (Hillier 1949). It can be seen that the dynamic modulus is still greater than the corresponding 'static' one and that the objection previously raised, that the dynamic measurements were made with much lower strains is not a serious one, for in this instance the strains used were identical.

Table 2. Values of Static Modulus

Temperature	17° c.	30° c.	40° c.
Cantilever	$6{\cdot}75\times10^8$	$5{\cdot}12\times10^8$	$4{\cdot}16\times10^8$
Filament	$6{\cdot}9^*\times10^8$	$5{\cdot}3\times10^8$	$4{\cdot}6\times10^8$

* By interpolation.

§ 6. CONCLUSIONS

A satisfactory method of measuring the dynamic elasticity at frequencies about 20 c/s. to 100 c/s. has been designed and operated, and measurements accurate to within one to two per cent can be obtained.

Preliminary results indicate that for polythene of the grade used no abrupt changes in the dynamic modulus occur in the complete range 20 c/s. to 20 kc/s. at temperatures between 20° c. and 40° c. The dynamic value of Young's modulus throughout the complete range of frequency so far investigated by the two methods is still greater than the 'static' value which has now been measured in two different ways with good agreement. The results confirm those of Lethersich (1950) already reported on the same grade of polythene for shear experiments and indicate that the dynamic value of Poisson's ratio remains essentially the same, throughout the range of compared frequencies, as that measured 'statically'.

Further extensions of the frequency range towards the 'static' time of application of force are obviously desirable as the gap still existing appears to be an important frequency range for this type of polymer.

ACKNOWLEDGMENTS

The author wishes to thank Dr. H. Kolsky and Mr. D. G. Christie for helpful discussions and suggestions during this work and Mrs. M. J. Moore for mathematical assistance and especially for computing the resonance values of the theoretical expressions. He would also like to acknowledge the help of Miss P. M. Prince and Mr. T. C. Welch, who carried out the tedious measurements necessary to obtain the resonance curves.

REFERENCES

Alfrey, T., 1948, *Mechanical Properties of High Polymers* (New York : Interscience).
Bosworth, R. C. L., 1949, *Aust. J. Sci. Res.* A, **2**, No. 3, 394.
Cole, K., and Cole, R., 1941, *J. Chem. Phys.*, **9**, 341.
Davies, R. M., and James, E. G., 1934, *Phil. Mag.*, **18**, 1023.
Hillier, K. W., 1949, *Proc. Phys. Soc*, B, **62**, 701.
Hillier, K. W., and Kolsky, H., 1949, *Proc. Phys. Soc.* B, **62**, 111.
Lethersich, W., 1950, *Brit. J. Appl. Phys.*, **1**, 294.
Lethersich, W., and Pelzer, H., 1950, *Brit. J. Appl. Phys.*, **1**, 1.
Nolle, A., 1948, *J. Appl. Phys.*, **19**, 753 ; 1950, *J. Polymer Sci.*, **5**, 1.
Prescott, J., 1946, *Applied Elasticity* (New York : reprinted by Dover Publications), chap. ix.
Suyehiro, K., 1928, *Proc. Imp. Acad. Japan*, **4**, 263.
Trouton, F. T., 1906, *Proc. Roy. Soc.* A, **77**, 426.

A Simplified Shearing Interferometer

By R. L. DREW
H. H. Wills Physical Laboratory, Bristol

Communicated by W. J. Bates; MS. received 28th March 1951, *and in final form 2nd July* 1951

ABSTRACT. A simple new design of interferometer based on the wave-front shearing principle is described and illustrations given of its application to the solution of a variety of 'through-type' and autostigmatic testing problems.

§ 1. INTRODUCTION

It is the purpose of this paper to describe a new design of interferometer based on the wave-front shearing principle which fulfils the requirement that it shall be of maximum simplicity consistent with adequate performance. In figuring two types of microscope mirror pairs (Drew 1949), 'through-type' testing methods were found desirable if an unnecessarily elaborate and cumbersome experimental arrangement was to be avoided. The design now to be described also enables one to dispense with an error-free reference wave front and yet retain some of the preferred advantages associated with direct interferometry.

Bates (1947) has shown that precise information concerning asphericities having revolution symmetry is contained in the interferogram in the overlap region of mutually displaced views of a convergent wave front. The essential requirement of such an instrument is that it shall so divide an incoming convergent wave front that recombination of the two components after any desired amount of shear—that is, mutual displacement about a suitable axis—can occur without change of path length between them.

§ 2. PRINCIPLE OF THE INSTRUMENT

Consider the principal ray W of a convergent wave front of angular aperture η, incident at angle ϕ on a plane parallel dividing plate at point A (Figure 1). Subsequent rays AB and AC after reflection and refraction respectively, suffer further reflections at plane mirrors B and C such that recombination occurs at D after a similar process. Orientation of mirrors B and C parallel to and equidistant from the plate ensures equality of path length in the two circuits. Rotation of mirror B about a vertical axis through the point of incidence of the principal ray results in rotation of the principal ray about this point as imaged at I, but without change of path length. Thus, location at point I_2 of the apex of the cone of aperture η associated with the principal ray enables rotation of B to occur, whilst identical path lengths are retained for individual rays. This results in mutual lateral displacement between the wave fronts F_L and F_R via B and C respectively. Rotation of B through an angle θ results in shear through an angle 2θ between displaced sights F_L and F_R of the same wave front, and an overlap region of angular aperture $\eta - 2\theta$ in a horizontal direction, in which interference can occur.

Spatial separation of the images at I due to B and C results in interference fringes perpendicular to the direction of separation, and we have the conditions for lateral shear with horizontal or vertical fringes. Mutual rotation of mirrors B and C about horizontal axes, so that they are symmetrically disposed each at an angle α to the plate (Figure 2), results in spatial separation of the images I and I_1'', due to B and C respectively, by a vertical amount $S = t \sin 2\alpha/(\mu^2 - \sin^2 \alpha)^{1/2}$, where t and μ are the thickness and the refractive index of the plane parallel plate. This is equivalent to mutual rotation of the wave-fronts about a horizontal diameter of such an amount as to give at the upper and lower edges of the aperture η an effective separation $\delta = N$ wavelengths.

Writing the focal ratio as f/n, where n expresses the ratio l/d of the wave front, we see from Figure 2 that the separation $\delta = S/2n = N\lambda$ results in $4N+1$ horizontal fringes across the field, including a central 'black' fringe. Thus to obtain 10 fringes across the field associated with an $f/30$ output cone of a micro-objective would require B and C each to be rotated through an angle $\alpha = 20'$.

§ 3. COMPENSATION

A plate of thickness 8 mm. and refractive index 1·5 introduces into an $f/4$ cone incident at an angle of 35° (the maximum of the present instrument), about 19·3 fringes of astigmatism, 4 fringes of primary coma and 0·2 fringes of primary spherical aberration in a wavelength of 5×10^{-5} cm. (Bates 1947). It is necessary that compensation of these aberrations should fall within the testing tolerance required, say one-tenth of a wavelength.

Define a new principal ray passing through the centre of the interference aperture and consider the case when the images I and I_1'' (Figure 2) are coincident, that is, a single 'fluffed out' fringe covers the field of view. Such a ray traverses the plate horizontally at an angle $\sin^{-1}[\sin(\phi+\theta)/\mu]$ to the normal, having a glass path length $p=\mu t/[\mu^2-\sin^2(\phi+\theta)]^{1/2}$ in either arm. This equality of path lengths holds for any other overlapping pair of rays, so that errors introduced by the plate are exactly compensated for all values of shear.

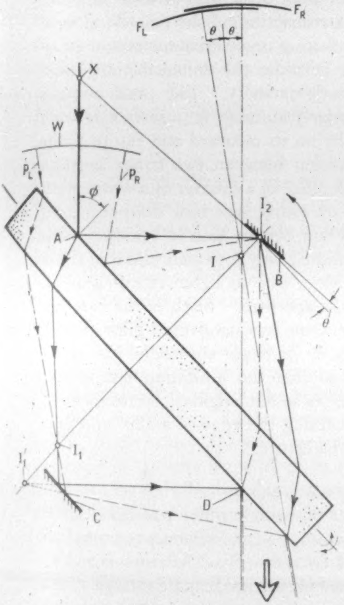

Figure 1.

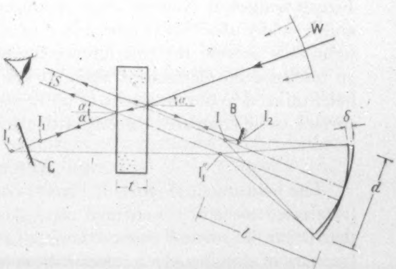

Figure 2.

Compensation errors arise only when the plate and mirror C are rotated to give the required number of horizontal fringes across the field, as in Figure 2, but these can be kept within the testing tolerance. For example, with ten fringes across the field of an $f/4$ cone the rotation required results in uncompensated plate errors amounting to one-tenth of a fringe (1/20 wavelength) of astigmatism and 1/100 fringe of coma. The natural procedure in order to appreciate progressively 'slower' (longer period) errors is to reduce the number of fringes across the field. This results in an increase in the nominal sensitivity of the test in the sense that the wider spacing of the fringes gives a better appreciation of the error. The associated decrease in the uncompensated coma and astigmatism is automatically brought within any tolerance required.

§ 4. MODES OF OPERATION

In 'through-type' testing, the wave front converging to an image is merely the output of the particular optical system on test. In such a case, retention of the visibility of the fringes, defined as $(\text{Intensity}_{\max} - \text{Intensity}_{\min})/\text{Intensity}_{\max})$ requires that the size of such an image be restricted in a direction parallel to the direction of shear. An $f/20$ output cone from a micro-objective of initial magnification $\times 60$ sheared through a distance equal to one-tenth of the field radius requires a slit image $5{\cdot}2 \times 10^{-3}$ cm. wide for 50% visibility. This implies the use of a slit object of actual width 1×10^{-4} cm., for example a fine scratch on an aluminized slide, with correspondingly wider slits for smaller apertures or shears. It is not difficult to obtain visibilities greater than 50% over a wide range of apertures and shears, but inevitably there is a restriction on the amount of light available, and this may become important in testing unsilvered surfaces.

In such cases it may be advantageous to consider the enhanced range and sensitivity of the instrument when used autostigmatically. The small number of surfaces in the instrument make it particularly suitable for use in this way. When the light traverses the system identically on its outward and return paths the errors are seen doubled, so that a separation between two fringe maxima or minima corresponds to an actual height difference of a quarter of a wavelength (instead of half a wavelength). Restrictions on source size now disappear, and it is possible to use an extended source with consequent gain in intensity even for very large values of shear. Such a use is limited only for small values of shear by the fact that the fringe visibility is only 50%, due to light returning along unwanted paths and falling in the interference aperture. Such is the case for Fizeau fringes or Newton rings produced between two unsilvered glass plates, and in many uses this is tolerable. In any case, for larger shears the unwanted light falls outside the interference aperture so that the limitation disappears. In testing deep menisci for Schmidt systems, these autostigmatic features have been utilized to obtain shears of up to 30°, enabling the edge of a 120° aperture surface to be compared directly with that at the centre.

§ 5. APPARATUS

The instrument (Figure 3, Plate*) consists of a single plane parallel plate P (a selected piece of commercial plate glass 8 cm. × 1·5 cm. × 8 mm.) mounted so that it can be rotated about a horizontal axis by screw S_R. Mirrors B and C (sections of aluminized microscope slides selected for flatness) can be rotated about vertical axes by screws S_S and S_1 (not shown) respectively, and adjusted in altazimuth setting by screws S. The screw S_P operates an arm carrying mirror C and adjustments to give the initial path length setting by rotation about the point X (Figure 1).

§ 6. EXPERIMENTAL

The initial setting of the instrument can be made to a high order of accuracy by utilizing the phenomenon of Brewster fringes produced between the plate and each mirror. The focus of the incoming wave front is arranged to coincide with the axis of B by observing through D that no positional change of the image occurs on rotating B, this also correctly locating the mirror surface in a plane through the axis of rotation. When mirror C is obscured and one views in the direction CD, a Brewster fringe system is seen, due to front and back surface plate reflections at A, thence to mirror B, and again to the front and back surfaces of the plate. The surfaces can be made parallel by appropriate adjustment of the mirror about a vertical axis, and the plate about a horizontal axis. The fringe pattern thus obtained gives a direct estimate of any errors of plate homogeneity and thickness or the departures from flatness of the surfaces.

---

* For Plates see end of issue.

Coincidence of image fields F_L and F_R is established by viewing beyond D, adjusting mirror C to give parallelism and operating the path length control until a 'fluffed-out' fringe covers the field. Rotation of C and the plate about horizontal axes through angles 2α and α respectively gives the required number of horizontal fringes across the field and establishes the instrument in its correctly compensated setting at zero shear. Operation of the shear control S_s is now the only one required, and this is continuously variable over any desired range. A test of the compensation is to examine the fringes at zero shear, when they should be straight and uniformly spaced as in Figure 4(*a*) (Plate), and for all values of shear the orientation separation and 'blackness' of the fringes should remain constant apart from the asphericities of the wave front on test.

§ 7. INTERPRETATION

In general, the fringe pattern is antisymmetrical about the centre point of the interference aperture, and indicates directly height differences $h_{r+\Delta r}-h_r$ between adjacent portions of the surface or wave front. These height variations are interpreted differently in the range of large and small shears. A single zone will show in the fringes as a 'hill and dale' and the magnitude of the error will increase to a constant value, indicating directly the height error when the zone is sheared clear of itself.

In the region of small shear (for example, where it is required to test a highly aspheric wave front) an integration is required. For surfaces having rotational symmetry $h=f(r)$, so that the height differences expressed by the fringe pattern can be expanded as a Taylor series of the form $h_{r+\Delta r}-h_r=\Delta r(dh/dr)+\ldots$ plus higher terms which for slow errors and small shears can be neglected. Since the shear is Δr, the slope dh/dr of the wave front at a particular radius is then indicated directly by the departure from straightness $(x\lambda)$ of the fringes at that radius, that is, $x\lambda/\text{shear}=\text{slope}$.

Taking a reference line at an arbitrary angle to the shear direction is equivalent to a focus shift, so that by choice of a particular reference line we can refer the information contained in the interferogram to a mean focus. These functions of the instrument are thus analogous to the operation of knife-edge testing, except that slopes are indicated directly in terms of fringes per unit distance and may be referred to a mean focal position without movement of the instrument. True height differences are obtained by integration of the area between the mean and actual slope curves, either graphically or, in some cases, mentally.

Figure 4(*b*) shows the interference pattern given by a 5 in. diameter nominal sphere of aperture $f/12$ at a shear of $r/5$. The variation of slope with increasing radius (Figure 5(*a*), full line) referred to the mean centre of curvature (dotted line) implies the true height differences indicated in Figure 5(*b*). Colour photographs of this event show clearly the differential fringe separation due to the constituent wavelengths in the mercury light used.

The interferogram given by an achromatic doublet of diameter $1\frac{1}{2}$ in. and focal length 4 in. tested between arbitrary conjugate points is shown in Figure 4(*c*).

An interesting feature is that the asphericities of the wave-front profile as shown in Figure 5 (*c*) are directly related to the spherical aberration correction of the doublet. A colour photograph would further exhibit the associated secondary spectrum so that, in principle, complete information concerning the doublet is obtainable from a single colour photograph.

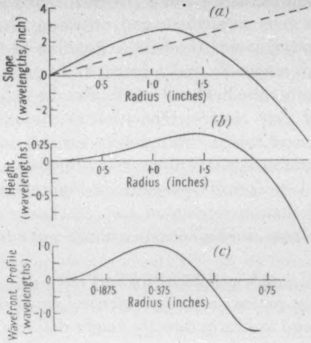

Figure 5.

Figure 4 (*d*), (*e*) and (*f*) show interferograms of the output wave front of a commercial immersion apochromat of N.A. 1·3 focusing at −1 cm., 0, and +4 cm. with respect to the correct optical tube length. These clearly exhibit local zonal error and overall 'lemon peel' of about one-tenth of a fringe. The spherical aberration due to working at an incorrect tube length amounts to 2 and 8 fringes, as shown in Figure 4 (*d*) and (*f*), and indicates that for a tolerance of a quarter of a fringe the tube length should be correct to better than 1 mm.

The resemblance between the present instrument and that of Mach and Zender has been pointed out to the author, but the shearing principle used here is somewhat different. It is hoped that the earlier discussion has illustrated the fact that 'shearing' instruments, even of relatively simple design and construction, can play a useful part in the solution of many practical problems.

ACKNOWLEDGMENTS

The author is indebted to Dr. C. R. Burch, Mr. J. M. Burch and his colleagues in the laboratory for helpful advice and discussion and to the Ministry of Education for financial assistance during the course of the work.

REFERENCES

Bates, W. J., 1947, *Proc. Phys. Soc.*, **59**, 940.
Drew, R. L., 1949, *Nature, Lond.*, **164**, 360.

LETTERS TO THE EDITOR

An Unusual Kind of Fringe System

The author once formed Newton's rings of large diameter for which a low power equi-convex lens and a concave lens (instead of the usual combination of convex lens and plane surface) were used, and published a photomicrograph of a part of the rings formed between them (Dhavale 1947). In order to obtain rings of large diameters the difference between the curvatures of the surfaces forming the rings had to be very small. Apart from the Newton's rings seen with monochromatic or even with white light, it was found that if this combination was held so as to reflect the light from an electric bulb, among the various images of the bulb there was one which was crossed with localized white light fringes. These fringes were not part of the Newton's rings. Further investigation showed that: (i) by moving the eye, the image in which the fringes are formed moves over the surface of the lens and the fringes can then be traced over the surface; (ii) these fringes are usually curved, having large radii of curvature and are sometimes even straight, depending upon the position of the point of contact of the two lenses and the angle of reflection; (iii) the central white light fringe of the new system passes approximately through the centre of the usual Newton's rings; (iv) the image in which the fringes are seen can be identified as the second flare image by reflection of the electric bulb as would be formed by the convex lens, but (v) by separating the upper convex lens away from the lower concave lens this image breaks up into *four* separate images. It is possible to show how these four images are formed due to the two surfaces of the convex lens and the near surface of the concave lens which latter has very nearly the same curvature. By blackening the lower surface of the concave lens it can be shown that it has no share in the formation of these images or of the fringes. The photograph (Figure 1) shows the new fringes obtained with white light superposed on Newton's rings.

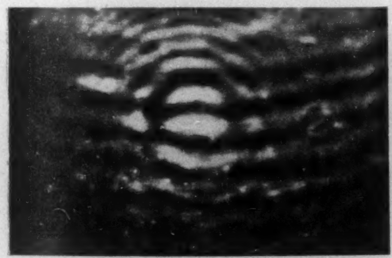

Figure 1.

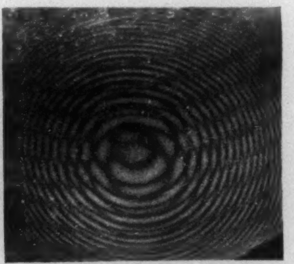

Figure 2.

(vi) When the white light is replaced by monochromatic light it is found that, if the flare image is brought to the point where the usual Newton's rings are formed (for this the point of contact between the lenses has to be moved away from the centre of the system, as otherwise all possible images overlap), there now appear *two* sets of Newton's rings. The separation between these two sets increases as the angle of incidence increases. The two ring systems give nodal lines exactly like those given by two identical sources of spherical waves. The pattern, in fact, looks like that given by a double source in a ripple projector when the waves are stabilized by a synchronized stroboscope. It is these nodal lines which form the dark bands of the fringes when white light is used. A greatly enlarged photograph of these double Newton's rings obtained with the mercury green line is reproduced in Figure 2. (vii) The two systems of rings show no difference in polarization. Polarization due to reflection according to Brewster's law is found in both systems in the same direction; thus the doubling in this case is not an effect of birefringence. (viii) The two ring systems are obviously due to two pairs of the four flare images mentioned in (v) above. (ix) The diameter of the first ring is not the same in the two systems. These white light fringes are obviously *localized* fringes of superposition and are therefore of the same type as Brewster's bands. Raman and Datta (1925–26), following a suggestion by Schuster (1924), have given a detailed explanation of the production of Brewster's bands by the superposition of two sets of non-concentric Haidinger rings. *Localized* fringes of superposition between two silvered sheets of mica have been obtained by Tolansky (1949) in his studies in multiple beam interferometry.

A comparison between the earlier observations and the contents of this note may now be in order. The double ring system in the present work is obtained as a result of a peculiar type of reflection and interference phenomenon. Brewster's bands formed by the superposition of two non-concentric Haidinger ring systems are located at infinity. When the Brewster's bands are obtained with white light the Haidinger rings disappear. In the present work the bands are localized and can be seen at the same time as the circular rings (Figure 1). While Brewster's bands, whether localized as in Tolansky's work or non-localized, require *four* surfaces for their formation the fringes obtained in the present case are given by only three surfaces. These differences are easily explained. The localization is a result of the surfaces being curved; three surfaces are sufficient to produce the fringes of superposition as a result of the internal reflections which form the flare images, and the three surfaces *can* give rise to four emergent rays.

Thus it may be said that the novelty of the present observation consists not in any new principle but in the peculiar circumstances in which the fringes are obtained.

Department of Physics,
University of Poona.
8th August 1951.

D. G. DHAVALE.

DHAVALE, D. G., 1947, *J. Univ. Bombay*, **15**, Part 5, 22.
RAMAN, C. V., and DATTA, S. K., 1925–26, *Transactions of the Optical Society*, **27**, 51.
SCHUSTER, A., 1924, *Phil. Mag.*, **48**, 609.
TOLANSKY, S., 1949, *Nature*, **163**, 637.

Certain Properties of Electrostatic Fields encountered in Electron Lenses

In a recent paper " Certain Properties of Electrostatic Fields encountered in Electron Lenses " by Dr. P. A. Lindsay (1950), it is suggested that the equipotential lines in a two-cylinder electrostatic lens show two points of inflection, at distances off the axis of about one-third and two-thirds of the lens radius. This is contrary to our experience in general, and has not been confirmed by our check of the particular problem treated in the paper. We find in this case, as in many other similar cases, that the equipotential lines are quite smooth curves, of strictly parabolic shape up to nearly one-half lens radius distance from the axis (Maloff and Epstein 1938, Figure 4.1, which shows also some 'kinks', referred to in Dr. Lindsay's paper, is of rather low accuracy, the asymmetry about the axis being even more marked than the 'kinks').

From the original data of his field plots, which Dr. Lindsay was good enough to make available to us, and which agree quite closely with our check of this particular problem, one can prove that the deviations of the equipotential lines from smooth curves are well *within the error limit* which one would have to expect from the numerical errors of the original field data and the subsequent process of interpolation. These deviations are therefore not significant, and they are, moreover, so small that they would not be noticed in a graph of the size of Figure 1 of Dr. Lindsay's paper. The representation of the results in this Figure and the conclusions drawn from it are therefore in error.

Research Laboratory,
Associated Electrical Industries Ltd.,
Aldermaston, Berks.

M. E. HAINE.
G. LIEBMANN.

LINDSAY, P. A., 1950, *Proc. Phys. Soc. B*, **63**, 699.
MALOFF, I. G., and EPSTEIN, D. W., 1938, *Electron Optics in Television* (New York: McGraw-Hill).

The issue between Dr. Liebmann, Mr. Haine and myself is whether the ' kinks ' or 'flattening' of the equipotential lines shown in my work on electron lenses, and previously indicated by Maloff and Epstein (1938) are significant or whether they are merely due to numerical and experimental errors.

Dr. Liebmann and Mr. Haine state that the ' kinks ' are within the limits of numerical errors of my field calculations. I should like to point out, however, that in field plots which I have made available to them the ' kink ' is caused by a 4% change in the slope of equipotential lines. Since the slope was calculated with an accuracy of the order of 1–2% it is clear that the ' kink ' could hardly be said to lie ' well within the error limits ' of numerical computations.

The existence of the ' kinks ' has been further questioned by Dr. Liebmann and Mr. Haine on the grounds that they have never themselves come across such irregularity in calculating potential fields in electron lenses. I have consulted Messrs. Maloff and Epstein on the matter, and in a letter they have pointed out to me that the ' kinks ' appearing in the equipotential lines were originally questioned at the time of collecting data for Figure 4.1 on p. 74 of their book, but repeated experiments seemed to indicate some irregularity in this region of the lens. Although the accuracy of the measurements was not high enough to verify conclusively their existence, Dr. Epstein expressed the view that some irregularity is, in general, to be expected on theoretical grounds when the gap between the cylinders is finite.

In view of the fact that Dr. Liebmann and Mr. Haine used numerical and not analytical methods in calculating their results, no finality can be attached to the statements they have made about the shape of equipotential lines. On the other hand, the fact that two entirely independent lines of approach seem to indicate similar results would suggest with a fair degree of probability that some irregularity in the shape of the equipotential lines exists in this part of the lens.

18 Aspley Road,
London, S.W. 18.
6th September 1951.

P. A. LINDSAY.

MALOFF, I. G., and EPSTEIN, D. W., 1938, see reference above.

The Acceleration of Electrons to Energies above 10^9 ev.

The main difficulties in designing an electron synchrotron for energies above 5×10^8 ev. are the needs to relate the accelerating radio frequency accurately to the increasing magnetic field, and to provide the high radio-frequency voltages necessary to replace the energy lost by radiation (Schiff 1946). The first difficulty may be met by injecting at an energy so high that a fixed radio frequency may be employed, and the second by the use of a ' race-track ' design (Crane 1946), with an all-metal resonator in a field-free part of the orbit. Initial betatron acceleration is not recommended for a large synchrotron because of the low injection magnetic field and increased gas scattering. The extra cost of an external injector is justifiable, and a magnet C-shaped and facing outwards has the important advantage of accessibility.

On the basis of these principles a $1{\cdot}3\times10^9$ ev. synchrotron could be made with the following characteristics :

Magnet. Radius 300 cm. ; mass of steel 160 tons; $H_{\max}$ 15,000 gauss; stored energy 5×10^5 joules; peak ampere turns $1{\cdot}3\times10^5$; inductance $2{\cdot}6\times10^{-4}$ henry; useful doughnut aperture 7×23 cm^2; windings air-blast cooled.

A.C. Generator. Frequency 25 c/s.; repetition rate 12·5 pulses per second; peak potential 2·7 kv.; peak current $6{\cdot}6\times10^4$ amp.

R.F. Generator. Peak power 15 kw.; fixed frequency 36 Mc/s. (fourth harmonic of electron revolution frequency); voltage amplitude modulated from 30 to 120 kv.; copper losses 1 kw. peak; beam loading (for injection current 100 ma.) 12 kw. peak.

The copper loss is for a quarter-wave resonator of inner diameter 30 cm. and outer diameter 270 cm., or a cavity of comparable size. In practice a much smaller resonator could be used.

Injection would be at 3 MEV. from a linear accelerator (Fry 1947) because of the large currents available. The injection field is then 33 gauss, and the radius of the orbit changes by only 1% as the particles are accelerated. The estimated acceptance time is 2×10^{-7} sec. and 3×10^{10} particles might be injected per pulse. The radiation loss at full energy is 100 kev. per revolution. Amplitude modulation is employed to restrict the radial spread of the beam due to the initial phase oscillations.

The magnet could be used to accelerate protons to only 750 MEV. The Birmingham $1{\cdot}3\times10^{9}$ ev. proton synchrotron (Oliphant *et al.* 1947) uses a magnet of mass 1,000 tons, the stored energy being 5×10^{6} joules*. The smaller magnet for $1{\cdot}3\times10^{9}$ ev. electrons makes possible a substantially higher repetition rate for a comparable source of power, the rate proposed being 125 times greater than for the Birmingham synchrotron; this entails the use of transformer laminations instead of ½-inch steel plates. Further, because of the high injection current, the number of particles injected per pulse would be of the same order.

Physics Department,
The University, Birmingham.
3rd September 1951.

L. RIDDIFORD.

---

* $1{\cdot}8\times10^{6}$ calories.

CRANE, H. R., 1946, *Phys. Rev.*, **69**, 542.
FRY, D. W., *et al.*, 1947, *Nature, Lond.*, **162**, 859.
OLIPHANT, M. L., *et al.*, 1947, *Proc. Phys. Soc.*, **59**, 666.
SCHIFF, L. I., 1946, *Rev. Sci. Instrum.*, **17**, 12.

Thermo-Electric Measurements on Semiconductors

In a recently published discussion, Boltaks (1950) reviews an earlier paper by the author on the thermo-electric and conductive properties of blue titanium dioxide (Henisch 1948). The present note is intended to clarify some of the misunderstandings which have evidently arisen, probably through an inaccurate translation of my original remarks.

The polarity of the thermo-electric effect is widely used as a criterion for the type of charge carrier in semiconducting materials. This procedure is theoretically justified, unless the substance is intrinsically conducting at the temperature of the experiment and unless the surface of the specimen is contaminated in various ways (Granville and Hogarth 1951). Non-uniform distribution of impurity centres constitutes a further possible source of error. Under suitable conditions which, for purposes of demonstration and study, were purposely established in some of my experiments, such heterogeneity can give rise to 'distributed thermo-e.m.f.s' which may be of either sign and which may dominate the measured thermo-electric response. It is thus necessary to interpret thermo-electric tests on new specimens with caution and, in general, to supplement them with simple tests for homogeneity and surface contamination. The view that thermo-electric tests can *never* be used as a criterion for the type of charge carrier was not implied in the original publication. When allowance was made for the heterogeneity of the specimens, the experimental results were in good agreement with theory and were not materially affected by experimental shortcomings of the type mentioned by Boltaks.

Department of Physics,
University of Reading.
31st August 1951.

H. K. HENISCH.

BOLTAKS, B. I., 1950, *J. Tech. Phys. U.S.S.R.*, **20**, 1039 (see also *Science Abstracts*, 1951, **54**, 719).
GRANVILLE, J. W., and HOGARTH, C. A., 1951, *Proc. Phys. Soc.* B, **64**, 488.
HENISCH, H. K., 1948, *Elect. Commun.*, **25**, 163.

REVIEWS OF BOOKS

An Introduction to Electron Optics, by L. JACOB. (Methuen's Monographs on Physical Subjects.) Pp. x + 150. (London: Methuen, 1951.) 8*s*. 6*d*.

Though there is no lack of good textbooks on electron optics, there is certainly a demand for a short and compact representation of the essentials. Dr. Jacob's intention to fill this gap will be certainly appreciated by many students and non-specialists. It is unfortunate that his monograph contains passages which are likely to mislead or to puzzle the uninitiated. Here are some examples, all taken from the first pages. On page 4 Fermat's principle is introduced, without disclosing that the v which figures in it is the phase velocity, and the beginner may well be wondering why v appears here in the denominator, while in the principle of Least Action, on the next page, it is a factor of ds. On page 5 the author forgets to mention that the action function is a difference of two functions, one depending on the initial, one on the final position only, and he forgets to state what the symbol U, the potential energy, is meant to represent. On page 6 the problem is stated to depend on the conditions imposed ' by the motion ', when what is meant is ' on the motion ', or ' by the field '. On page 8 he starts to talk suddenly of the analogy with ' thick glass lenses ' though on page 7 only the refraction at a plane interface has been explained, and the reader is left wondering how the electron can cross the normal and converge to an ' axis ' of which not a word has been said previously. On page 10 most of the optical definitions are wrong, partly because the author fails to distinguish between the off-axis angle of a marginal ray and of a general ray, to which he gives the same symbol α, and he speaks, rather surprisingly, of the ' numerical aperture *of a ray* ' (italics mine).

In the later, more practical chapters, the author is on firmer ground, and these contain much useful material. The bibliography is good and comprehensive, but contains many indecipherable abbreviations.

D. G.

Photometric Atlas of the Near Infra-Red Solar Spectrum, by ORREN C. MOHLER, A. KEITH PIERCE, ROBERT R. MCMATH and L. GOLDBERG. Pp. 7 + 234 tracings. (Ann Arbor, Michigan: University of Michigan Press, 1950; obtainable in London through the Oxford University Press.) $4.

The elaborate Utrecht Atlas produced by Minnaert, Mulders and Houtgast in 1940 has for several years provided solar physicists with an accurate photometric map of the solar spectrum for wavelengths shorter than $\lambda 8771$. The infra-red solar spectrum beyond this limit has been mapped photometrically with various types of heat detector up to 24μ, but the resolution obtained has not been comparable with that obtained in the photographic region. In the Utrecht Altas, for example, the resolving power $\lambda/d\lambda$ is of the order of 10^5; Adel's map of the region 7–14μ has a resolving power of about 10^4.

Under a ' guest-investigator ' arrangement between the Mount Wilson and Palomar Observatories, and the McMath–Hulbert Observatory, investigators from the McMath–Hulbert Observatory have been able to use an infra-red spectrometer with a Cashman PbS detector in conjunction with the 24 in. Snow Telescope of Mount Wilson to produce high resolution direct intensity recordings of the near infra-red solar spectrum from $0{\cdot}8\mu$ to $2{\cdot}5\mu$. The resolving power of about 30,000 is unprecedented in the region covered, and the published results form a natural extension of the Utrecht Atlas, which they overlap by several hundred Ångströms.

Those who are more familiar with the appearance of the visible spectrum will at once notice the regions of total atmospheric absorption which obscure the solar spectrum in the regions $1{\cdot}4\mu$, $1{\cdot}8\mu$ and $2{\cdot}5\mu$.

The region preceding the first absorption was already well known from photographic and other studies. The main interest in the Atlas will undoubtedly centre in the newly displayed contents of the two ' windows ' at $1{\cdot}65\mu$ and $2{\cdot}20\mu$, where hundreds of new lines are now revealed. About half of the observed lines are atmospheric, being due to the molecules O_2, CH_4, N_2O, H_2O, and to CO_2 and its isotopes. The CO_2 band structure is completely resolved. Many of the several hundred newly discovered solar lines have been identified. The elements concerned are those which are known to be relatively common in the solar atmosphere. The significant feature of these new lines is the fact that they nearly all have high ionization potentials, and are heavily concentrated in number and intensity in the window of shorter wavelength. Goldberg has pointed out that the negative hydrogen ion absorption coefficient has a minimum near $1{\cdot}65\mu$, and that the abundance of solar lines in this region may be due to the consequent reduction of solar opacity.

The individual line contours in the Atlas are of course determined almost entirely by instrumental effects, but a great deal of information will be obtainable from their measured equivalent widths.

The Atlas consists of 234 tracings, each of which covers a range of about 80A., reproduced with a superimposed grid by the photo offset process. Each page contains two such tracings. The zero intensity level is given and wavelengths are marked for three lines on each trace. This is a departure from the more convenient procedure of the Utrecht Atlas, in which the wavelength scale is printed. The sheets are very lightly bound together without boards.

This Atlas is a major contribution to infra-red solar spectrophotometry, and will become a standard work of reference for all engaged in solar or atmospheric spectroscopy. The companion volume containing wavelengths, equivalent widths and identifications will be eagerly awaited. In the meantime, the authors of the Atlas are to be congratulated on their promptitude in making these important records generally available. P. J. TREANOR.

Progress in Metal Physics: II, edited by BRUCE CHALMERS. Pp. viii + 213. (London: Butterworth's Scientific Publications, 1950.) 45*s*.

Since the Editor is a distinguished experimentalist, it is not surprising to find that experiment, rather than theory, is emphasized in the articles which he has brought together in this second volume on metal physics. Not that laboratory techniques are described, but rather that experimental results and their broad physical interpretations are the prevailing interests. The reader is not required to be a great mathematician, and little special knowledge is assumed on his part beyond a general notion of the structures and properties of metals.

The first article is a very readable essay by Dr. H. Lipson on *Order–Disorder Changes in Alloys*. The study of both long-range and short-range order by X-rays and other methods is described in detail, and the broad principles underlying the ordering process are outlined, together with an interesting suggestion about superlattice Brillouin zones. Mr. I. I. Betcherman's account of *Rate Processes in Physical Metallurgy* deals with the application of chemical rate theories, of the Eyring type, to processes such as diffusion, precipitation, creep, and recrystallization. This article amply demonstrates the truth of Sir Cyril Hinshelwood's remark, made several years ago, that " the real unities underlying the interpretation of chemical changes are seldom open and apparent but tangled in a confusion which here and there might well appear inextricable, did not a broader view prevail that through the tangle ran certain threads bright enough to show a plan. The strongest and brightest of these threads is the idea of the activation energy."

A very sure touch is discernable in the excellent survey of *Anisotropy in Metals*, by Messrs. W. Boas and J. K. Mackenzie. They begin with a short introduction to vector and tensor relations, and then use this mathematical framework to discuss a surprisingly wide variety of topics, from amplitudes of thermal vibrations to weathering of rocks. The following article, on *Developments in Magnesium Alloys*, by Mr. H. G. Warrington will interest the production metallurgist, but is out of place in a book on metal physics, unless it is meant to illustrate the proposition that, in physical metallurgy, physics flies out by the window when economics enters by the door.

The last three articles in this volume, by Messrs. R. W. Cahn, A. Guinier and J. Tennevin, and C. Crussard, F. Aubertin, B. Jaoul and G. Wyon, together form an interesting *Symposium on Polygonization*. There is a rather exciting stop-press flavour about them; here the reader can actually see metal physics in progress. Polygonization, not even named until four years ago, is the process whereby plastically bent crystals reduce their lattice strains by developing block structures. It is attracting much interest at present, partly because it provides good evidence for dislocations in crystals, and partly because it seems to be a key to the still unsolved problem of recrystallization.

Judged solely on the basis of length against price, this is an expensive book. One imagines that many research students, and it is they who stand to gain most from it, will hesitate before digging as deeply into their meagre book allowances as its purchase requires. This would be unfortunate, because it contains articles of high scientific value and is elegantly printed on excellent paper.

(The reviewer has also written a survey of this publication from the metallurgical standpoint for the *Journal of the Institute of Metals*.) A. H. COTTRELL.

Negative Ions, by H. S. W. MASSEY. (Cambridge Monographs on Physics.) Pp. x + 136. 2nd Edition. (Cambridge: University Press, 1950.) 12*s*. 6*d*.

The first edition of this excellent monograph was reviewed in the *Proceedings of the Physical Society* in 1938. This second edition is better bound with hard covers, has a bibliography, and is nearly 30% larger, the increase being due mainly to the complete re-writing of the last chapter on modern developments in the study of negative ions.

The first four chapters closely follow those of the first edition apart from small modifications due to later work. Chapter I discusses the theory and structure of negative atomic ions and describes experimental determinations of electron affinities. (There are two small misprints in the last paragraph: 10^{12} being printed for 10^{-12}, and O^- being printed for O^{--}.) Chapter II discusses the nature of molecular ions in general, and of the simple cases H_2^-, O_2^-, halogen ions and OH^- in particular. Chapter III deals with modes of formation of negative ions: it discusses fully the various processes of electron attachment. Calculations are given of free-electron radiative capture by atoms of hydrogen and of oxygen, and capture by Na, Hg, Cl is also considered: then follows a discussion of the possibility of experimental confirmation of these theoretical results. Attachment in three-body collisions is next examined, and attachment by molecules (a form of three-body problem) is discussed. The two groups of experiments on electron attachment are then described: (i) the homogeneous electron beam method of Tate and Lozier and the mass spectrograph of Hagstrum and Tate at low pressures; (ii) the electron group methods such as the filter method of Loeb and Cravath and the diffusion method of Bailey at higher gas pressures. A good review of the main results is given. This important chapter closes with a survey of other modes of ion formation by capture of bound electrons from neutral atoms or metals. The next chapter discusses processes of electron detachment in the light of the principle of detailed balancing. This discussion is mainly theoretical, and reflects the lack of experimental data in this field; in fact, one of the features of this book is the emphasis it lays on the need for more experimental data on these collisional processes, since many of the views now held are, of necessity, conjectural.

Detachment is more difficult to study experimentally than attachment, as the main desideratum is a high value of the ratio of negative ion to electron concentration, whereas for attachment the more readily obtained low values of this ratio are required.

The last chapter occupies more than a quarter of the book, and deals with applications of negative ions and interpretation of collisional processes, whether in glow discharge tubes or in the terrestrial or stellar atmospheres. Some possible effects of negative ions in glow discharges are outlined qualitatively. Many new data on the earth's upper atmosphere are included, and a careful summary of its properties is given in tabular form. The Chapman theory of ionized layer formation is outlined. The influence of negative ions in solar and stellar atmospheres is discussed, and it is shown in some detail how negative ions of hydrogen practically determine the spectral distribution of solar continuous radiation over the observable frequency range.

This book is very readable, and can be highly recommended for its treatment of the subject. F. LLEWELLYN JONES.

CONTENTS FOR SECTION A

PAGE
Prof. J. RAYSKI. On the Quantum Theory of Reciprocal Fields and the Correspondence Principle 957
Dr. J. R. MACDONALD. Ferromagnetic Resonance and the Internal Field in Ferromagnetic Materials 968
Dr. R. W. WRIGHT. The Effect of the Mean Free Path of Electrons on the Electrical Properties of Non-Metals 984
Mr. C. CANDLER. The Magnetic g-Factors of a Nucleon 999
Dr. J. W. JEFFERY. X-Ray Diffraction by a Crystal Possessing Periodicities within the Unit Cell 1003
Dr. W. T. DAVIES and Dr. D. F. SHAW. A Search for Sudden Large Changes of Energy of Beta-Rays in a Cloud Chamber 1006
Dr. O. THEIMER. The First Order Raman Effect in Crystals, particularly in Diamond 1012
Dr. P. G. KLEMENS. Electrical Conductivity of Metals at Low Temperatures: Equilibrium between Electrons and Phonons 1030
Prof. ERWIN SCHRÖDINGER. A Combinatorial Problem in Counting Cosmic Rays 1040
Dr. J. C. BARTON. Observations of the Penetrating Non-Ionizing Component of the Cosmic Radiation 1042
Letters to the Editor:
  Dr. A. F. GIBSON, Mr. W. D. LAWSON, and Dr. T. S. MOSS. The Long-Wave Limit of Infra-Red Photoconductivity in PbSe 1054
  Dr. F. A. EL-BEDEWI, Mr. R. MIDDLETON, and Mr. C. T. TAI. Angular Distributions of the Neutron Groups from the Reaction ^{12}C(d, n)^{13}N . 1055
  Mr. J. J. WILKINS and Mr. F. K. GOWARD. The Reaction ^{12}C(γ, 3α) and a 16·9 MEV. Level of ^{8}Be Emitting Alpha-Particles 1056
  Dr. K. MENDELSSOHN and Mr. H. M. ROSENBERG. The Thermal Conductivity of Cadmium in a Magnetic Field at Low Temperatures 1057
Contents for Section B 1058
Abstracts for Section B 1059

ABSTRACTS FOR SECTION A

On the Quantum Theory of Reciprocal Fields and the Correspondence ***Principle***, by J. RAYSKI.

ABSTRACT. A method of quantization of non-local fields whose interaction is expressible by means of integral equations is given. The S-matrix is constructed by Yang's method. The non-local field theory is free of the usual convergence difficulties. It is possible to satisfy generally either the postulate of reciprocity or the postulate of correspondence, but it seems impossible to satisfy both principles simultaneously.

Ferromagnetic Resonance and the Internal Field in Ferromagnetic Materials, by J. R. MACDONALD.

ABSTRACT. A classical treatment of the domain energy terms of a homogeneous ferromagnetic solid leads to a formula for the internal field contributions from these terms. With this result, modifications in the resonance condition of ferromagnetic resonance arising from self energy, exchange energy, magnetocrystalline anisotropy, and applied or intrinsic stress are obtained and are applied to various crystalline anisotropy and stress conditions of interest in ferromagnetic resonance experiments. Finally, the bearing of the results on the anomalous g-values obtained in resonance experiments is considered.

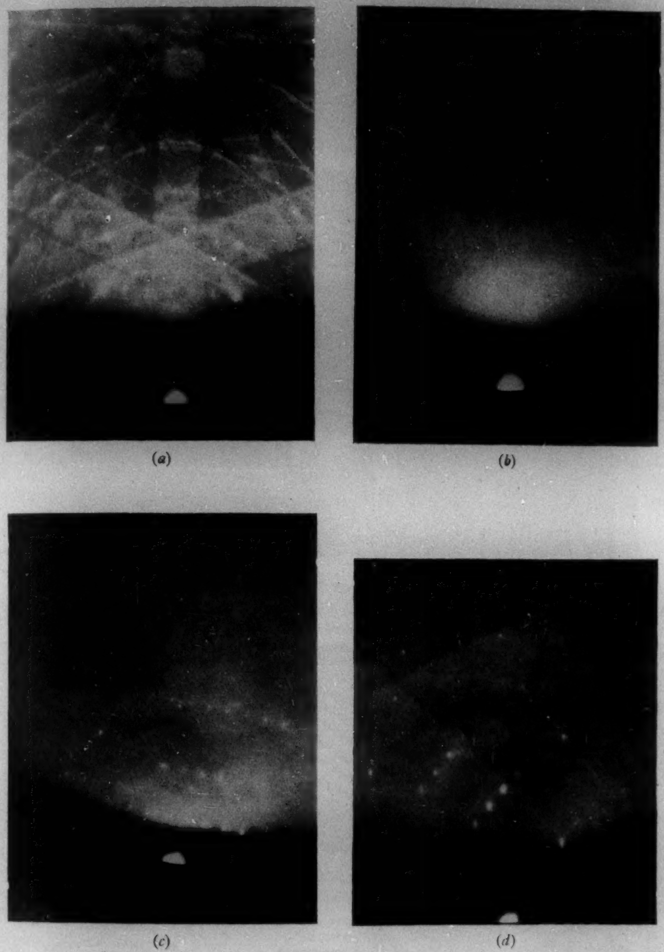

Figure 5. Electron diffraction reflection photographs of germanium surfaces ($L=25$ cm.; 75 kv.). (*a*) Polished and chemically etched. (*b*) Polished. (*c*) Polished and heat treated at 450° c. (*d*) Polished and heat treated at 850° c.

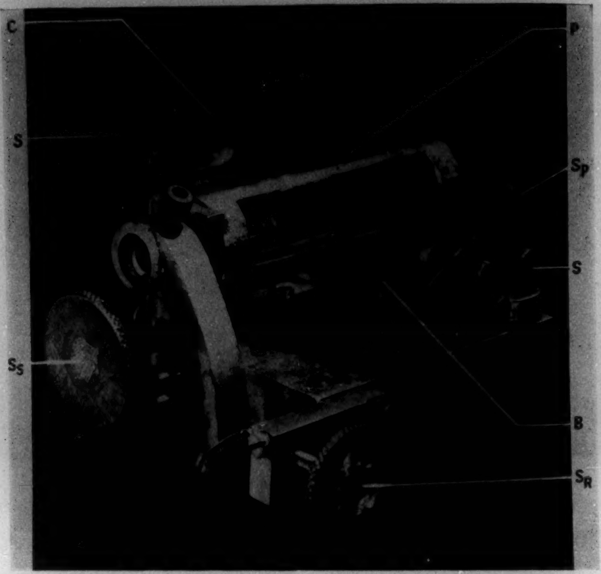
C
S
S_S
P
S_P
S
B
S_R

Figure 3.

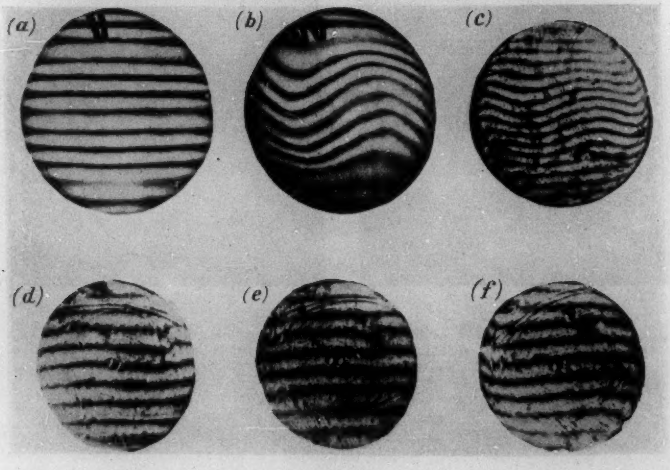

Figure 4.

The Effect of the Mean Free Path of Electrons on the Electrical Properties of Non-Metals, by R. W. Wright.

ABSTRACT. The theories of the mean free path of electrons in various types of materials, under various conditions, are discussed. The conductivity, thermo-electric power, Hall coefficient, fractional change of conductivity in a magnetic field, and the Nernst, Ettinghausen, and Righi–Leduc coefficients are all calculated upon the Lorentz–Sommerfeld theory for the various mean free path theories. The variations are discussed with particular respect to the changes of the reduced chemical potential η^*. The magnitude and sign of the coefficients are found to depend upon the mean free path theory assumed, that is, upon the type of material. In particular it is shown that the Ettinghausen and Nernst coefficients should be negligible in the majority of semiconductors with ionic lattices. Some of the assumptions usually made in semiconductor theory are shown to lead to erroneous conclusions. Experimental evidence is discussed and is found in general to support the theory given, both in impurity metals and semiconductors, except perhaps in the case of the thermo-electric power. No experimental results in non-metals are known for the thermo- and galvano-magnetic effects apart from the Hall coefficient, and it appears likely that such measurements will produce interesting information.

The Magnetic g-Factors of a Nucleon, by C. Candler.

ABSTRACT. The nuclear magnetic moment is a two-valued function of the spin, and Schmidt's argument is used in reverse to induce the orbital and spin g-factors. g_l is shown to be unity in odd-proton and zero in odd-neutron nuclei, as theory has assumed, but g_s varies from nucleus to nucleus with a mean value about half that found in the free proton or neutron. The magnetic spin ratio G, defined as $g_s/g(\mathrm{p})$ in odd-proton and as $g_s/g(\mathrm{n})$ in odd-neutron nuclei, measures the approach of an empirical moment to a Schmidt line; it is shown to obey much the same rules in odd-proton and odd-neutron nuclei.

X-ray Diffraction by a Crystal Possessing Periodicities within the Unit Cell, by J. W. Jeffery.

ABSTRACT. The Fourier transform of a crystal is used to explain the appearance of the X-ray reflections from the true crystal lattice of tricalcium silicate as satellites of the strong reflections corresponding to a pseudo-lattice. Similar but more general diffraction effects are also discussed.

A Search for Sudden Large Changes of Energy of Beta-Rays in a Cloud Chamber, by W. T. Davies and D. F. Shaw.

ABSTRACT. Measurements are presented of the changes of curvature of β-ray tracks in a cloud chamber containing air at approximately N.T.P. situated in a magnetic field of 400 gauss. These are examined for evidence of processes involving the reversible production of electrons of rest mass a small multiple of the normal value. Indications from a study of earlier investigations, that such processes might exist, are not substantiated, and the results confirm and extend those of Bleuler. It is shown that this type of cloud chamber investigation is unsuitable for obtaining useful information on inelastic scattering of fast β-particles, and that multiple scattering and observational bias are adequate to explain the anomalies previously reported.

The First Order Raman Effect in Crystals, particularly in Diamond, by O. Theimer.

ABSTRACT. The theory of the first order Raman effect in crystals is presented in a form which takes into account the finiteness of the wavelength of the incident radiation. The theory is applied to calculate the relative intensities of the first order Raman line and of the Brillouin components of diamond, which are interpreted as the Stokes and anti-Stokes Raman lines produced by those elastic vibrations, whose wave vector $\mathbf{Q}$ fulfils the condition $\mathbf{Q}=\mathbf{Q}''-\mathbf{Q}'$. ($\mathbf{Q}'$ and $\mathbf{Q}''$ are the wave vectors of the incident and scattered radiation.) The calculated intensities are in good agreement with experiments of Krishnan. A formula derived by Leontowitsch and Mandelstamm is discussed and is shown to be inadequate to calculate the intensities of the Brillouin components.

Electrical Conductivity of Metals at Low Temperatures: Equilibrium between Electrons and Phonons, by P. G. KLEMENS.

ABSTRACT. The Bloch theory of electrical conductivity of metals assumes that the phonon distribution does not deviate from equilibrium. Peierls has criticized this assumption, showing that in the presence of an electric field a stationary state is achieved only through processes which do not conserve the total wave vector. These can be *Umklapprozesse* involving electrons and a phonon, or phonon–phonon interaction of the type responsible for thermal resistance in dielectric solids. He estimates that if only the latter were to act, strong deviations from Bloch's formula would occur below 50° K. He therefore concludes that the electrical resistance at low temperatures is determined by *Umklapprozesse.*

A more detailed treatment of the statistical equilibrium of phonons and electrons shows that the relaxation times of the important phonons is smaller than estimated by Peierls by a factor of about 100; consequently one would not, as a result of phonon–phonon interactions, expect important deviations from the Bloch theory above 10° K. It is thus unnecessary to consider *Umklapprozesse*. Since *Umklapprozesse* require a special shape of the Fermi surface in wave-vector space, Peierls has concluded from the apparent agreement with Bloch's theory that the Fermi surface has this special shape. Hence it is now shown that this shape is not necessary.

A Combinatorial Problem in Counting Cosmic Rays, by ERWIN SCHRÖDINGER.

ABSTRACT. The probability is computed that precisely m out of r counters be hit by at least one out of n cosmic particles, each of which has the probability $1/r$ of hitting any particular counter. The estimation of n from given r and m is discussed.

Observations of the Penetrating Non-Ionizing Component of the Cosmic Radiation, by J. C. BARTON.

ABSTRACT. An anticoincidence arrangement of Geiger–Müller counters was used to detect that part of the non-ionizing component which is capable of penetrating 10 cm. of lead. Measurements were made at sea level and at an altitude of 3,560 metres. The mean absorption length of the non-ionizing particles was found to be 170 ± 5 gm. cm^{-2} in air, 190 ± 35 gm. cm^{-2} in carbon and 400 ± 25 gm. cm^{-2} in lead. The secondary particles were strongly absorbed in a few centimetres of lead. Studies were made of the angular distribution of the secondaries and of the production of two or more secondary particles in a single process. Less than 0·5% of the non-ionizing particles were found to be associated with extensive air showers, but about 10% appeared to be produced by ionizing particles interacting in the lead above the apparatus.

The angular distribution of the secondary particles produced in carbon was approximately proportional to cos θ.

The nature of the non-ionizing particles is discussed and it is concluded that the only known particles which could explain the results are high energy neutrons. On this hypothesis, their energy spectrum and intensity at the two altitudes are calculated.

PROFESSOR S. CHAPMAN, M.A., D.Sc., F.R.S.,
President of the Physical Society 1949–1950.

(*Note*—Prof. Chapman's Presidential Address is published in the October 1951 *Proceedings*, Section B, page 833.)